FSO Channel Characterization for Continental Fog Environments

Dissertation submitted by

MUHAMMAD SAEED KHAN

to the Faculty of Electrical Engineering and Information Technology

Graz University of Technology, Austria

in partial fulfillment of the requirements for the degree of

Doctor der Technischen Wissenschaften (Ph. D)

at the

Institute of Microwave and Photonic Engineering

Graz, January 2012

Supervisor and 1st Reviewer: Prof. Dr. Erich Leitgeb

2nd Reviewer: Prof. Dr. Gorazd Kandus

Declaration - EIDESSTATTLICHE ERKLÄRUNG

Ich erkläre an Eides statt, dass ich die vorliegende Arbeit selbstständig verfasst, andere als die angegebenen Quellen/Hilfsmittel nicht benutzt und die den benutzten Quellen wörtlich und inhaltlich entnommenen Stellen als solche kenntlich gemacht habe.

Graz, am:————- (Unterschrift)————————..

STATUTORY DECLARATION

I declare that I have authored this thesis independently, that I have not used other than the declared sources / resources and that I have explicitly marked all material which has been quoted either literally or by content from the used sources.

Graz, dated:————- Signature————————..

Dedication

To my beloved parents, fiance, brothers and sisters, to whom I owe, the love and the strive for wisdom and knowledge.

Acknowledgements

In the name of Allah the most Beneficent and the most Merciful, the one who rules all over the earth, heavens and everything that is present in between. All praise is to Allah for all His power, His blessings, His majesty, His sovereignty and every thing related to Him, whether we know it or not. Peace and prayer be upon our beloved Prophet Muhammad (S.A.W), his family and all of his companions. I am very thankful to Allah who has blessed me with the abilities to complete my PhD research course; with out His guidance and vision I would not have been capable of completing this dissertation.

This thesis finds me indebted to all my colleagues and the scientists, who helped me in many ways for the completion of this task. First of all, I am highly obliged to my colleagues Andreas Merdonig, Pirmin Pezzei, Thomas Plank, ex-colleagues Sajid Sheikh Muhammad, Muhammad Saleem Awan, Benno Flecker, Michael Gebhart and Farukh Nadeem at institute of Microwave and Photonic Engineering (formerly Institute of Broadband communications (IBK)) who helped me in a number of ways, giving all possible and valuable suggestions, using all of their knowledge. I am also thankful to my Pakistani colleagues in Graz, Austria especially Abid Ali Minhas, Amir Hayat, Asim Mansha, Muhammad Zahid, Tahir Mushtaq who have helped me through their noble guidance and confabulate with me on every topic giving me their full support and company. I want to pay special thanks to Prof. Carlo Capsoni and Roberto Nebuloni of Politecnico di Milano (Milan, Italy), V. Kvicera and M. Grabner of Department of Frequency Engineering, Czech Metrology Institute, (Prague, Czech Republic); who helped me by giving critical reasoning and helpful suggestions for improvement of my work, during the course of my PhD research.

Last but not least acknowledgement is for my advisor Prof. Dr. Erich Leitgeb who supported me in all possible ways by giving his advice, encouragement and all required resources to accomplish the task. He is a role model and the main driving force in providing me the power to cope with the challenges and to accomplish them during the course of thesis. I would like to thank Prof. Dr. Gorazd Kandus to take part in my examination committee and above all his valuable suggestions helped me to refine my work.

I am highly obliged for the financial support of Higher Education commission of Pakistan, which leads to the completion of the task; the Europe-wide network of excellence in Satellite Communications (SatNEx) and COST actions 291 and IC0802 played a vital role in the dissemination of the research results.

My heart is being filled with the sensation of thankfulness especially for my parents, brothers, sisters, friends and my well-wishers who prayed for my success and have remained the binding force in my life all through this work. I am highly grateful to my fiance for her care, patience and support. During the thesis many people have been supportive and deserve my heartiest gratitude. Thanks to anybody, I missed whosoever deserves a mention! May Allah Al-Rehman gives reward to all those who helped me and prayed for me during my research. Ameen.

Muhammad Saeed Khan

TU Graz, Graz, January 2012

Abstract

Ever since the inception of free-space optical links as a potential "last mile" access technology; the atmospheric attenuators have played a detrimental role in its widespread acceptance. Free-space optical links are supposed to operate through the atmosphere and achieve high reliability. The local weather conditions, in general, degrade the system performance and also reduce visibility. Among all the different atmospheric channel attenuators, fog remains the toughest to combat.

A detailed analysis of fog attenuation measured at Graz (Austria), Milan (Italy), and Prague (Czech Republic) has been presented. The thesis further explores the linearity or homogeneity analysis of optical attenuations. It is observed through the linearity analysis of optical attenuation that general assumption of linearity can not be valid for longer path lengths. This thesis further provides in detail the analysis of visibility based optical attenuation models and provides new insight about these empirical models. The error characteristics of a free-space optical (FSO) channel are significantly different from the fiber based optical links and thus require a deep physical understanding of the propagation channel. In particular different fog conditions greatly influence the optical transmissions and thus a channel model is required to estimate the detrimental fog effects. This thesis presents the probabilistic model for radiation fog from the measured data over an 80 m FSO link installed at Graz, Austria and 100 m FSO link installed at Prague, Czech Republic.

The fog events are classified into dense fog, thick fog, moderate fog, light fog and general fog based on the international code of visibility range for measured data of Graz while the measured data of Prague has been considered only for general fog case. The detailed analysis of liquid water content (LWC) modeling for FSO links is provided. Five months measurement of optical attenuations and the LWC have been used to draw a new model for direct estimation of optical attenuation from the LWC. The model proposed can be used conveniently in the range of wavelengths from 800 - 1600 nm for estimation of optical attenuation based on LWC with reasonable accuracy.

Zusammenfassung

Seit dem Aufkommen von optischen Freiraumübertragungssystemen (Free Space Optics - FSO) als mögliche Technologie zur Anbindung der "Last Mile" spielten die atmosphärischen Dämpfungseinflüsse die meistlimitierende Rolle in Bezug auf eine gröSSere Verbreitung der Technologie. FSO-Links sollen im freien Raum eingesetzt werden und eine hohe Zuverlässigkeit erreichen. Die lokalen Wetterbedingungen beschränken jedoch die Systemperformance und haben Einfluss auf die Sichtweite. Unter allen atmosphärischen Einflüssen stellt der Nebel die gröSSte Hürde für die terrestrische Freiraumübertragung dar.

Detaillierte Analysen der Dämpfung von Nebel an verschiedenen Orten (Graz, Mailand, Prag) wurden präsentiert. In der Arbeit wird die Linearität bzw. Homogenität von optischen Dämpfungen in Relation zur Pfadlänge untersucht. Anhand der Ergebnisse der Linearitätsuntersuchungen von FSO-Verbindungen ergibt sich, dass die Dämpfung auf längeren FSO Strecken nicht linear ansteigt. Diese Arbeit bietet genaue Analysen von auf die Sichtweite basierenden optischen Dämpfungsmodellen und neue Erkenntnisse über diese Modelle. Die Fehlermerkmale eines FSO-Kanals unterscheiden sich fundamental von jenen der Glasfaser, deshalb ist ein genaues Verständnis über die physikalischen Grundlagen notwendig. Insbesondere verschiedene Nebelereignisse beeinflussen den optischen Link in hohen MaSSen, deshalb ist ein Kanalmodell zur Abschätzung der Einflüsse notwendig. Ein Wahrscheinlichkeitsmodell über das Verhalten bei Nebel basierend auf Messwerten einer 80 Meter langen FSO-Verbindung in Graz und einer 100 Meter langen FSO-Verbindung in Prag wird erarbeitet.

Die Nebelereignisse in Graz wurden gemäß internationalen Richtlinien in Bezug auf die Sichtweite nach "dichter Nebel", "dicker Nebel", "moderater Nebel" und "leichter Nebel" eingeteilt, währen bei den Messungen in Prag nur generell über Nebelereignisse diskutiert wird. Auch die Rolle des (Flüssig)-Wassergehalts in der Luft (bei Nebel) als Auswirkung auf FSO-Links wurde untersucht. Messungen über fünf Monate lieferten Daten und Erkenntnisse, um ein neues Modell zur Abschätzung der Dämpfung anhand des Wassergehalts zu etablieren. Das vorgestellte und verifizierte Modell kann für Wellenlängen zwischen 800 und 1600 Nanometern verwendet werden.

Contents

List of Figures

List of Tables

1 Introduction

This thesis presents investigations on probabilistic channel model for terrestrial Free-Space Optical (FSO) links in different continental fog conditions, liquid water content (LWC) modeling for terrestrial FSO links and detailed statistical analysis of optical attenuation measured in Graz, Prague and Milan. The work is multidisciplinary and evokes knowledge of FSO, fog modeling for FSO and statistics of optical attenuation among many others. The main emphasis of the work is on probabilistic model for FSO links, LWC modeling for FSO links under continental fog conditions by using measured data of Graz and Prague and linearity analysis of optical attenuations.

1.1 An overview to FSO

Recent years have witnessed considerable interest in employing free space optics (FSO) or optical wireless communication (OWC) to a number of futuristic applications dealing with terrestrial and ground-space communication links . Over the last decade, the data rate demands (for many communication applications, like video conferencing, online video transmission, etc.) have been increasing to tens gigabit per second [1]. FSO has emerged in telecommunication industry as a viable source for providing high data rates to meet the needs of bandwidth hungry communication applications [2]. Initially FSO was mainly considered as a solution to the last mile access problem but now it is being investigated for high speed data transfer applications involving links between fixed and mobile platforms e.g. High Altitude Platforms (HAPs), Unmanned Aerial Vehicles (UAVs), Geostationary (GEO) and Low Earth Orbit (LEO) satellite terminals. Over last thirty years, FSO has become an improved and rising technology of the modern world, and is much more advanced than Radio Frequency (RF) and microwave/millimeter-wave (MMW) technology. Commercially, FSO is proved to be a strong alternative for complementing existing line-of-sight technologies (RF and MMW links) [3, 4]. A general overview of FSO system is provided in Fig. 1.1.

Usually FSO employs modulated beams of visible or infrared light to transmit huge data volumes between line of sight (LoS) transceivers through the free-space atmospheric channel by means of low powered lasers or LEDs. A narrow beam of light is triggered at transmission station which after passing through the atmosphere is received at the receiver station. FSO links require clear line-of-sight availability between the transmitter and receiver to establish a communication link. The optical carrier frequencies in the range of 20-300 THz (Fig. 1.2) makes FSO links as an important technology for future bandwidth

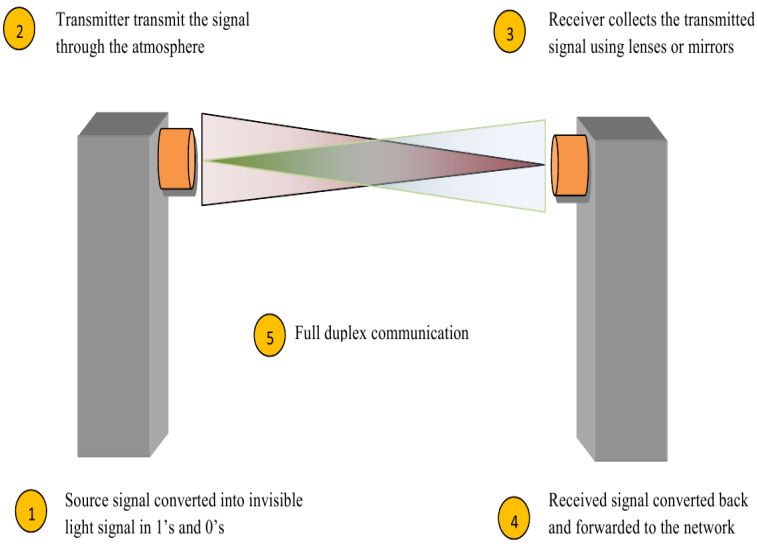

Figure 1.1: General overview of FSO links [5]

hungry communication applications [4]. FSO uses the similar concept of fiber optics except that no cabling is required. Considering the factors of speed and bandwidth, FSO has similar potential as that of fiber optic [6].

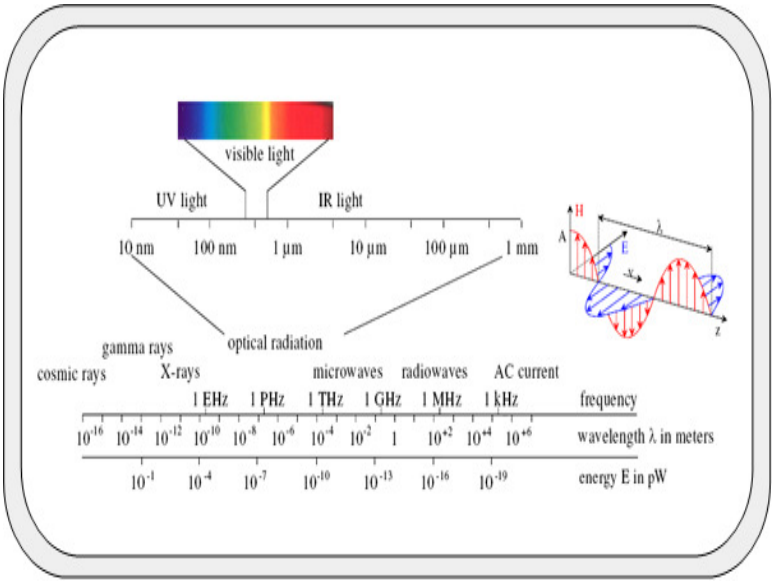

Figure 1.2: Electromagnetic wave spectrum [7]

The major applications of FSO include short, mid and long range communication applications when there is a need to transmit high data volumes (100 Gb/s range). Practical

fields of interest of FSO include satellites, high altitude platforms (HAPs), aircrafts and other nomadic communications which are used in military as well as civilian purposes, because of the favor of bandwidth, spectrum and security issues which are helpful for the adoption of FSO [8, 9]. The FSO is a low cost technology therefore, it is mostly used in the situations where the physical connections are impractical due to high costs or other considerations [10]. FSO has the ability to cope with the problems of bandwidth required for high data rate communication applications, thus, providing internet facilities in remote places especially in rural areas and to deal with emergency situations i.e. for disastrous situations [11]. Daily life applications of FSO include electronic commerce, streaming audio and video, web browsing, real-time medical imaging transfer, business networking and is considered as a last mile solution. Typical applications of FSO are secure and speedy service delivery of high bandwidth access to fiber networks, temporary network installation for special events and purposes, re-establishing high speed connections in case of emergency or disaster recovery, ship-to-ship high data rate communication and communication between ground and spacecraft or between spacecrafts including elements of a satellite constellation, unmanned aerial vehicles (UAVs) and low earth orbit (LEO) satellite terminals [12, 11]. The fixed FSO links for terrestrial usage have long been well established and today it has become a well known technology for commercial usage in local and metropolitan area networks [13]. The mobile and long-range applications of FSO require pointing and tracking accuracy because the transmitted beams have small beam divergences. This requires a thorough investigation to fully exploit the benefits of optical links. The detailed application scenerio is described in Fig. 1.3.

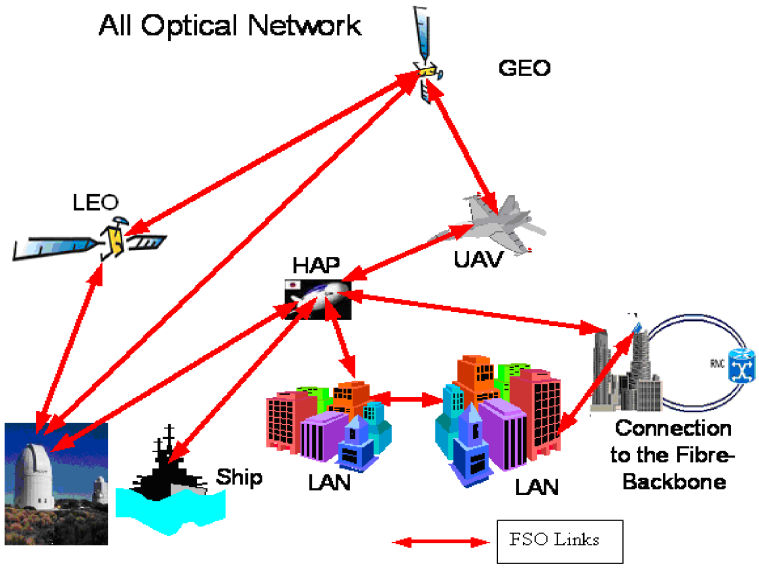

Figure 1.3: Application scenarios of FSO links [14]

There were certain experiments performed to explore the benefits and advantages of FSO

links for different terrestrial and space applications. The details of these experiments are given in Table 1.1 [15].

Table 1.1: Important FSO experiments

	Ground	**LEO Satellite**	**GEO Satellite**
Ground	Many Experiments	KODEN (2006) TerraSAR-X (2008)	ETS-VI (1994) GeoLITE (2006) SILEX (2001)
LEO Satellite	KODEN (2006) KIODO (2006) TerraSAR-X (2008)	TerraSAR-X-NFIRE (2008)	SILEX (2001) OICETS (2005)
GEO Satellite	ETS-VI (1994) GeoLITE (2006) SILEX (2001)	OICETS (2005)	No Experiment

Advantages of Free Space Optical Communication are significant cost savings, speed of deployment and ease, wiretapping safety and avoidance of electro-magnetic pollution [16, 6]. Moreover, FSO provides flexibility of establishing links therefore, helps in finding niche applications both in military as well as commercial service sectors [17, 18]. Several studies and experimentations are laid down for the development of optical wireless terminals having reduced size, mass, power consumption and increased data transmission [19, 20, 21].

FSO systems are supposed to operate through the atmosphere. Earth's atmosphere highly affects near-earth optical communication system because of variability in atmospheric conditions. Optical communication network for near-earth application scenarios is shown in [22]. Fig. 1.4 shows the operational scenario for FSO links.

Earth's atmosphere contains fog, clouds, dust, smoke, smog and some charged particles [9]. All these mentioned hydrometeor quantities act as attenuator for FSO links. Among all of them, fog is the most challenging attenuator [24] and have remained a research topic for FSO links over the years. Fog can be characterized by many physical parameters i.e. liquid water content, particle size distribution, temperature and humidity. The main attenuation contributing effect is the Mie scattering phenomena causing attenuations of the order of 480 dB/km [25] in dense maritime fog environments and 130 dB/km in continental fog environments [26]. This is mainly due to the Mie scattering phenomena that occurs if the spatial variations in the real part of the complex refractive index are on the order of transmitted wavelength. These variations in the real part of complex refractive index are caused by fog particles due to statistical fluctuations in its density. Rain causes attenuation of 20-30 dB/km at a rain rate of 150 mm/h [27] while, 45 dB/km specific attenuation can be caused through snow.

Laser power attenuation through the atmosphere is variable and difficult to predict, which is a main disadvantage of FSO [28]. Wave front distortion, beam wandering and beam spreading, which are responsible for signal loss, are also caused by absorption and scattering of laser beam propagating through the atmosphere, while, system losses even in the

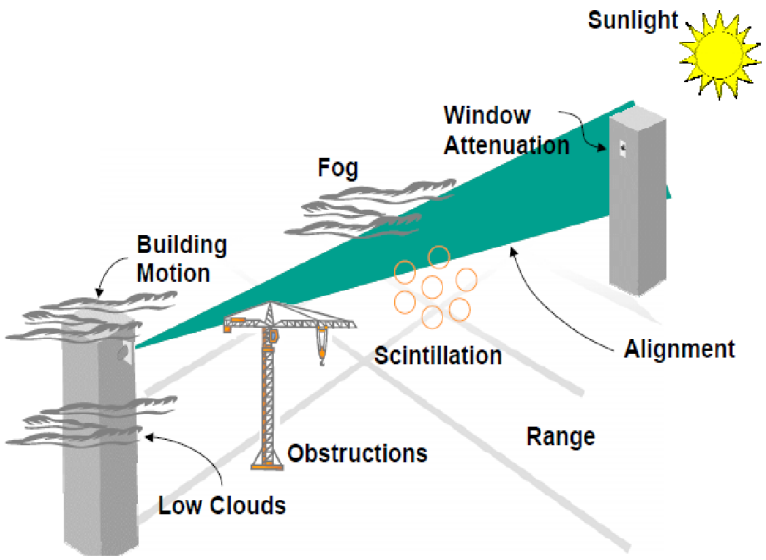

Figure 1.4: Operational scenario for FSO link [23]

absence of atmospheric particles (fog, rain, snow and clouds), some times tend to increase BER [29]. There is an exponential increase in turbulence with altitude which is found remarkable at an altitude of 25 km and stochastic in space and time showing fade signals on a time scale of several milliseconds [30, 31]. Fog and clouds mostly affect lower atmosphere extending upto 10-12 km. Furthermore, long-haul optical links through the atmosphere are highly effected from strong fading, due to variation in index-of-refraction turbulence (IRT) and link blockage; caused by obscuration such as clouds, snow and fog.

1.2 History of FSO

FSO has gained a very popular place in the modern communication industry, but it has roots in the primitive times as the communication methods employed today prevailed in the old forms for centuries before the work of Claude chappe in the year 1792, when he demonstrated semaphore system for the transmission of messages between towers, but the transmitted information was very limited until the invention of optical telegraph at the end of 18th century which helped in communication over long distances. FSO became available after the invention of laser as a source of light. First working laser was described as stimulated emission by Albert Einstein in 1905 and then by Ruby Laser in 1960 by Theodore Maiman and it was proved to be a milestone for optical technology which lead to the discovery of optical communication based on optical fibers [32].

With the expansion of developments of low attenuation optical fibers and semiconductor lasers emitting continuously at room temperature in 1970-71 explosion of wired optical telecommunications took place which dominated the fields of terrestrial long-distance transmissions starting from 10 km (for cables) to metropolitan networks thus becoming

an integral part of the whole world [22]. The network infrastructure which is based upon silica mode glass fibers in buried cables has now been deployed in many European countries. Terrestrial applications having longer distance directive radio links are used in special cases but main medium for shorter distances non-directive applications (access segment of networks) is radio frequency. Major examples of radio frequency links are the digital cellular telephone network (GSM, UMTS), WLAN for data transmission in smaller cells, or DVB-T for digital television broadcasting [22, 33].

The transmission capacity of wired communication systems is constantly increasing (doubling) every year from telegraph systems to Dense Wavelength Division Multiplexing (DWDM). New creations in this art of technology for performing analogous functions are carried out in both electrical and electronic domains, which are further accelerated at an average rate of doubling after every 18 months with the help of single mode fibers. Prior to optical communications, Electrical coaxial cables are used to transmit data signals at a maximum bit rate of 565 Mbit/s over 1 km distance between electrical regenerators. The transmission capacity has reached upto 2.5 Gbits/s over a distance of 100 km with the introduction of single-mode fibers, while in early 1990s the development of Erbium Doped Fiber Amplifiers (EDFA) took place which was designed to combine many optical channels in frequency domain for the amplification of optical signal from all channels and at the end, the transmitted stream signal was demultiplexed at receiver end [34].

Fiber-optic communication has gained considerable place for different telecommunications applications, FSO technology is relatively new and provides similar bandwidth and transmission abilities as fiber optics. FSO was originally developed by the military and NASA. Now it has been more than three decades that FSO is getting importance for a variety of communication applications. Recent advances in FSO technology have increased the importance of FSO for short, medium and log range communication applications [35].

1.3 Motivation

FSO operates through a challenging scenario (Fig. 1.4). Fog and turbulence are the most prominent atmospheric particulates which have been studied and investigated for different application oriented scenarios. For FSO technology, to mature and reach mass acceptability, there is a need to investigate different weather impairments on FSO links and predict the attenuation of transmitted laser beam caused by atmospheric aerosols. Since, attenuations due to fog are the biggest concerns for terrestrial FSO links, so in this study the measured optical attenuations has been evaluated in continental fog statistically by comparing the attenuations for different probability distribution functions (PDF) and presenting their important statistics. FSO channel has been modeled under turbulent conditions widely but turbulence is less significant for terrestrial FSO links. There are certain attempts to model fog drop size distribution under fog conditions. Since, there was a lack of PDF estimate of received signal strength (RSS) and liquid water content (LWC) modeling for terrestrial FSO links, it made a lot of sense to investigate a probabilistic model for RSS using the

measured data of optical attenuation. The simultaneous measured data of optical attenuation along with liquid water content (LWC) made it possible to investigate and probe the relationship between Optical attenuation and LWC and the variation of optical attenuation with the variation of LWC.

1.4 Previous Work

FSO is an area of communication which is needed to be researched comprehensively [36, 37, 38, 1] . The basic concepts of light transmission through the atmosphere have been presented in [39, 40, 41, 42, 43]. The weather effects on the performance of FSO remained an active research area [25, 44, 45, 46, 47, 48, 49, 50, 51] and some solutions have been proposed to cope with such atmospheric effects [52, 53, 48]. The selection of an appropriate wavelength for FSO links has been considered in [28, 54, 55, 56, 57]. Availability and reliability analysis for FSO systems has been studied in [58, 59, 60, 61, 62, 63] to prove their importance in evolving the broadband network [64]. Hybrid FSO-RF links promise very high availabilities and are described in [65, 66, 67, 68, 69].

1.4.1 PDF estimation of received signal strength

Statistical characterization and modeling of fog can provide important inputs for better system design of FSO links. The FSO links are impaired by various atmospheric attenuators and this study provides a thorough statistical analysis of the RSS under a foggy channel. In the past years several PDF have been proposed to characterize the received optical signal. The log-normal (LN) distribution has been considered as best distribution to characterize under scintillation conditions [70, 71]. In [72, 73] have been shown that LN distribution assumption is not valid for strong turbulence conditions. Therefore, the K, gamma (G) and gamma-gamma (GG) distributions were presented as suitable PDFs [70, 71, 74]. RSS has been modeled as the Lognormal [75, 76] and Gamma [75] distribution based on selected fog event data.

1.4.2 LWC modeling for FSO links

For FSO technology, to mature and get widespread acceptability, there is the need to investigate different weather impairments on FSO links and predict the attenuation of transmitted laser beam caused by atmospheric aerosols [77]. The prediction of optical attenuation in lower atmospheric visibility ranges, due to water hazes, fogs and clouds, has been thoroughly investigated and researched [78, 28, 79]. In the literature there is a lack of empirical relationship between the LWC and optical attenuation based on directly measured values of LWC and optical attenuations, simultaneously. Though several efforts have been made to estimate extinction coefficient (extinction coefficient is measured in km^{-1}) [80, 81, 82] and attenuation [83, 84] for FSO links on the basis of the LWC.

1.5 Thesis Structure and Contributions

The attenuations caused by atmospheric aerosols have played a detrimental role in the widespread acceptance of FSO links [85]. FSO links are supposed to be operated through

the atmosphere and achieve high reliability. The local weather conditions, in general, degrade the system performance and also reduce visibility. Among all the different atmospheric channel attenuators, fog remains the toughest to cope with. In many real life situations, when fog attenuation was measured as high as 480 dB/km, [25] there remained little hope for keeping the link operational. However, if the fog attenuation remains within the link margin, then the need arises to develop a deep understanding on the characterization of such fog attenuation. Chapter 2 provides overview of fog modeling for terrestrial FSO links and different model comparisons which have been used extensively for FSO links.

Different measurement campaigns have been carried out to investigate the impairing effects of weather, mainly of fog, on FSO systems. The link distances of the measurement campaigns were selected carefully depending on the purposes, limitations and local weather conditions. In most of the free-space optical attenuation measurement campaigns, presented in [75, 86, 87] , specific attenuation, described in dB/km, is used for detailed analysis. Chapter 3 presents the different measurement campaigns and the linearity or homogeneity analysis of optical attenuation under continental fog conditions using the measured data.

Statistical characterization and modeling of fog can provide important inputs for better system design of FSO links. The FSO links are impaired by various atmospheric attenuators and this study provides a thorough statistical analysis of the received signal strength under a foggy channel. Chapter 4 provides the PDF estimate of RSS by using the measured data of Graz and Prague.

Atmospheric particles attenuate the optical beam, propagating through the line-of-sight FSO links. Among all these, fog is the most serious deterrent [2, 88]. Fog can be characterized by the liquid water content (LWC), optical visibility, drop size distribution and temperature [89]. The scattering, absorption and extinction of laser beam propagating through the atmosphere are associated with the size of fog droplets, their effective radii and the microphysical properties of fog, specifically the liquid water content [88, 81]. Chapter 5 discusses the LWC modeling for FSO links.

The main contributions of the thesis include the linearity analysis of optical attenuations and have been discussed in Chapter 3; PDF estimation of RSS using the measured data of Graz and Prague are discussed in Chapter 4, followed by the modeling of LWC for terrestrial FSO links (Chapter 5). The originality and significance of the above thesis contributions is reflected by publication of parts of this thesis in several refereed conferences proceedings and journals (Appendix A).

2 Fog modeling for FSO links

Fog is a collection of suspended water droplets or ice crystals near the Earth's surface that causes to reduce horizontal visibility below 1 km (5/8 of a statute mile) [90]. Typical diameter of water droplets or ice crystals is in the range of 5 to 50 μm [91]. Water droplets and ice crystals are formed as a result of super saturation generated by cooling, moistening and/or mixing of near surface air parcels of contrasting temperatures [92]. The suspended water droplets and/or crystals can render an object undistinguishable to a distant observer and thus causes reduction of visibility conditions. It happens due to reduction in brightness contrast between an object and its background by particle concentration and size-dependent scattering losses of the light propagating between the object and the observer and through the blurring effect of forward scattering of light caused by the water droplets or ice crystals [93, 94, 95]. There are different kinds of fog, among them radiation fog (continental fog) and advection fog (maritime fog) are the more prominent types.

Radiation fog: Radiation fog occurs mostly in winter and autumn season. The radiation fog is formed near the earth's surface and occured usually at night and remained till sunrise and some times can persist for all the day in winter. The radiation fog occurred when there is a low speed wind, high humidity and clear sky. The typical diameter and shape of fog droplets depend upon the geographical location but usually can vary from 0.17 μm to 50 μm [96, 97]. The moderate continental fog can have the droplet diameter of 2-4 μm and droplet diameter for dense continental fog can vary from 4-6 μm [98, 99].

Advection fog: Advection fog is formed when damp air is moved across the earth surface or water with contrasting temperature properties. The droplet diameter of advection fog is normally larger than droplet diameter of continental fog. The mode droplet diameter of moderate advection fog is 8 μm and in dense fog case the diameter is 10 μm with particle concentration of 20 cm^{-3} [98, 99]. It is also called sea fog.

Fog begins to form when water vapors condense at temperature range of $-5°C$ to $5°C$ and relative humidity above 100 % with light wind (4 m/s) or relative humidity between 80-100 % and in the presence of numerous condensations or water vapor sublimations at $-30°C$ and relative humidity below 80%. Fog is formed only when air is saturated enough with water vapors and enormous amount of condensation nuclei are available in the air. The air saturation happens when there is relative humidity of 100% and air temperature decreases to dew point [100].

In general, the probability of occurrence of fog is much higher in winter than in summer, for continental environments when temperature approaches upto $0°C$ and relative humidity

rises above 80% [101]. But this is not the case for the maritime fog environments which is not dependent on any particular season. We determine fog occurrence on the basis of visibility range estimate. There is fog when visibility range reduces to 1 km.

2.1 Fog effects on FSO

Fog particles are normally larger than 1 micron and these particles are suspended in the air near the earth surface. FSO links operating inside fog conditions can suffer from severe attenuations of the optical signal power as the fog can significantly affect transmittance in the visible and near-infrared wavelengths. However, the mid and long-wave infrared spectral regions are not as sensitive to fog. This is mainly due to the Mie scattering phenomena that occurs if the spatial variations in the real part of the complex refractive index are on the order of the wavelength. These variations in the real part of complex refractive index are caused by fog particles due to statistical fluctuations in its density.

According to international code of visibility fog can further be categorized into four distinct types. The four types of fog depending upon the visibility range are given in Table 2.1. Fog effects the availability and reliability of FSO links significantly. Optical attenuations

Table 2.1: International code of visibility range

Visibility range (m)	Description	Sp. Attenuation (dB/km)
40 - 70	Dense fog	250-143
70 - 250	Thick fog	143-40
250 - 500	Moderate Fog	40-20
500 - 1000	Light fog	20-9.3

caused by fog in continental fog environment are shown in Fig. 2.1.

In real life situations attenuation due to fog reaches upto 480 dB/km in maritime environments and 236 dB/km for continental fog conditions [25, 87]. Fog attenuations are generally estimated by a semi-empirical formula based on visibility range estimate.

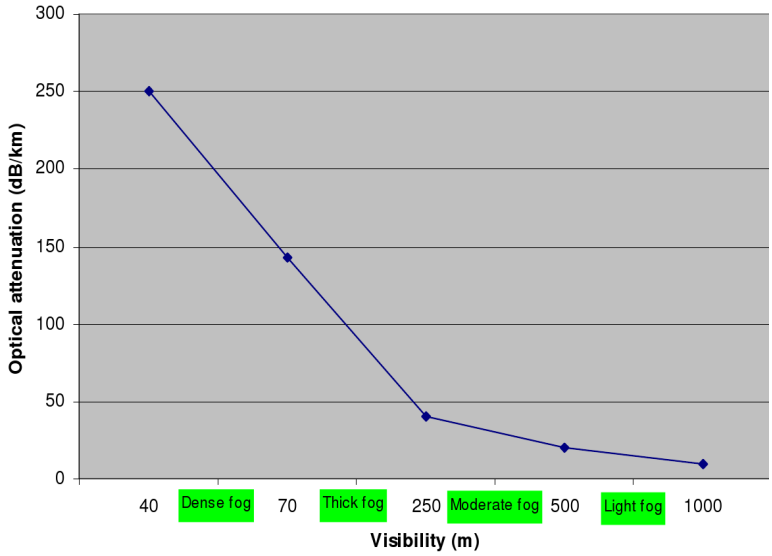

Figure 2.1: Optical attenuation caused by fog

2.2 Visibility based model

The standard visibility range is the distance to an object where the image contrast drops to 5% of what it would be if the object were nearby instead. There are three commonly used empirical models (Kim, Kruse and Al-Naboulsi models [28, 102, 79]) that employ visibility information to predict optical attenuations. The 1st model to estimate optical attenuation from visibility data was proposed by Kruse [102]. The visibility range data is readily available as it is collected at all airports around the world. This Kruse formula is essentially a combination of Koschmieder's visibility range formula and Beer-Lambert exponential attenuation law as presented in Equation 2.1 below and is applicable in case of fog attenuations [101, 2].

$$\Gamma(V,\lambda) = \frac{17.0}{V}[\frac{\lambda}{550}]^{-q} \tag{2.1}$$

where, V is the visual range in km, λ is wavelength in nm and Γ is the attenuation in dB/km, q is the size distribution coefficient of scattering and contains the information of meteorological conditions. 17.0 dB value is against 2% contrast, assumed for visibility range. The value 8.5 dB can be used instead of 17.0 dB value if 5% contrast is assumed for visibility range. The parameter q differentiate both Kim and Kruse models. The parameter q for Kruse model is given as

$$q = \begin{cases} 1.6 & \text{if V} > 50 \text{ km} \\ 1.3 & \text{if 6 km} < \text{V} < 50 \text{ km} \\ 0.585V^{\frac{1}{3}} & \text{if V} < 6 \text{ km} \end{cases}$$

Kim [28] showed that there is no preferential scattering of wavelengths by fog. Mie scattering calculations, transmission measurements, and simple observations indicate that optical attenuation from the visible to the near IR in fog is virtually independent of wavelengths [103]. Kruse model supposes lesser attenuation for longer wavelengths and fails to predict optical attenuation for lower visibility range (less than 1 Km). According to this assumption, longer wavelengths(like 1550 nm or 10 μm) could be used for future FSO systems to cope with problems of severe attenuation caused by atmosphere [104, 105].

The major drawback of Kruse model is that this model fails to approximate the attenuation for dense fog conditions especially when the visibility is less than 500 m, and 2nd limitation of Kruse model is that it does not consider different types and classes of aerosols. In Mie scattering theory, optical transmission measurements and simple observations show that attenuations caused by atmosphere are independent of transmitted wavelength, which allows to assign a fix value to parameter q for dense fog conditions(as approximated in Kim model). According to Kim, the parameter q can attain following values,

$$q = \begin{cases} 1.6 & \text{if V} > 50 \text{ km} \\ 1.3 & \text{if 6 km} < \text{V} < 50 \text{ km} \\ 0.16V + 0.34 & \text{if 1 km} < \text{V} < 6 \text{ km} \\ V - 0.5 & \text{if 0.5 km} < \text{V} < 1 \text{ km} \\ 0 & \text{if V} < 0.5 \text{ km} \end{cases}$$

The main difference between Kruse and Kim model is, Kruse assumes the wavelength dependency whereas, Kim rejects the wavelength dependency for dense fog conditions (visibility $\leq$ 500 m).

Al Naboulsi presented two different models for radiation and advection fog. The radiation and advection fog models are presented in Equation (2.2 and 2.3) respectively.

$$\gamma_{adv}(\lambda) = \frac{0.11478\lambda + 3.8367}{V} \tag{2.2}$$

$$\gamma_{rad}(\lambda) = \frac{0.18126\lambda^2 + 0.13709\lambda + 3.7502}{V} \tag{2.3}$$

where, V is the visual range in km, λ is wavelength in *nm*. The specific attenuation coefficient is provided in Equation (2.4)

$$a_{spec}(dB/km) = \frac{1000}{\ln 10} \cdot \gamma(\lambda) \tag{2.4}$$

The five months measured data of optical attenuations at Prague provided us a chance to compare these three models and find a best suitable model for continental fog environment.

Fig. 2.2 provides the time series of recorded specific attenuation in dB/km and visibility in meters for the representative fog event. The accuracy of the measurements is validated by the fact that as the visibility decreases the corresponding specific attenuation increases and vice versa.

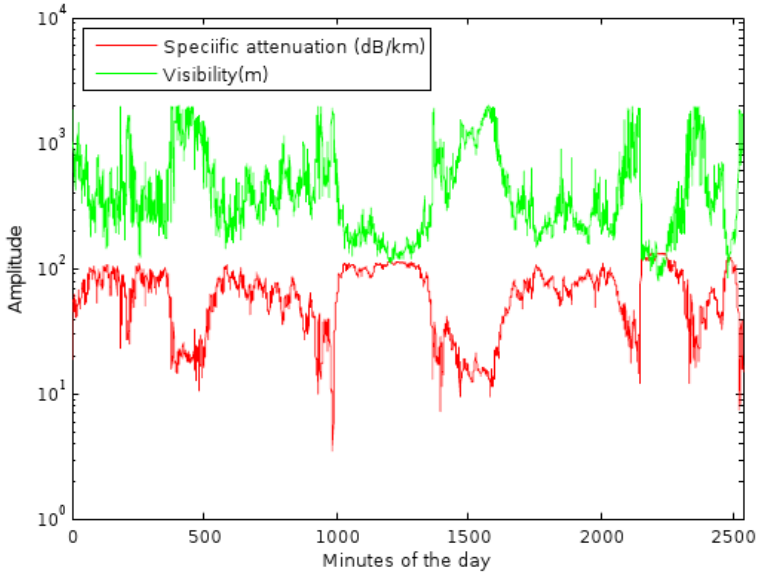

Figure 2.2: Time series of measured optical attenuations at a minute scale

The comparison of real time measured fog attenuations data with predicted specific attenuation using models of Kruse, Kim and Al-Naboulsi (radiation model) is illustrated in Fig. 2.3.

Analyzing Fig. 2.3, it is very difficult to decide which model is better suited to the recorded attenuations. Therefore, the root mean square error (hereafter RMSE) for all three models has been calculated using Equation 2.5.

$$RMSE = \sqrt{\frac{\sum_{i=1}^{n}(A_{p,i} - A_{m,i})^2}{n}} \tag{2.5}$$

A_p is predicted specific attenuation, A_m is measured specific attenuation and n represents the total number of observations in Equation 2.5.

The comparison of RMSE, using above mentioned three empirical models, is given in Fig. 2.4. For this particular recorded data the Al-Naboulsi radiation fog model has the least value of RMSE and thus appears to provide the best approximation.

It shall be considered in subsequent researches on visibility based attenuation models, that presenting a new model; through only a specific data set [106, 107], does not lead to significant scientific progress. The development of generic visibility based attenuation

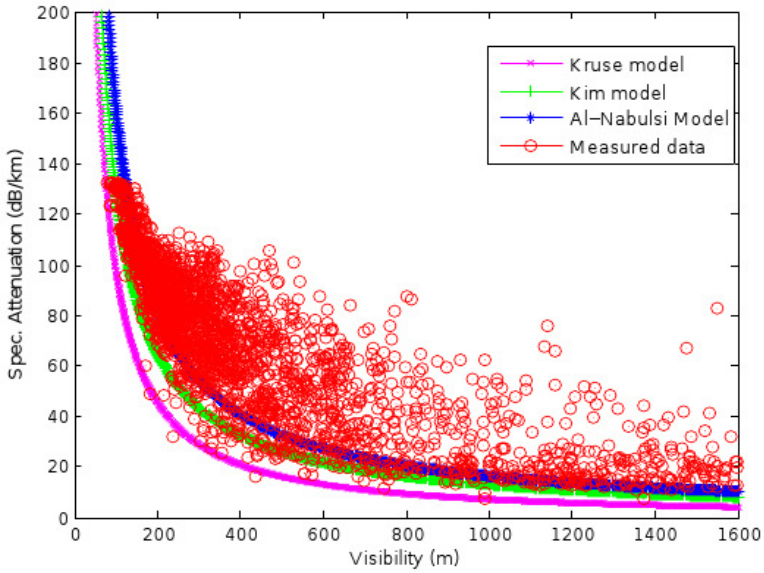

Figure 2.3: Comparison of different visibility based attenuation models with real data

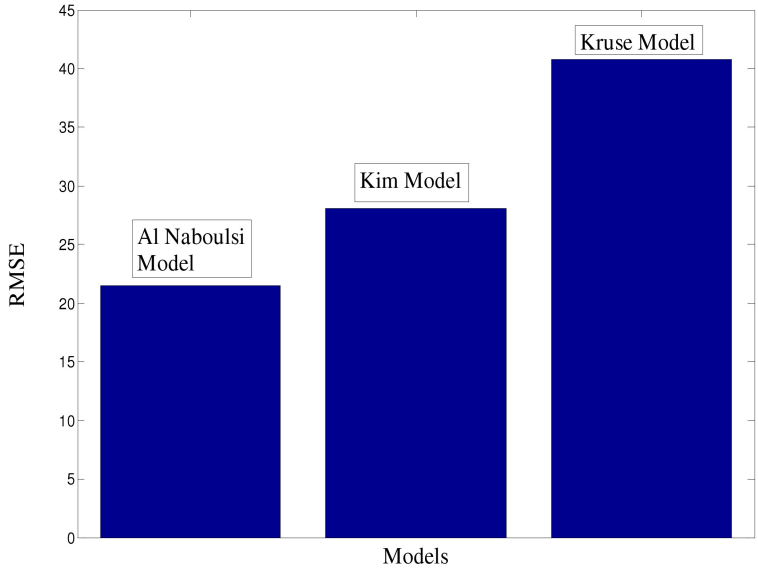

Figure 2.4: Comparison of RMSE for different models

model requires collection of data at various locations, and then a thorough analysis is needed to be performed for the complete global data bank. If this generic model does not attain the focus of the research community we would end up having numerous empirical models which would all have limited utility.

2.3 Scattering

When a transmitted laser beam interacts with atmospheric particles, some part of it looses the directivity and energy. When an electromagnetic wave encounters with an atmospheric particle, some part of the wave energy is redirected and re-radiated into a solid angle centered at it. The re-radiation or scattering depends on the particle size, refractive index (especially real part) and isotropy of the atmospheric particles. With the help of these mentioned parameters the scattering behavior can be determined well [15]. There are three different types of scattering depending upon the size of atmospheric particles.

If the wavelength of the transmitted laser beam is comparable to the size of atmospheric particles ($\lambda/10 \leq r \leq 10\lambda$), the transmitted wave is scattered into the direction of main forward lobe and some small part into side lobe. This is called as Mie scattering. Generally, the wavelength of optical frequencies spectrum range is comparable to fog particles. Therefore, fog causes severe attenuation for FSO links. If the wavelength of transmitted laser beam is greater than the size of atmospheric particles (if the size of atmospheric particle is approximately 10 percent the size of the transmitted wavelength, ($r < \lambda/10$)), the wave is scattered symmetrically in backward and forward lobe. This is called as Rayleigh scattering. If the transmitted beam is smaller than the size of atmospheric particle ($r > 10\lambda$) than the wave is scattered in a complex and irregular way. This is called geometrical scattering. Fig. 2.5 shows the illustration of all three types of scattering.

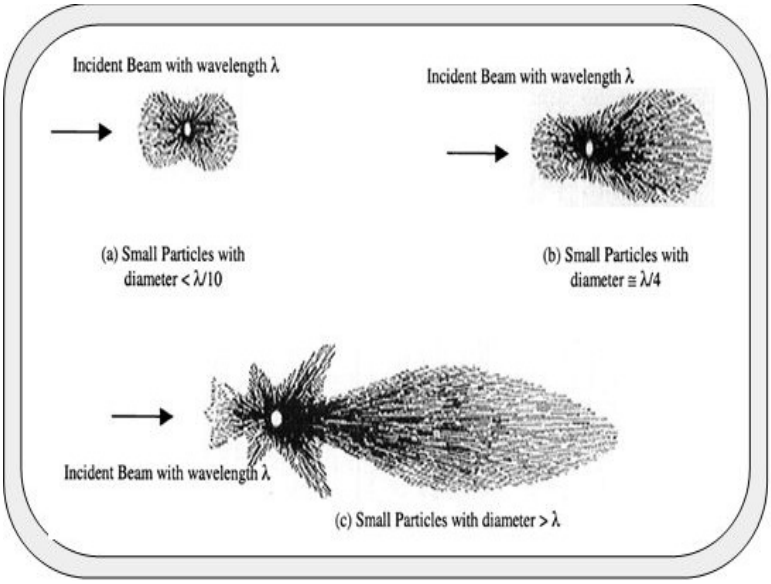

Figure 2.5: Illustration of different kinds of scattering patterns [108]

Table 2.2 presents the summary of different kinds of scattering for typical atmospheric radii at λ = 850 nm.

Table 2.2: Different kinds of scattering for typical atmospheric radii at λ = 850 nm

Type of atmospheric process	Radius(μm)	Type of Scattering
Air Molecules	0.0001	Rayleigh
Haze particle	0.01 - 1	Rayleigh - Mie
Fog droplet	1 - 20	Mie - Geometrical
Rain	100 - 10000	Geometrical
Snow	1000 - 5000	Geometrical
Hail	5000 - 50000	Geometrical

2.3.1 Simulation of scattering effects on FSO links

FSO links use atmosphere as a propagation medium. Nevertheless, a common problem that occurs from time to time is the emergence of moderate clouds and fog between the receiver and the transmitter. Absorption and scattering of radiation through fog, clouds, dust, snow and smoke cause attenuation of a laser beam propagating through atmosphere. Fog and clouds are typical dominating factors in atmospheric attenuation. However, other factors like rain and snow are generally less significant. Another major atmospheric process that affects the performance of FSO system is turbulence-induced atmospheric scintillation, which causes severe fluctuations in received signal power.

In FSO channel, scintillation and fog causes multiple photon propagation paths between the transmitter and the receiver which results into signal attenuation and multiple scattering. The underlying process will be multi-path propagation or dispersion. Generally, each of the multi-path components has different relative propagation delays and attenuations, which can result into signal fading. Some models exist in literature to study and to mitigate the effects of multiple scattering effects on Laser beam propagating through fog [109, 110, 111]. The simulation facility at Department of Electronics and Information (DEI), Politecnico di Milano has been used to simulate and see the scattering effects on Laser beam propagating through the radiation fog. Two simulators at DEI (Method I and Method II will be used hereafter for two models) have been used to study the scattering effects.

2.3.2 Method I for scattering analysis

Method I has been used to estimate the correction factor caused by dense fog conditions. Method I also estimates the received power and amplification factor required to reduce the effects of multiple scattering due to fog conditions.

2.3.2.1 Description of Method I

This is an analytical method based on radiative transfer equations [109, 110] which calculates the received power, correction factor and amplification factor required to mitigate the effects of multiple scattering . In this method different types of fogs (radiation and advection fog) can be simulated by changing different drop size distribution (DSD) parameters. The particle scattering function (i.e. the scattered complex amplitude as a function of the scattering angle) is approximated by a Gaussian function.

Based on a term-by-term integration of the small angle solution of the radiative transfer equations (RTEs) a correction factor has been simulated due to multiple scattering effects of all orders [109, 110]. In this simulation, correction factor has been computed and the results of simulation are compared with the measured data.

Received power by an open detector has been considered for any given multiple scattering medium, (i.e. there is no obstruction to its field of view) placed on the axis of a collimated or divergent monochromatic beam as a function of its distance from the source.

Optical depth (τ) is the product of path length (z) and the extinction coefficient (σ) of the population of particles (in fog case).

$$\tau = \sigma.z \tag{2.6}$$

A given value of the optical depth can be obtained by several combinations of path length and extinction coefficient. Moreover, for a given shape of the particle size distribution, optical depth depends upon the path length and particle concentration. In the simulation following parameters have been considered (Table 2.3).

Table 2.3: Input parameters for simulation

Serial No	Description	Parameter
1	DSD	Arbitrary(δ)
2	Scattering Function	Gaussian Approximation of the mainlobe (α)
3	Detector Type	Open detector (θ_v)
4	Beam type	Collimated or divergent (Gaussian beam)
5	Wavelength	1.06 μm
6	Receiver Diameter	1 cm
7	Spot size(ω_0)	$\gamma = 0.35 cm^{-1}$

The parameter spot size (line 7 of Table 2.3) and γ are related by following equation

$$\gamma = \frac{\sqrt{2}}{\omega_0} \tag{2.7}$$

2.3.2.2 Simulation results of Method I

Here, radiation fog has been considered in simulation. Simulation parameters for radiation fog are provided in [109, 110] and are given below.

- Receiver Diameter = 1cm

- Phase function divergence (α) = 28.20 (rad^{-1})
- Transmitted beam: Gaussian beam wave
- Fog DSD is modeled by a modified gamma distribution proposed in [109, 110] to characterize the radiation fog
- Extinction coefficient = 21.775 km^{-1}

The extinction coefficient due to multiple scattering is given as

$$\sigma_{ms} = \sigma_{ss}(1+C) \tag{2.8}$$

Where, σ_{ms} is an extinction coefficient due to multiple scattering, σ_{ss} is extinction coefficient due to single scattering and C is correction factor. The correction factor C has been introduced due to multiple scattering effects. The variation of correction factor and optical depth is provided in Fig. 2.6. In Fig. 2.6 we can see the correction factor is around 3% for optical depths up to 5; increasing to more than 5% when the optical depth is equal to 10 for radiation fog.

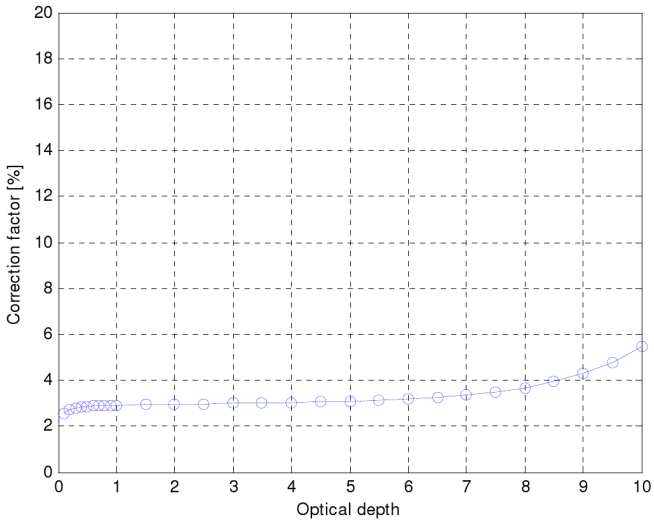

Figure 2.6: Plot showing Correction factor and Optical depth

The values of optical depth in Fig. 2.6 can be turned into corresponding path lengths through Equation (2.6); assuming the path is uniformly filled with the above radiation fog. The results are shown in Fig. 2.7.
It is obvious from Fig. 2.7 that for radiation fog (parameters are provided in [109, 110]), the path length is varying upto 460 m for an optical depth of 10. Optical attenuations have been calculated from optical depth for same DSD but with different particle concentrations.

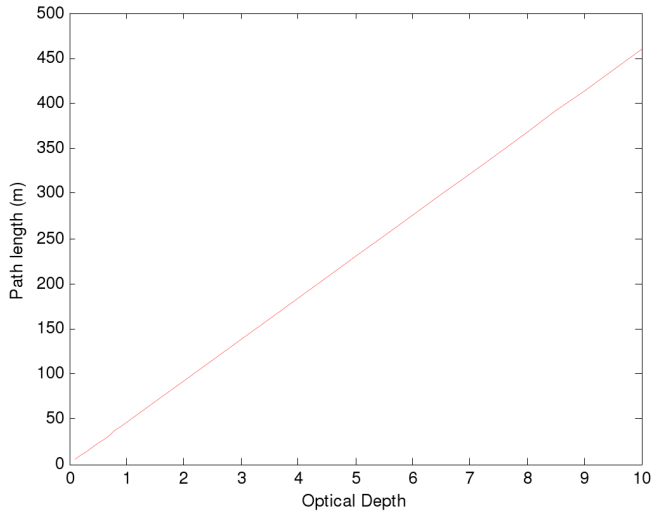

Figure 2.7: Plot showing path length and Optical depth

The effects can be seen in Table 2.4. If the optical depth is supposed to be 4 and correction factor is 3.04% (these values has been taken from simulations) having path length of 50, 100, 300, 500, and 1000 m then corresponding computed optical attenuations are provided in the Table 2.4.

Table 2.4: Computed optical attenuation from optical depth and path length

$\tau = 4$, Correction factor (3.04%)	Attenuation (dB/km)
Z =50, $\sigma = 80Km^{-1}$	347.2
Z =100, $\sigma = 40Km^{-1}$	173.6
Z =300, $\sigma = 13Km^{-1}$	56.42
Z =500, $\sigma = 8Km^{-1}$	34.72
Z =1000, $\sigma = 4Km^{-1}$	17.36

Simulated correction factor has been compared with the measured data. Table 2.5 shows the simulated correction factor, optical depth and measured values at Prague. If specific attenuation is 71.5 dB/km, measured at a path length of 100 m then it requires correction factor of 3% due to multiple scattering. These results show that the multiple scattering has minimal effect for the measured data of Prague.

In Table 2.5 the measured values are average values for four different fog events recorded in Prague. It is obvious that we got different particle concentrations with the assumption of radiation fog with same DSD.

Table 2.5: Verification of the simulated results

Measured attenuation (dB/km)	$\sigma(km^{-1})$	path length(Z(m))	τ	Correction factor
71.5	16.47	100	1.647	3%
75.83	17.47	100	1.747	3%
61.32	14.12	100	1.412	3%
95.48	22	100	2.2	3%

2.3.3 Method II for scattering analysis

Method II permits the characterization of the impulse response of the medium, by estimating the spread of time of arrival of photons at the receiver section. The further details of Method II are provided in subsequent sections.

2.3.3.1 Description of Method II

This simulator characterizes impulse response of the medium, by estimating the spread of the time of arrival for the photons at receiver section. The simulator tracks every single photon from transmitter to receiver to see the effects of fog. Following parameters are considered in this method.

- Number of photons
- Extinction coefficient
- Path length (1km)
- Wavelength(785 nm)
- Particle scattering function for every drop size distribution (DSD)
- Beam type
- Drop size distribution DSD

2.3.3.2 Simulation results of Method II

Scattering effects due to radiation fog have been simulated. The general form of the simulator is shown in Fig. 2.8

A line in Fig. 2.8 shows the path length. Transmitter is located at one end of line and receiver is located at the other end of line. It shows that 33.65 % of the total transmitted photons were received directly while, the rest 66.35 % of the total transmitted photons were scattered. A Gaussian beam was transmitted in this simulator and is shown in Fig. 2.9.

Fig. 2.9 shows that the transmitted beam having a diameter of $4cm$ was launched from transmitter section. Delay spread of arrival of photons was calculated. The probability

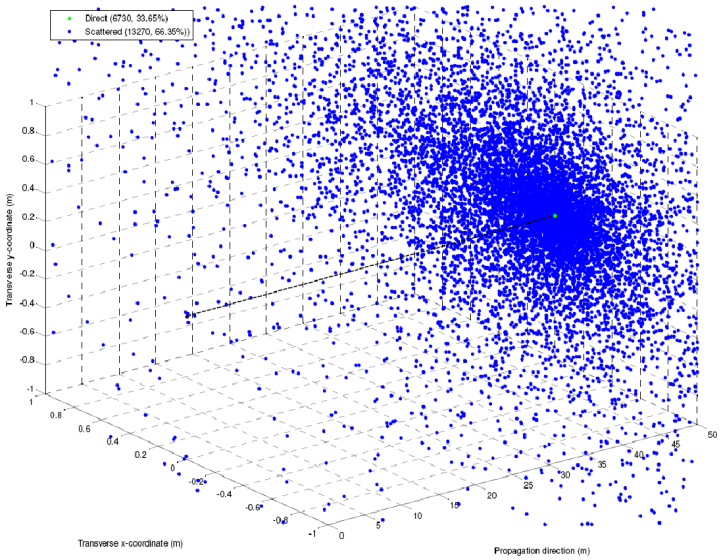

Figure 2.8: General form of the simulator

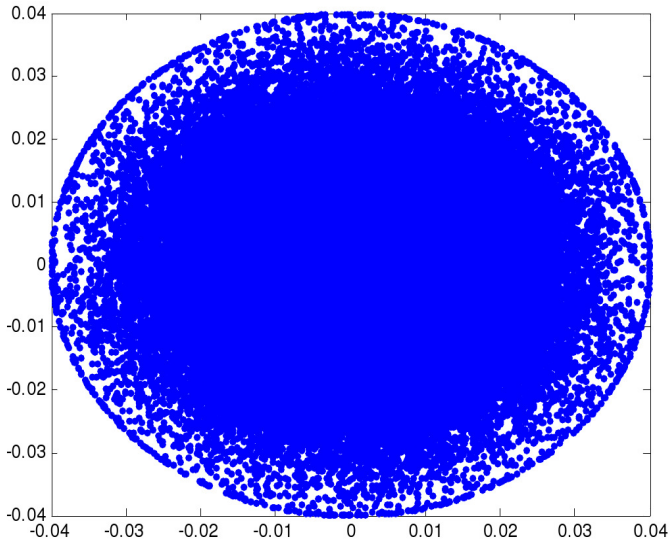

Figure 2.9: The 20,000 photons launched from the transmitter section

density function of delay spread of transmitted photon is provided in Fig. 2.10, indicating a delay spread of few Pico seconds over a path length of 1 km.

Fig. 2.11 and Fig. 2.12 show multiple scattering functions as a function of scattering angle. It is obvious from Fig. 2.11, that the multiple scattering is not so significant for

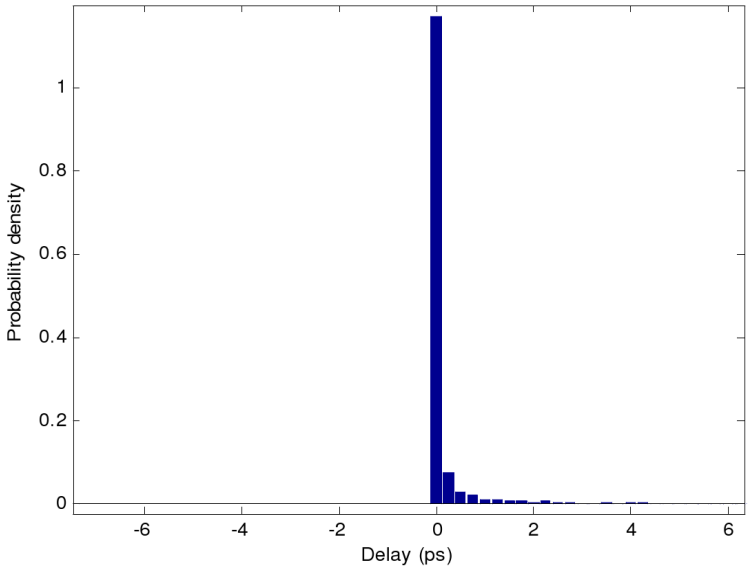

Figure 2.10: PDF of delay spread of Photon

a particle with diameter 1 μm. As the photons are scattered in every direction, they will lose the path because the scattering angle is very large. It is clear from Fig. 2.12 that multiple scattering is significant for particles having diameter of 50 μm. As the scattered light is almost parallel to the transmitted beam therefore, the scattering angle is very small. However, it is important to mention that particle concentration is an important factor which affects the multiple scattering.

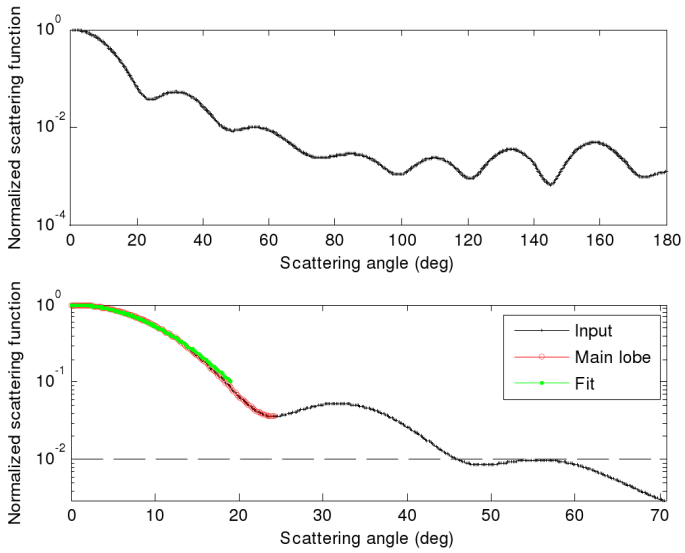

Figure 2.11: Multiple scattering for fog particle with a diameter of 1 micrometer

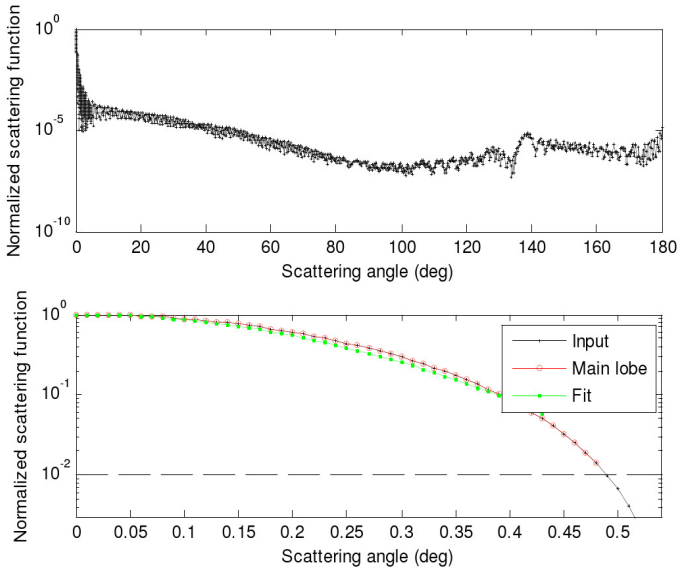

Figure 2.12: Multiple scattering for fog particle with a diameter of 50 micrometer

3 Analysis of Optical attenuations

Besides the popularity of terrestrial FSO links during recent years the attenuations caused by fog remained the main focus of the research community [112, 113, 114, 26, 115]. In this chapter the analysis of optical attenuation are discussed with the main focus of linearity or homogeneity of optical attenuation along with the path length. Various measurement campaigns have been carried out at different locations by several institutes to study the weather effects, mainly fog, on FSO links. Link distance between the FSO transceiver is different for most of the measurement campaigns depending upon the installation, weather conditions and the purpose of study. Specific attenuation with the unit of dB/km is widely used for the detailed analysis of the optical attenuation with the assumption that the fog is uniformly distributed along the path. The main focus of this chapter is to provide a detailed analysis and study of the linearity or homogeneity in optical attenuations measured across collocated links. However, this chapter also provides the analysis of optical attenuation measured at Graz (Austria), Prague (Czech Republic) and Milan (Italy).

3.1 Measurement at Graz

The research group Optikom at the Institute of Microwave and Photonic Engineering (formerly Institute of Broadband Communication) of Graz University of Technology conducted measurement campaign stared from September 2005 and remained active till April 2006. Graz is located at latitude of 47° 05', North and longitude of 15° 27' East having continental weather. The major focus of the measurement campaigns was to study the influence of fog on FSO links. The 1st measurement campaign by the Institute of Microwave and Photonic Engineering of Graz University of Technology, was carried out at Nice, France in June 2004. Nice has maritime environment. The 2nd measurement campaign was conducted at Graz to study the influence of continental environment on FSO links. In this chapter the analysis of continental environment is presented.

3.1.1 Measurement setup at Graz

The research group OptiKom at TU Graz is very active on FSO propagation studies and experiments in different weather conditions. We conducted experiments on optical signal transmissions in continental fog environments during winter months (Sept. 2005 - Feb. 2006) at Graz, Austria and in dense maritime fog conditions at Nice, France during June 2004. In this chapter we have provided the statistical data analysis of continental fog attenuations measured at Graz on 80 m FSO link. The specifications of the FSO transceiver used for attenuation measurements at Graz is tabulated in Table 3.1. The fog attenuation

Table 3.1: FSO system specifications

Parameters	850 nm FSO Link	950 nm FSO Link
Tx Wavelength	850 nm	950 nm
Tx Technology	LED	LED
Rx Technology	Si-APD	Si-APD
Tx avg. optical power	8 mW	1mW per diode
Avg. radiated power	3.5 mW	4 mW
Tx aperture diameter	1 X 25 mm convex lens	4 X 25 mm convex lens
Rx aperture diameter	98mm	98 mm
Tx divergence angle	2.4 degree	0.8 degree
Rx acceptance angle	1.7 degree	1.7 degree
Rx sensitivity	Min -35 dBm	Min -35 dBm
Specific link margin	224 dB/Km	224 dB/Km
Link distance	79.8m	79.8m

data obtained from the measurement campaign was post processed in MatLab and LabView software.

The link distance was selected carefully as a compromise between accuracy and allowable attenuation range, depending on the expected maximum fog attenuation. The system provided a dynamic range of 25 dB at each wavelength. The link distance of 79.8 m allowed us to measure specific attenuation up to 310 dB/km. The measured data was processed and evaluated in MATLAB. Specific attenuation in dB/km is generally used for analysis of the data as a standard.

3.1.2 Analysis of fog attenuations measured at Graz

Various measurement campaigns were conducted to study the fog effects on FSO links. The optical attenuations have been measured reaching up to 120 dB/km averaged on a minute scale over a link distance of 79.8 m. The maximum specific attenuation that was recorded, reached up to 236 dB/km. One of the most successful measurement campaign was started on September 27, 2005 and continued till March 1, 2006 for 156 days. During the whole measurement campaign 18 major fog events were observed, the details of which are tabulated in Table 3.2.

It is important to mention that the minimum duration of these 18 fog events is three and a half hour. Table 3.2 shows the attenuation statistics of 18 major continental fog events recorded at Graz. We observed that the measured attenuations were in high correlation

Table 3.2: Statistics of fog attenuation measurement campaign at Graz, Austria [116]

ID	Start date	End date	Start time	End time	Duration	50%	90%	Max.
1	29.9.2005	29.9.2005	02:00:00	07:29:59	5:30	2.39	37.63	83.9315
2	25.10.2005	25.10.2005	03:00:00	10:59:59	08:00	38.29	93.19	112.1198
3	26.10.2005	26.10.2005	01:30:00	03:59:59	03:30	7.0810	110.8667	118.0525
4	10.11.2005	11.11.2005	16:00:00	09:59:59	18:00	12.9737	29.3020	71.4139
5	11.11.2005	12.11.2005	14:00:00	11:00:00	23:00	10.5382	33.8819	63.3891
6	22.11.2005	22.11.2005	00:00:00	05:59:59	06:00	5.9392	100.7586	113.8157
7	25.11.2005	28.11.2005	19:00:00	09:59:59	63:00	8.0926	19.6037	66.8660
8	28.11.2005	29.11.2005	22:00:00	05:59:59	08:00	9.2515	113.8157	124.6511
9	30.11.2005	30.11.2005	06:00:00	11:59:59	06:00	7.3776	103.2164	116.2736
10	02.12.2005	02.12.2005	01:00:00	17:24:59	16:25	0.9405	4.5956	96.4585
11	13.12.2005	14.12.2005	21:00:00	11:59:59	15:00	9.7898	62.4800	97.3173
12	25.12.2005	28.12.2005	19:32:00	13:30:59	65:59	6.4271	13.5516	42.8042
13	09.01.2006	09.01.2006	05:00:00	09:59:59	05:00	72.1849	109.5157	116.2022
14	09.01.2006	10.01.2006	22:00:00	04:59:59	07:00	1.0790	100.7586	121.5819
15	30.01.2006	31.01.2006	21:00:00	09:59:59	13:00	20.8970	81.7411	165.0155
16	31.01.2006	01.02.2006	15:00:00	08:59:59	18:00	46.6857	154.7429	225.7779
17	01.02.2006	02.02.2006	20:00:00	10:19:59	14:20	87.3802	168.3753	217.0663
18	02.02.2006	03.02.2006	21:00:00	07:59:59	11:00	28.9490	159.9085	236.0736

with the fog intensity and were highly dependent on the density and distribution of the fog particles.

The optical signal attenuations (specific attenuation (dB/km)) were computed from the received signal power using an appropriate model (implemented in LabView), based on the hardware specification of the self-developed FSO system. The analysis of these 18 fog events indicated that last four fog events belong to dense fog type having optical attenuations higher than 143 dB/km. The remaining fog events were of thick fog types. The 9th column (last column) in Table 3.2 shows the maximum value of specific attenuation reached for respective fog event.

In the area of Graz, the continental fog events tend to occur in the winter season, usually from September to the end of February. During our measurement campaign of year 2005-06, we measured 18 low visibility fog events; all having durations more than three and half hour. We analyzed measured attenuations of these 18 major fog events and found out that 04 out of 18 fog events were dense continental fog events. The specific attenuations easily exceeded 143 dB/km and visibility range was less than 70 m. The remaining 14 fog events were some kind of thick continental fog events with visibility range lying between 70 m and 250 m. The important feature of the dense continental fog events was that they all occurred in January and February 2006, while the thick continental fog events occurred in between September 2005 to December 2005. The maximum attenuation measured was about 236 dB/km averaged on a second scale corresponding to the most dense fog event of 2nd February, 2006 A time series of all 18 continental fog events having measured

attenuations averaged on a minute scale is shown in Fig. 3.1 and a representative dense fog event is shown in Fig. 3.2 respectively.

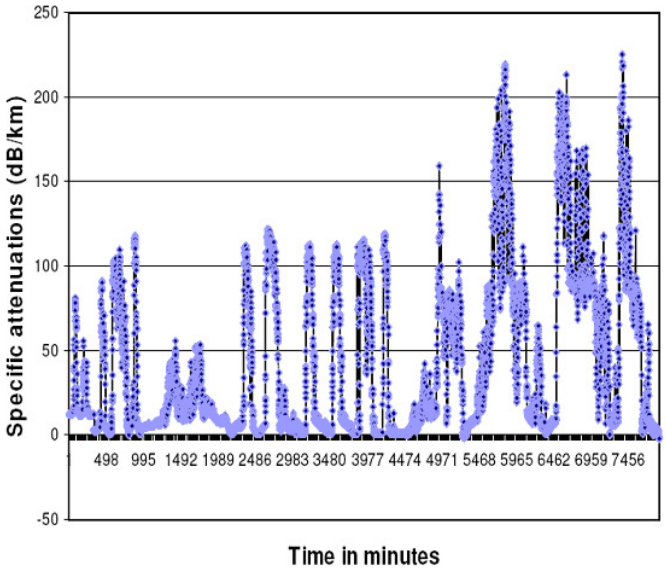

Figure 3.1: Time series of 23 fog events attenuations averaged on a minute scale

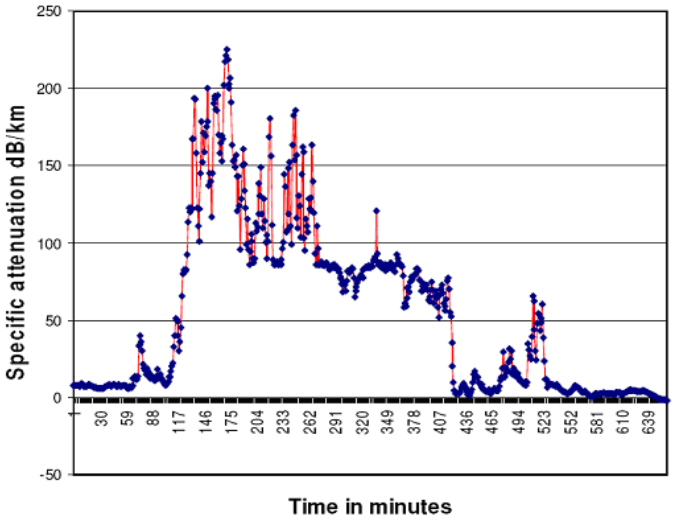

Figure 3.2: Time series analysis of densest continental fog event

3.2 Measurement at Prague

Department of Frequency Engineering, Czech Metrology Institute (CMI) Prague, Czech Republic, conducted measurement campaign to study the atmospheric effects on FSO links. The FSO links were operational at wavelengths of 1550 nm and 830 nm at two different path links. Here, the analysis of five months measured data is presented.

3.2.1 Measurement setup at Prague

The measurement campaign was carried out at the Department of Frequency Engineering, Czech Metrology Institute (CMI) Prague, Czech Republic from 08.01.2009 till 31.05.2009. Prague is located at latitude 50° 05' 12" N longitude 14° 24′ 59″ E and at altitude of 191 m. Prague has continental weather having the air mean temperature of 10.4 °C since 1971-2000 [117]. The technical specifications of the experimental installation in Prague are given in Table 3.3. The FSO systems were installed 26 meters above the ground level.

Table 3.3: Technical details of the FSO links

Description	**1550nm Link**	**830nm Link**
Wavelength	1550 nm	830 nm
Link distance	100 m	100 m
Transmitted Optical power	3.5 dBm	13 dBm
Lens Diameter	18 cm	15 cm
Fade Margin	13 dB	18 dB
Modulation Scheme	OOK Intensity modulation	OOK Intensity modulation

The link margin of the two FSO systems allowed the measurement of specific attenuation up to 180 dB/km for 830 nm wavelength systems and 130 dB/km for 1550 nm systems. Optical calibration was performed before deploying the FSO devices. A received power is obtained from the calibrated Received Signal Strength Indicator (RSSI) signal of the FSO link.

Meteorological conditions were identified by means of a color video camera and an automatic weather observation system located near the FSO receivers. The system used Vaisala sensors for the measurement of temperature, humidity, air pressure, velocity and direction of the wind.

The VAISALA PWD 11 equipment measured the atmospheric visibility (5% definition) values in the range from 50 m up to 2000 m using forward scattered light in the angle of 45°. The PVM-100 device was used to measure liquid water content LWC (g/m^3) and integrated particle surface area PSA (cm^2/m^3) of fog.

The meteorological data was synchronized in time with the hydrometer attenuation measurement. The received FSO signal levels and the meteorological data were recorded synchronously on a PC's hard disk. In this chapter five months real time measurement data of fog attenuations (observed using 1550 nm optical wavelength) are analyzed. The reason for selecting attenuation data for analysis against this wavelength is its increasing importance for future FSO system. Few sample data points taken against a representative fog event of 9 January 2009 are tabulated in Table 3.4.

Table 3.4 presents the day and the time alongside the attenuation values in dB for 830 nm and 1550 nm systems over 100 m link. The recorded values of LWC (g/m^3), PSA (cm^2/m^3) and the visibility in meters are also shown.

Table 3.4: Some sample data points recorded on January 9, 2011

day.mon.year	hour:min	Att_830nm[dB]	Att_1550nm[dB]	LWC[g/m3]	PSA[cm2/m3]	Vis[m]
09.01.2009	01:26	9.57	10.19	0.042	200	319
09.01.2009	01:27	9.7	9.95	0.019	160	359
09.01.2009	01:28	9.41	10.44	0.08	310	339
09.01.2009	01:29	8.39	9.36	0.056	270	351
09.01.2009	01:30	9.85	9.72	0.054	233.8	314
09.01.2009	01:31	10.86	10.32	0.058	271.2	285
09.01.2009	01:32	11.95	10.75	0.069	285	145
09.01.2009	01:33	10.98	10.55	0.097	390	212
09.01.2009	01:34	10.45	10.43	0.067	275	155
09.01.2009	01:35	10.64	10.63	0.075	305	151
09.01.2009	01:36	9.83	10.2	0.036	177.5	224
09.01.2009	01:37	8.47	9.29	0.013	133.8	240
09.01.2009	01:38	7.54	8.48	0.006	128.8	365
09.01.2009	01:39	8.33	9.19	0.002	80	280
09.01.2009	01:40	8	8.32	0.024	156.2	270
09.01.2009	01:41	8.27	8.6	0.058	258.8	324
09.01.2009	01:42	6.52	7.7	0.002	140	262
09.01.2009	01:43	5.13	6.06	0.002	37.5	338
09.01.2009	01:44	6.59	7.05	0.008	116.2	568
09.01.2009	01:45	6.53	7.13	0.031	168.8	607
09.01.2009	01:46	5.42	6.12	0.018	152.5	625
09.01.2009	01:47	7.36	7.53	0.003	108.8	522
09.01.2009	01:48	9.19	8.78	0.025	162.5	451
09.01.2009	01:49	9.17	9.15	0.074	363.8	384
09.01.2009	01:50	9.05	9.34	0.045	238.8	335

3.2.2 Analysis of fog attenuations measured at Prague

The measurement campaign was performed at the Department of Frequency Engineering, Czech Metrology Institute (CMI) Prague, Czech Republic from 08.01.2009 till 31.05.2009. Two FSO systems were installed at a path link of 100 m and 853 m using wavelength of 1550 nm. A time series analysis of the representative fog event measured on 20-21 January 2009 is shown in Fig. 3.3.

The vertical axis of the Fig. 3.3 shows the attenuation in dB/km and horizontal axis shows the minutes of the day. This fog event was recorded on midnight of 20-21 January 2009. It shows the interesting insight of fog formation, fog dissipation and mature fog stages. The total duration of this fog event was 6 hours. The fluctuations of few initial minutes starts from 23:00 and persists till 23:30, it shows the fog formation stage when the visibility starts decreasing and optical attenuations start increasing. During the mature fog stage the attenuations are a bit stable. Fog took one hour to dissipate. Fog dissipation starts around 04:06 till end. In fog event shown in Fig. 3.3 the maximum recorded attenuation was 114.32 dB/km, whereas, minimum recorded attenuation was 50.465 dB/km. 50 % of the attenuations remains below 103.57 dB/km. During the measurement campaign of five months at Prague a total of six fog events were recorded. The 1st fog event was observed on

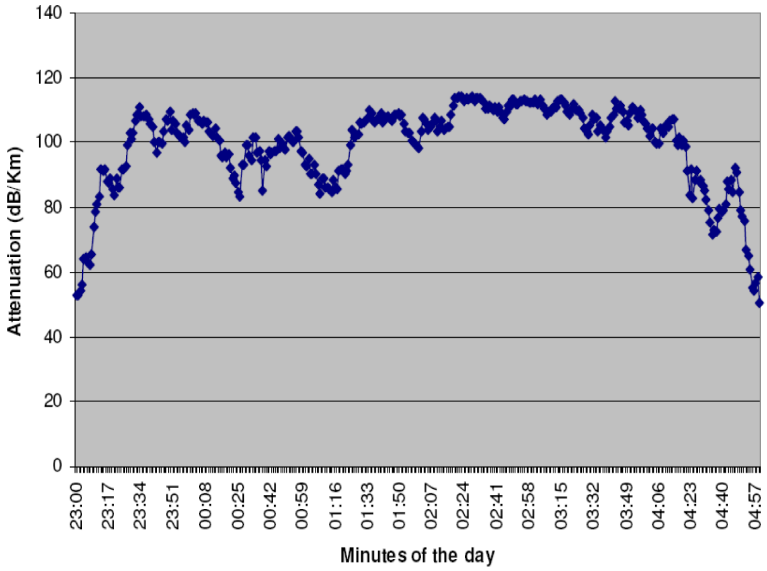

Figure 3.3: Time series of analysis of a representative fog event

08.01.2009 at 23:15 till 09.01.2009 at 06:51, 2nd fog event was measured on 16.01.2009 at 17:00 till 17.01.2009 at 03:05, the third fog event was recorded on 20.01.2009 at 23:00 till 21.01.2009 at 04:59, 4th fog event occurred on 07.02.2009 at 01:02 till 07.02.2009 at 11:05, 5th fog event was observed on 19.04.2009 at 04:09 till 19.04.2009 at 07:31 and the last 6th fog event was recorded on 31.05.2009 from 00:57 till 31.05.2009 at 04:21. The last fog event contains interesting information that this fog event occurred at the end of May. It is also important to mention that during a five months measurement campaign, no dense fog event was observed in Prague.

3.3 Measurement at Milan

The Department of Electronics and Information (DEI), Politecnico di Milano, conducted measurement campaign to study the weather influence on FSO links. Milan is located at Latitude 45° 25′ N and Longitude of 09°12′E with continental environment.

3.3.1 Measurement setup at Milan

A commercial FSO system, Terescope 3000, was installed at the Politecnico di Milano (Campus Leonardo) at a path length of 319 m. The FSO system consisted of two identical transceivers working at wavelength of 785 nm and were capable of transmitting the data of 155 Mbps. The transmitter contained three identical and independent semiconductor laser diodes with output power of 10 mW and beam divergence of 2.5 mrad. Optical transmissiometer (Model 6100) was used to measure visibility. A weather station was installed to measure different weather quantities like temperature, relative humidity, solar radiation, rain rate etc. The optical attenuations were sampled at every minute. The measurement campaign started in 2003 and remained active till 2006.

3.3.2 Analysis of fog attenuation measured at Milan

The analysis of a sample fog event recorded from 00:00 of 8-Jan-2005 to 23:59 of 15-Jan-2005 has been presented. The optical attenuation data was sampled at one sample per minute. The time series analysis of the attenuation data is presented in Fig. 3.4.

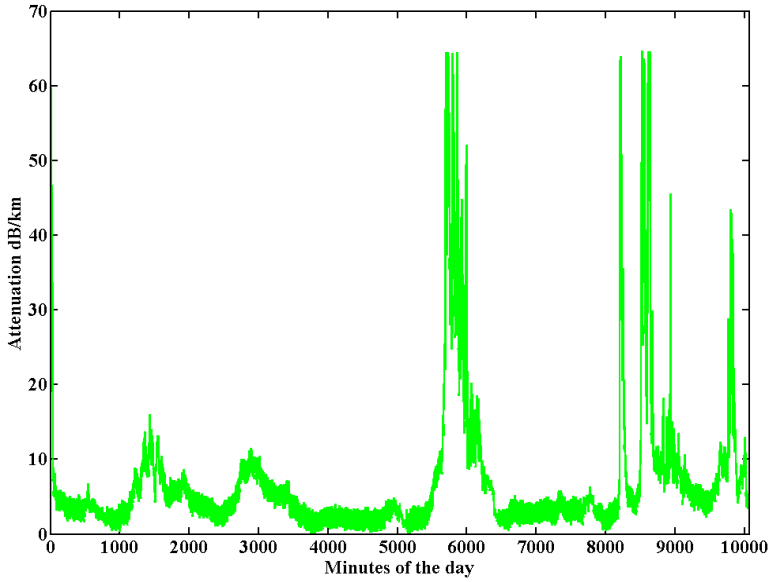

Figure 3.4: Time series of densest continental fog event attenuations measurement

The summary statistics of attenuation is presented in Table 3.5. It is obvious from Table 3.5 that 95% of the attenuations remained below 23.63 dB/km. It shows that in Milan for most of the time only moderate fog occurred. Only 5% of the optical attenuations are going as high as 64.71 dB/km.

Table 3.5: Summary of the measured data at Milan

Description	**Value**
Sample Size	10068
Range	64.693
Mean	6.6138
Variance	80.151
Standard Deviation	8.9527
Minimum	0.02433
Maximum	64.718
25% (Q1)	2.3189
50% (Median)	4.0406
75%(Q3)	7.122
95%	23.631

3.4 Linearity in optical attenuations

The department of Frequency Engineering at Czech Metrology Institute is conducting measurement campaign at path links of 100 m and 853 m using the wavelength of 1550 nm. The fog attenuation data of five months was collected to investigate the linearity or homogeneity of optical attenuations over the two mentioned path lengths. The recorded data of optical attenuations measured using the wavelength of 1550 nm was selected for the analysis, keeping in view, the increasing importance of the 1550 nm window for future FSO system. Fig. 3.5(a) provides the graphical illustration of measured optical attenuations in dB/100 m and dB/853 m and real time measured visibility in meters for the recorded data at path lengths of 100 m and 853 m. Fig. 3.5(b) provides the graphical analysis of specific attenuation (dB/km) and visibility in meters for the recorded data of both links.

The accuracy of the measurements of Fig. 3.5(a) and 3.5(b) is validated by the fact that as visibility decreases, the attenuation in Fig. 3.5(a) and specific attenuation in Fig. 3.5(b) increases and vice versa. The fade margin of 853 m path link is about 15 dB which allowed the measurement of maximum specific attenuation of 17.58 dB/km. When a fog event occurred the 853 m path link is saturated and the effects can be seen in Fig. 3.5(a) and 3.5(b) respectively, where the link is saturated under fog conditions. The fade margin of 100 m path link was 13 dB which allowed the measurement of maximum specific attenuation of 130 dB/km and Fig. 3.5(a) and 3.5(b) shows that the link remains under saturation. It is obvious from Fig. 3.5(a) and 3.5(b) that there occurred certain fog events during this measurement campaign showing high levels of optical attenuations (dB/km) having corresponding visibility well below 1000 m. Therefore, we carefully selected sample fog events recorded on 8th - 9th January, 9th January, 16th January and 20th - 21st January 2009 for further analysis. Fig. 3.6 provides the graphical illustration of optical attenuations measured in dB/100 m and dB/853 m and specific attenuations for selected fog events are shown in Fig. 3.7.

Fig. 3.6(a) corresponds to the fog event observed on 8th - 9th January 2009, Fig. 3.6(b) shows the fog event of 9th January 2009, Fig. 3.6(c) provides the fog event of 16th January 2009 and the graphical analysis of fog event measured on 20th - 21st January 2009 is given in Fig. 3.6(d). Horizontal axis of Fig. 3.6 represents minutes of the day while the vertical axis represents the attenuation in dB/100 m (for 100 m path link) and dB/853 m (for 853 m path links), respectively. When the visibility decreases well below 1000 m the attenuation level increases and the 853 m path link comes to saturation level (as shown in Fig. 3.6) while the 100 m path link remains under saturation level due to higher value of fade margin.

If we assume that fog is uniformly distributed along the FSO path link, then optical attenuation measured at two different path links under the similar conditions shall be linearly correlated. Regression analysis has been done to observe the linear relationship between the optical attenuation measured at two different path links. A fog event recorded on 20th - 21st January 2009 has been selected carefully for regression analysis. The path link was

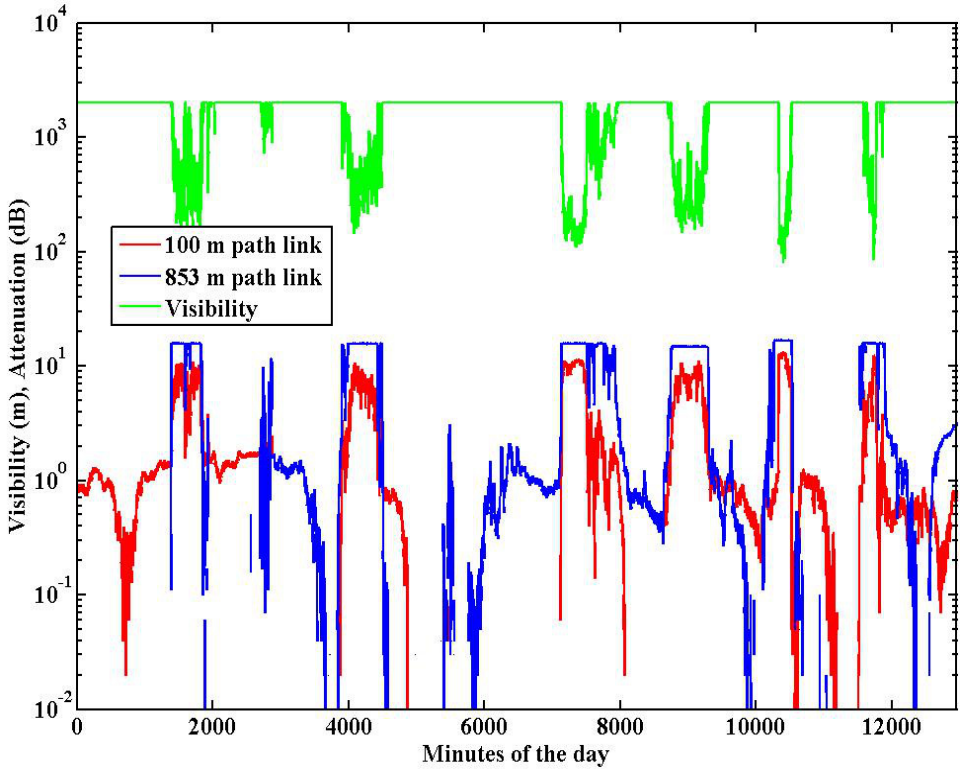

(a) Time series analysis of visibility and optical attenuations

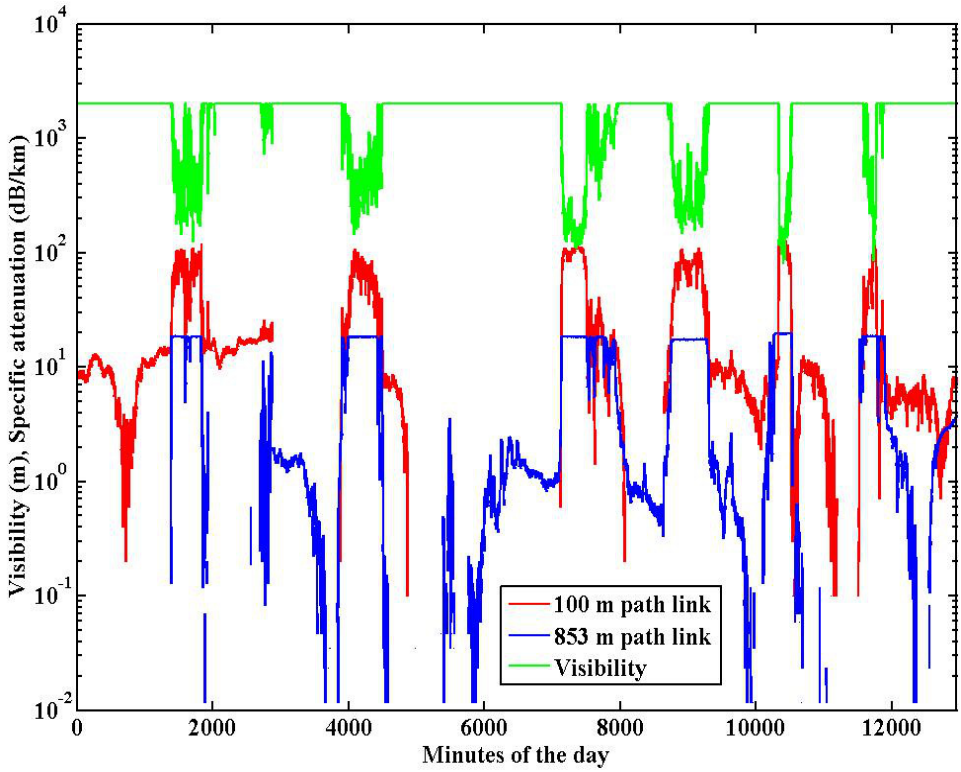

(b) Time series analysis of visibility and specific attenuations

Figure 3.5: Time series analysis of measured attenuation

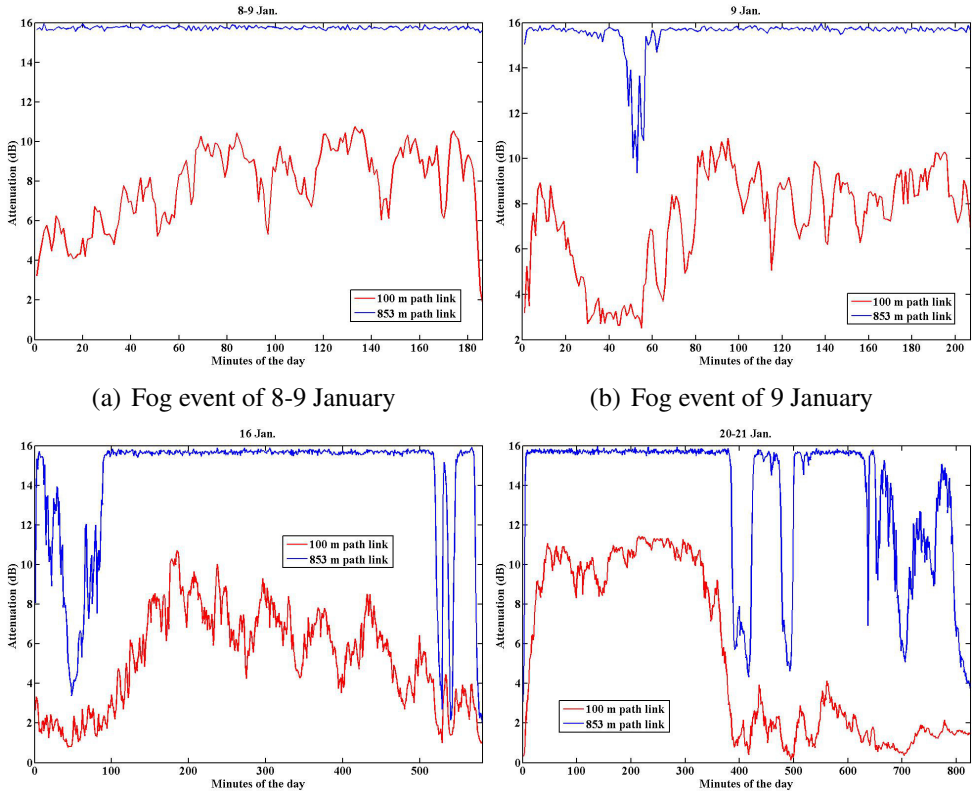

(a) Fog event of 8-9 January

(b) Fog event of 9 January

(c) Fog event of 16 January

(d) Fog event of 20-21 January

Figure 3.6: Analysis of optical attenuation for selected fog events

853 m and 100 m with an operational wavelength of 1550 nm. The time series analysis of optical attenuations measured at this fog event is presented in Fig. 3.8 (for the two mentioned path lengths).

The horizontal axis in Fig. 3.8 represents the minutes of the day and vertical axis shows the specific attenuation in dB/km. The results of regression analysis over the recorded attenuation data of selected fog event are shown in Fig. 3.9.

By analyzing the plot as shown in Fig. 3.9, we observe partial linearity/homogeneity of the recorded optical attenuations which indicates that for the shorter path link, fog is linearly distributed while for longer path link it is not. This may be due to the fact that measured attenuation data is quite scattered as shown in Fig. 3.9. The following linear relationship has been found between the optical attenuation measured at two different path lengths.

$$Y = 0.3531X + 9.0013 \tag{3.1}$$

where, X in equation 3.1 represents the specific attenuation measured over 100 m path

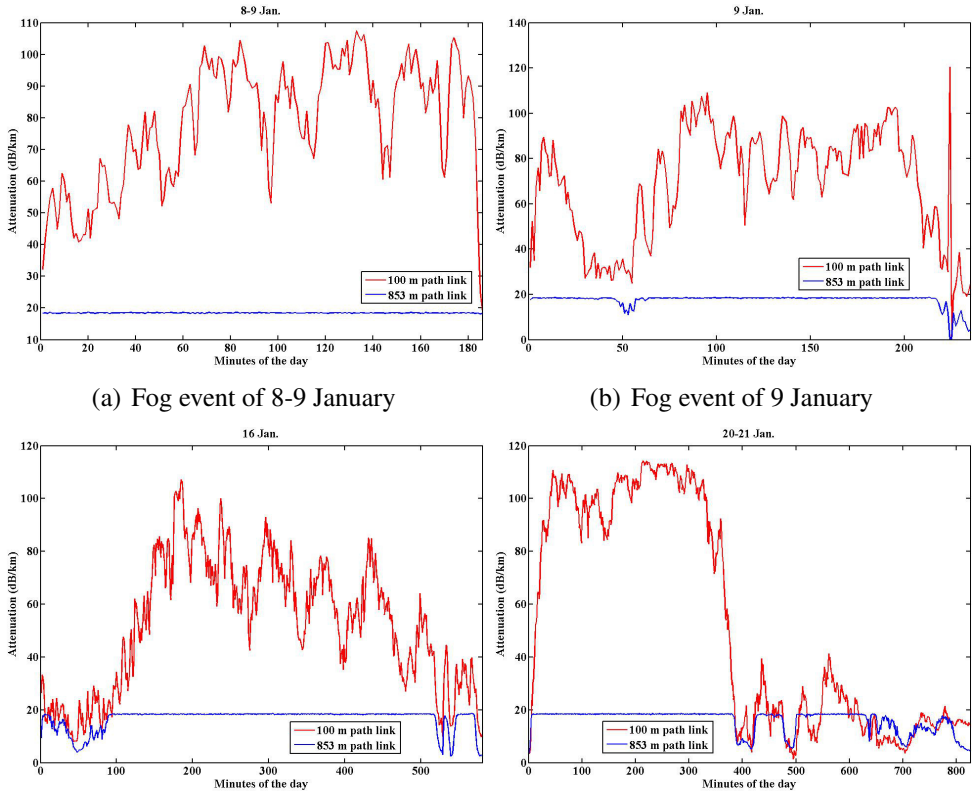

(a) Fog event of 8-9 January

(b) Fog event of 9 January

(c) Fog event of 16 January

(d) Fog event of 20-21 January

Figure 3.7: Analysis of specific attenuation for selected fog events

link and Y represents the specific attenuation measured over 853 m path link. The value of coefficient of determination (R- squared) or R^2 for linear model (0.26 or 26%) is quite less. Here, the value of *Rsquared* shows that we can not predict the optical attenuation of one link while having the measured optical attenuation of another link under the same circumstances or more precisely simple division of the measured optical attenuation of a link with the link distance would not accurately calculate the specific attenuation. Further, we found the following power relationship between the optical attenuation measured at two different path lengths, with R-squared value of 0.39 (or 39%).

$$Y = 4.99X^{0.39} \tag{3.2}$$

where, X in above Equation (3.2 represents the specific attenuation measured over 100 m link distance and Y represents the specific attenuation measured over 853 m link distance. The R-squared value in the above equation is higher than a linear relationship and mathematically quantifies the nonlinearity of the measured optical attenuation at the two different path lengths.

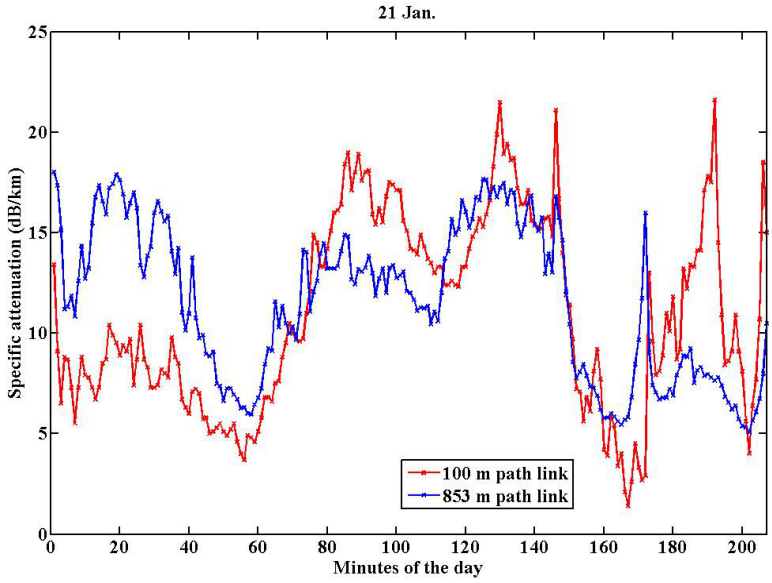

Figure 3.8: Time series analysis of a specific fog event selected for linearity analysis

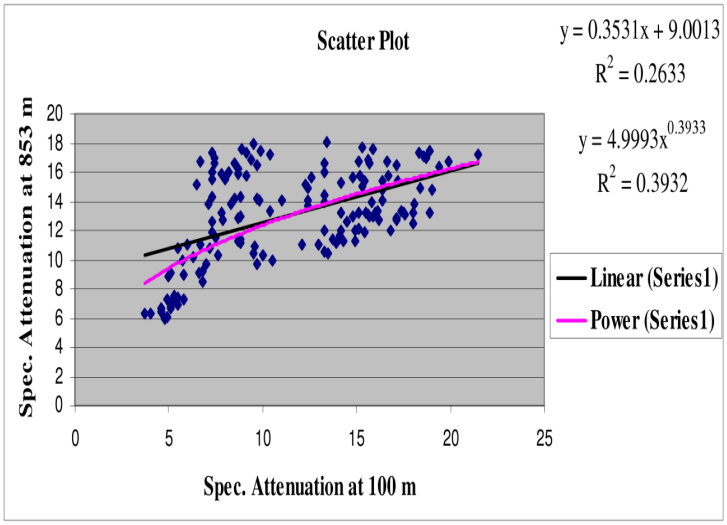

Figure 3.9: Regression analysis of a selected fog event

The linearity of the measured optical attenuations has been investigated by comparing the data of 100 m and 853 m path link. Although the correlation is not strong enough, we found that the optical attenuation in 100 m and 853 m is partially linearly correlated which is consistent with the general assumption of the homogeneity of the fog events in a short distance link. The possible reason for such less correlation in the current result is the measurement error in which the fade margin of 853 m path link is about 15 dB. Thus, some

optical attenuations of 853 m path link are saturated and can not be precisely compared with that of 100 m path link. Some studies need to be conducted in the future to strengthen our current findings and this study could be done by using some fog sensors in between the transceivers.

At the end we can summarize that the optical attenuation at a dense fog event measured for a short link (as example 100 m) can be calculated for 1 km (specific attenuation). But if we extrapolate from this specific attenuation (at 1 km) the attenuation for a 3 km link for example, it is possible and very probable that we will get a different result on optical attenuations (compared to a real measured 3 km FSO-link). Such a disagreement can occur because the fog is usually not of the same density over the whole distance of 3 km.

4 Probabilistic Model for FSO Links Under Continental Fog Conditions

The demands of high bandwidth communication applications are increasing day-by-day. FSO links are of prime importance in order to meet the needs of future high bandwidth terrestrial and ground-space communication applications [9] because FSO links operate at a license-free frequency band and offer virtually unlimited bandwidth at high data rates with a high security [118].

Widespread acceptability of FSO communication systems is hindered by its susceptibility to certain weather conditions (fog, snow, clouds etc.) and atmospheric variations (wind, temperature and humidity variations etc.). Received signal strength is highly influenced by some internal parameters or system parameters (system pointing and tracking induced fading) and many physical effects like absorption and scattering due to fog and scintillation. These atmospheric effects cause attenuation, temporal and spatial fluctuations of the received signal respectively. For terrestrial FSO links scintillation effects can be mitigated by increasing transmission power. There are also some other proposed techniques available to mitigate the scintillation effects like, wavelength diversity [119], multiple transmit beam [120] and multiple receiver [121]. The proposed techniques could be the only way to reduce the effect of scintillation but can not guarantee error-free channel [122]. The main impairing factor for terrestrial FSO links is fog [123]. There is a need for thorough investigations and studies to handle the effects of fog and additional techniques to reduce the effects of fog on FSO links.

Fog is characterized by several physical parameters such as liquid water content, particle size distribution, temperature and humidity. Since the size of fog particles is comparable to the transmission wavelength of optical and near infrared waves, Mie scattering is mainly responsible for causing high attenuation in different fog conditions [12].

The development of efficient design of FSO system is needed to consider fog channel model. There are alot of physical parameters which effect the performance of FSO system, therefore, it is very difficult to propose a model which can characterize all physical parameters. This can be done by studying the statistical description of received signal. The statistical description is derived from actual measurement data. Most commercially available FSO systems are based on intensity modulation with direct detection (IM/DD) using on−off keying (OOK) or pulse position modulation; therefore, the focus of this work is on channel modeling for such systems.

There are some probalistic models available for fog. The most significant work in this direction was presented by E. P. Shettle [98]. E. P. Shettle used modified Gamma distribution to model fog and cloud's drop size distribution (DSD). There are some other efforts to provide a statistical channel model for fog conditions. Sajid et. al. [75], presented the PDF estimates of two selected continental fog events. Sajid et. al. [75] concluded that the Lognormal and Gamma PDF have been found to be the two closest fit for continental fog at Graz. Wakeby distribution was proposed in [124] for dense continental fog conditions. B. Epple [122] presented the PDF models for turbulence as gamma-gamma or log-normal. B. Epple [122] considered three different scenarios for FSO i.e. maritime-mobile link, a land-mobile link, and a satellite downlink. He presented the data collected from four different projects, ATENAA, LCT-Marine, KIODO 40 cm, KIODO 5 cm having the total duration of 50 minutes. In this study long term measured data of optical attenuations measured at Graz and Prague has been presented to find best fit PDF.

Measured Optical attenuations under continental fog conditions were evaluated statistically by considering the measured data of Graz and Prague. Different PDFs were evaluated on the basis of their best fit (from quantile-quantile (Q-Q) plot and probability-probability or percent-percent (P-P) function plots) for actual measured attenuation data and have plotted their cumulative distribution functions (CDF).

Here, we utilized the measured data of Graz and Prague to find the best fit statistical distribution model. Due to high range of optical attenuation measured at Graz, the Graz data has been analyzed for different fog conditions. The Graz measured data of optical attenuations has been divided and analyzed into dense fog, thick fog, moderate fog, light fog and general fog types . In case of Prague, the measured data has been analyzed only for general fog conditions because the density of fog occurred in Prague is relatively less as compared to that of Graz.

In order to study the influence of different fog types and to suggest distribution model of each fog type for terrestrial FSO links, the whole set of attenuation data recorded over the period of six months is categorized into four distinct classes of fog types based on the international code of visibility as mentioned in Table 2.1. By this way, all the attenuation values higher than 143 dB/km were taken in the bin of dense fog, optical attenuations between 40-143 dB/km was taken as thick fog, 20-40 dB/km as moderate fog and 9.3-20 dB/km was included into the bin light fog. The main focus of this chapter is to find the best fit probabilistic model using the 6 months measured data of optical attenuation at Graz and 5 months recorded data at Prague.

4.1 Background

Probabilistic model for FSO links can be very useful not only for having prior estimate of attenuation PDF but also to understand the behavior of the channel. All the distribution functions were compared to find the best fitted distribution, which can describe the properties of the FSO channel under continental fog conditions in a better way through

Q-Q plot and P-P plot. The results of Q-Q plot and P-P plot suggested that Kumaraswamy distribution can be used to describe the characteristics of the FSO channel under general fog conditions. Wakeby distribution is the best fit model under dense continental fog conditions [124]. While Logistic distribution is the best fit model for thick fog and Johnson S_B distribution is the best fit for moderate and light fog measured data, respectively and the distribution functions for the above mentioned models are given in subsequent section.

4.1.1 Wakeby distribution

Wakeby distribution best fits the measured attenuation data for the dense fog conditions as this distribution can overcome certain deficiencies associated with traditional distributions. It can absorb more degrees of freedom than those distributions which are currently in use. The Wakeby distribution assumes that the observations of each sample are independently and identically distributed and there is no serial correlation and they are non-stationary. The density distribution of Wakeby is based on the five-parameters; neither the higher sampling moments nor even the sample variance are used to estimate those parameters. In traditional estimation procedures, the smallest observation can have a substantial effect on the right-hand side of the distribution. But the left-hand side does not necessarily add informations to an estimate of a quintile on the right-hand side. There is also some reason to believe that none of the standard distributions have the properties on their left-hand sides that may, in fact, reflect nature. The Wakeby distribution is defined as an inverse distribution function [125] and is given by Equation 4.1,

$$X = -a(1-F)^b + c(1-F)^d + e \tag{4.1}$$

Where, F is uniformly distributed (0, 1) and a, b, c and d are continuous and positive parameters, whereas, e is sometimes positive. The first and second order moment about mean are given in Equation 4.2 and 4.3 respectively,

$$\mu_1'(x) = e - [\frac{a}{b+1} - \frac{c}{1-d}] \tag{4.2}$$

$$\mu_2'(x) = \frac{c^2}{1-2d} + \frac{2ac}{1+b-d} + \frac{a^2}{1+2b} - [\frac{c}{1-d} - \frac{a}{1+d}]^2 \tag{4.3}$$

4.1.2 Logistic distribution

The logistic distribution is similar to normal distribution but this distribution is quicker to calculate than the normal distribution [126]. Another advantage over the normal distribution is that it has a closed form CDF but has longer tails and a higher kurtosis than the normal distribution. The distribution function of logistic function is given in Equation 4.4.

$$f(x) = \frac{\alpha}{\beta}[\frac{x-\gamma}{\beta}]^{\alpha-1}[1 + [\frac{x-\gamma}{\beta}]^{\alpha}]^{-2} \tag{4.4}$$

and parameters are

α- Shape parameter ($\alpha > 0$)
β - Scale parameter ($\beta > 0$)
γ- Location parameter ($\gamma = 0$, yields the two-parameters Log-Logistic distribution)

4.1.3 Johnson S_B distribution

The Johnson S_B distribution, or alternatively the 4-parameter lognormal model, is appealing on theoretical grounds as a candidate probability distribution function for ratios, or variates constrained by extremes [127]. It has found applications in a variety of fields including ambient air pollution , rainfall distribution and forestry . The distribution function of Johnson S_B distribution function is provided in Equation 4.5.

$$f(x) = \frac{\delta}{\lambda.\sqrt{2\pi}.z[1-z]} \exp[-\frac{1}{2}[\gamma + \delta.\ln[\frac{z}{1-z}]]^2] \tag{4.5}$$

and parameters are
α- Shape parameter ($\alpha > 0$)
β - Scale parameter ($\beta > 0$)
γ- is continuous shape parameter
δ- Continuous shape parameter ($\delta > 0$)
λ - Continuous scale parameter ($\lambda > 0$)
ξ -Continuous location parameter
And domain is $\xi \leq x \leq \xi + \lambda$

4.1.4 Kumaraswamy distribution

Kumaraswamy distribution is a two-parameter family of distributions which has many similarities to the beta distribution and a number of advantages in terms of tractability (it also, of course, has some disadvantages) [128]. Kumaraswamy distribution has its genesis in terms of uniform order statistics, and has particularly straightforward distribution and quantile functions which do not depend on special functions (hence afford very easy random variate generation). The distribution might, therefore, have a particular role when a quantile-based approach to statistical modeling is taken, and its tractability has appeal for pedagogical uses. To date, the distribution has seen only limited use and developed for the modeling of hydrological parameters. The distribution function of Kumaraswamy distribution is provided in Equation 4.6.

$$f(x) = \frac{a_1 a_2 z^{a_1-1}(1-z^{a_1})^{a_2-1}}{b-a} \tag{4.6}$$

where,

$$z \equiv \frac{x-a}{b-a} \tag{4.7}$$

and parameters are,
a_1 - shape parameter($a_1 > 0$)
a_2 - shape parameter ($a_2 > 0$) a, b - boundary parameters ($a < b$)
and domain is $a \leq x \leq b$

4.1.5 Performance analysis

Graphical ways for performance analysis (goodness-of-fit) such as Q-Q plot and P-P plot has been used for Graz data, whereas, Kolmogorov-Smirnov test is also included and used for Prague data.

4.1.5.1 Q-Q Plot

The graphical analysis of the data can refer a basic shape of the distribution. Several distribution models can be compared intuitively. The easiest way to do this comparison is through Q-Q plot. The Q-Q plot is a plot of the points (Q(pr), x(r)), i.e., the n data quantiles, x(r), against the corresponding model quantiles, Q(pr). Where, Q(p) is a suitable model, x(1), x(2), x(3), ..., x(n) are the n-ordered observations and pr, r = 1, 2, 3, ... n, are the corresponding probabilities; pr = (r - 0.5)/n. This plot will approximate a good model by a straight line since the model gives the p-quantiles, xp, as a function of p; xp = Q(p) and the line should be at 45 degree. In practice, Q(p) is often a model fit to the set of data, denoted by (p). Hence, the plot of ((pr), x(r)) is called the fit-observation diagram and the 45 degree line is the line of perfect fit. An inappropriate model will show some systematic curvature. For models with unknown position and scale parameters, the straightness of the line of the Q-Q plots can still be examined. For unknown shape parameters, there will be a need to give numerical values to the parameters to enable the Q-Q plot to be drawn. If the plot veers away at the ends, it indicates that the distribution need to have either shorter or longer tails at that end [129].

4.1.5.2 P-P Plot

A probability-probability (P-P) plot is used to see if a given set of data follows some specified distributions and it should be approximately linear if the specified distribution is the correct model. The probability-probability (P-P) plot is constructed using the theoretical cumulative distribution function, F(x), of the specified model. The values in the sample of data sorted in order from smallest to largest, are denoted as x(1), x(2), ..., x(n). For i = 1, 2, ..., n, F(x(i)) is plotted against (i-0.5)/n . Concerning how the distribution composing a single P-P plot compare , a P-P plot that lies on 45 degree line indicates that the two distributions are identical, whereas, a P-P plot strictly above or below 45 degree line indicates that one distribution stochastically dominates the other [130].

4.2 PDF estimation of Graz Data

In this section detailed analysis and simulation results of measured optical attenuations data of Graz have been presented. Curve fitting techniques were applied on measured data

for all kinds of fog (Different types of fog are given in Table 2.1) to get the most appropriate probabilistic model for terrestrial free-space optical communication links under different continental fog conditions. All continuous distribution functions were compared through Q-Q plot and P-P plot for the actual measured data and selected only the two best fit distribution models for each kind of fog. Although histogram is a convenient way to get insight into the probability distribution associated with the continuous random variable but PDF and CDF are presented for analysis. PDF, though, is a common way to visualize a distribution but for statistical analysis, CDF is better suited than the PDF. The integral of the PDF calculated from histogram should be equal to 1, but this is not true in some cases. To circumvent this inaccuracy, the use of empirical CDF (ECDF) can be helpful as all data points have to be normalized by the maximum value for an accurate representation of ECDF. To avoid uncertainty , both PDF and CDF are used because these are also the two general ways of defining a distribution. The analysis of the measured data resulted in the calculation of some basic parameters for different types of fog i.e. dense, thick, moderate and light fog, along with whole range of fog conditions. Table 4.1 quantify some basic features of the measured optical attenuations data. These parameters are given in Table 4.1. As evident from Table 4.1 taht sample size and mean is different for all types of

Table 4.1: Descriptive statistics of all fog events

Description	Dense fog	Thick fog	Moderate fog	Light fog	General fog
Sample Size	25451	183290	86355	225259	520355
Mean	171.82	78.318	27.364	13.338	46.306
Variance	376.3	457.33	30.706	8.6605	1849.9
Std. Error	0.12159	0.04995	0.01886	0.0062	0.05962
Skewness	0.79165	0.25302	0.56434	0.53469	1.4397
CV x 100	11.2897218	27.31	20.25	22.06	92.88

fog, therefore, coefficient of variation (CV) is used as a standard quantity to describe the variation. The coefficient of variation (CV) is presented in last line of Table 4.1. CV is a ratio of the standard deviation to the mean and it is a useful statistics for comparing the degree of variation. Here, CV in Table 4.1 under each fog type tells us about the variation in specific attenuations for a particular fog type. From the Table 4.1, it is visible that the dense fog has least variations and so is the most stable as compared to the other fog types, whereas, general fog has most variation, which gives some insight about the variations of fog. It means that in case of dense fog the behavior of the channel remains almost constant, whereas, in case of general fog variations in channel are very high. The main reason behind this is that during the fog formation and fog dissipation, fog changes rapidly. The 4th line indicates the skewness. The skewness for all kinds of fog is positive which indicates that data are skewed right. Skewed right means that the right tail of the distribution of the data is long relative to the left tail. The skewness of general fog is highest value, whereas, thick fog has less value. If we see figures 4.2(a) and 4.5(a), it is clearly indicated that the higher attenuation of general fog are more symmetric as compared to thick fog.

For the detailed statistical analysis of the specific attenuation(dB/km) of received signal, 18 fog events from terrestrial free-space optical communication demonstrations have been

used. The measurements data represent some typical areas where FSO links were deployed.

4.2.1 Dense fog

In order to statistically evaluate the attenuation data for dense continental fog, and to observe its characteristics we selected fog attenuation values exceeding above 143 dB/km measured on a second scale on 80 m FSO link. The descriptive statistics of the selected attenuation data set are presented in Table 4.1, curve fitting is applied on the sampled attenuation data by comparing different probability distribution functions. It is found that Wakeby distribution best fits the measured attenuation data for the dense fog condition. For dense fog, the histogram of PDF and CDF along with Q-Q plot and P-P plot are given in Figs 4.1(a), 4.1(b), 4.1(c) and 4.1(d) respectively.

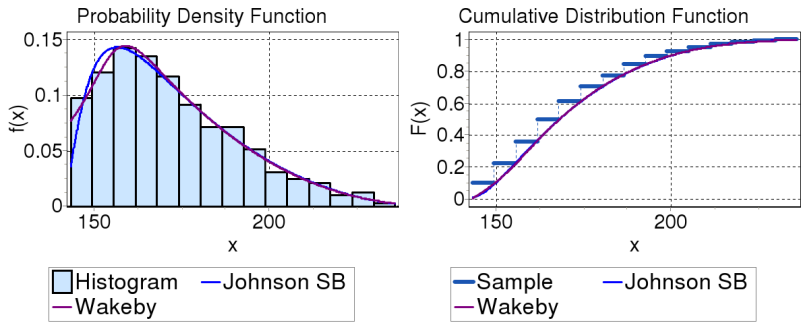

(a) pdf of the dense fog

(b) cdf of the dense fog

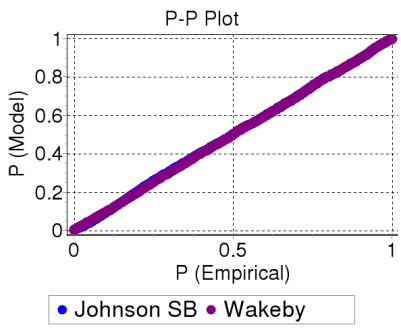

(c) P-P plot of the dense fog

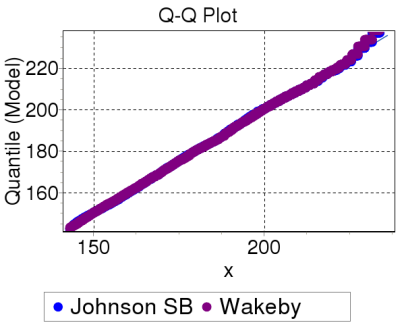

(d) Q-Q plot of the dense fog

Figure 4.1: Statistical analysis of the dense fog

By comparing the histogram of measured data and the plots of PDF and CDF as shown in Fig. 4.1(a) and Fig. 4.1(b), the Wakeby distributions seem to have more accuracy as compared to other density functions for our measured attenuation data. Furthermore, if we observe the Q-Q plot for these density functions in Fig. 4.1(d), Wakeby distribution seems to be a better fit. Fig.4.1(c) shows the P-P plot for the selected distribution functions.

The parameters for selected distribution for every kind of fog were calculated, these parameters are given in Table 4.2. Note that * in Table 4.2 indicates the best fit distribution

Table 4.2: The calculated parameters for the selected distribution functions

Description	Distribution	Parameters
Dense fog	Wakeby*	a =51.517, b =8.4422, c =30.569, d = -0.29677, e =142.79
	Johnson S_B	γ=1.1237, δ =1.033, λ =111.86, ξ =139.82
Thick fog	Logistic*	σ =11.79, μ =78.318
	Nakagami	m =3.5126, Ω =6591.0
Moderate fog	Johnson S_B*	γ=0.53036, δ =0.62405, λ =20.894, ξ =19.886
	Wakeby	α =11.123, β =0.44992, γ =0, δ=0, ξ =19.693
Light fog	Johnson S_B*	γ=0.51767, δ =0.65162, λ =11.315 , ξ =9.2184
	Wakeby	α =6.1241, β =0.48097, γ =0 δ=0, ξ =9.2025
General fog	Kumaraswamy*	α_1 =0.45233, α_2=1.6528, a=9.3395, b=236.09
	Gen. Gamma (4P)	k=1.0277, α =0.58616, β =62.564, γ =9.3395

according to the results of Q-Q plot and P-P plot. Table 4.2, shows the two best fitted distributions on our data against every kind of fog.

4.2.2 Thick fog

Thick fog is characterized when the visibility range is 40 - 70 m and attenuation level is 143-40 dB/km. In order to evaluate statistically the attenuation data for thick fog, and to observe its characteristics fog attenuations values exceeding from 40 and less than 143 dB/km measured on a second scale on 80 m FSO link, were selected. The descriptive statistics of the selected attenuation data set are presented in Table 4.1. Curve fitting is applied on the sampled attenuation data by comparing different probability distribution functions. We found that logistic distribution best fits the measured attenuation data for the thick fog conditions, by comparing, several distributions on the attenuation data for the thick fog through visualizing Q-Q plot and P-P plot. The results of Q-Q plot and P-P plot suggest that Logistic distribution and the Nakagami distribution are the two best fitted distributions for thick fog. The PDF over the histogram of the measured data for two best fitted distribution is given in fig 4.3(a). While, goodness of fit is tested with the help of Q-Q plot and the P-P plots for the two mentioned distributions. The results are shown in Figs 4.2(a), 4.2(b), 4.2(c), 4.2(d) for attenuations corresponding to thick fog. In figure 4.2(a) probability density plot shows that Logistic density function has better fit for thick fog data. Fig. 4.2(b) shows the cumulative distribution function of logistic distribution which is a good approximation. Figs 4.2(c) and 4.2(d) shows that P-P plot and Q-Q plot, respectively. P-P plots and Q-Q plots are not continuous which shows some unusual peaks in the histogram. These breaks represent that during fog formation or fog dissipation the channel is changing abruptly. For thick fog it is very difficult to decide which distribution is better on the basis of P-P plot and Q-Q plot because both plots are overlapping. Here, we can use CDF for decision. If we observe fig 4.2(b) the logistic distribution is more linear

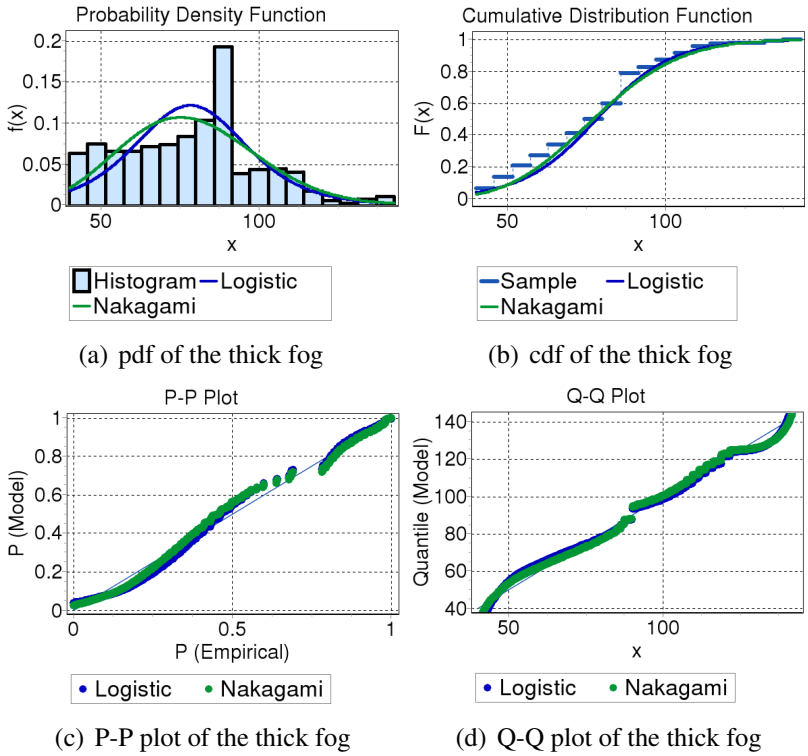

(a) pdf of the thick fog (b) cdf of the thick fog

(c) P-P plot of the thick fog (d) Q-Q plot of the thick fog

Figure 4.2: Statistical analysis of the thick fog

as compared to Nakagami distribution. CDF confirms that logistic density function have better fit for thick fog. The calculated parameters for logistic and Nakagami distributions are given in Table 4.2.

4.2.3 Moderate fog

Fog attenuation values in the range of 20-40 dB/km measured on a second scale on 80 m FSO link for the statistical evaluation of the attenuation data for moderate fog and observing its characteristics, were selected. Table 4.1, presents the descriptive statistics of the selected attenuation data set. Curve fitting has been applied on the sampled attenuation data by comparing different probability distribution functions. Johnson S_b and Wakeby distribution model has better results as compared to any other distribution model. It was found out that Johnson S_b distribution best fits the measured attenuation data for the moderate fog conditions. For moderate fog, the histogram over PDF and CDF along with Q-Q plot and P-P plot are given in Figs 4.3(a), 4.3(b), 4.3(c), 4.3(d). It is evident from figure 4.3(a) that probability density plot for that of Johnson S_b density function has better fit for moderate fog attenuation data. Figure 4.3(b) shows the cumulative distribution function of Johnson S_b and Wakeby distribution for moderate continental fog. Figures 4.3(c) and 4.3(d) shows the P-P plot and Q-Q plots, respectively. If we see figure 4.3(d), the Q-Q plot for Johnson S_b distribution is converging at the end while for Wakeby distribution it

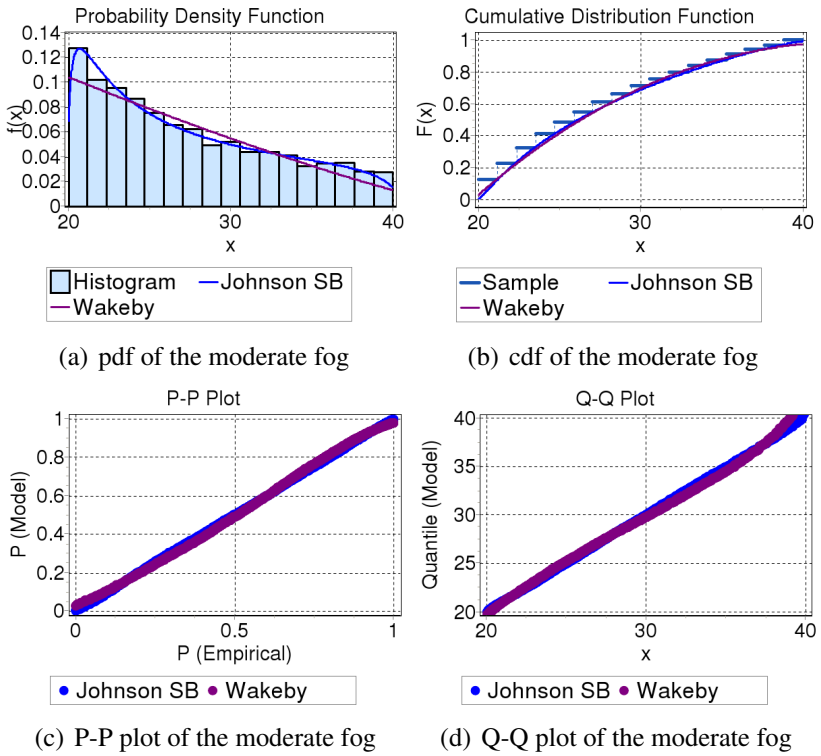

(a) pdf of the moderate fog (b) cdf of the moderate fog

(c) P-P plot of the moderate fog (d) Q-Q plot of the moderate fog

Figure 4.3: Statistical analysis of the moderate fog

is diverging, which shows that Johnson S_b distribution is a better model for moderate fog data. The calculated parameters for Wakeby and Johnson S_b are given in Table 4.2.

4.2.4 Light fog

The data in the range of 9.3-20 dB/km measured attenuation data on a second scale on the 80 m FSO link for the statistical evaluation for light fog conditions is considered and find to be the best suited probabilistic model. Table 4.1 illustrates the descriptive statistics of the selected attenuation data set. Curve fitting on the sampled attenuation data were applied to find the best model and different PDFs were compared for light fog. It was found out that Johnson S_b distribution best fits the measured attenuation data for the light fog condition. For light fog, the PDF over histogram and CDF along with Q-Q plot and P-P plot are given in Figs 4.4(a), 4.4(b), 4.4(c), 4.4(d). From figure 4.4(a) probability density plot, it is evident that Johnson S_b density function has better fit for light fog attenuation data. Figure 4.4(b) shows the cumulative distribution function of Johnson SB and Wakeby distribution for light continental fog. Figures 4.4(c) and 4.4(d) shows the P-P and Q-Q plots. If we see figure 4.4(d), the Q-Q plot for Johnson S_b distribution is converging at the end while for Wakeby distribution it is diverging, which shows that Johnson S_b distribution is a better model for moderate fog data. The calculated parameters for Wakeby and Johnson S_b are given in Table 4.2.

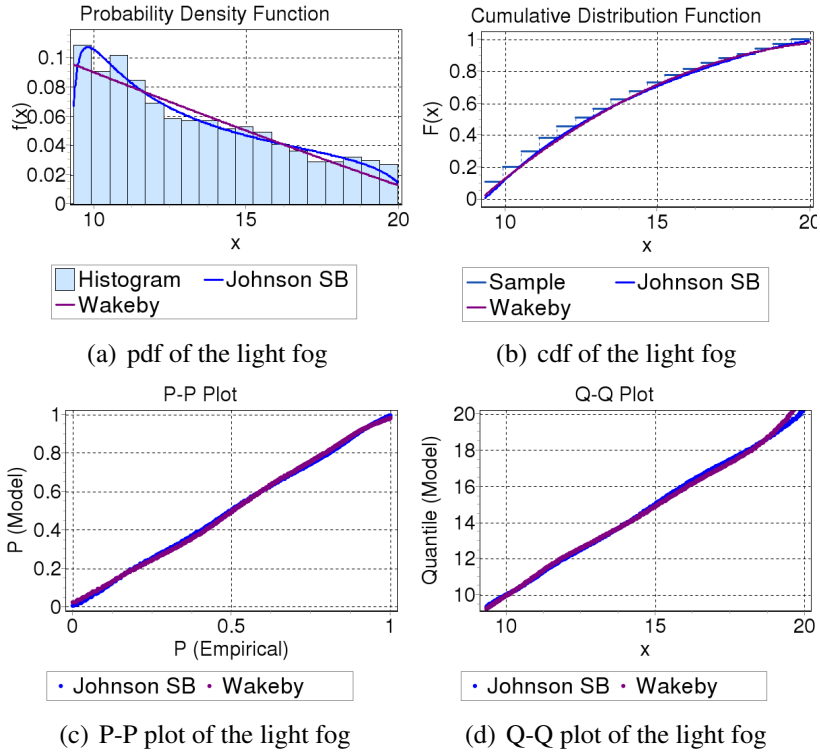

(a) pdf of the light fog

(b) cdf of the light fog

(c) P-P plot of the light fog

(d) Q-Q plot of the light fog

Figure 4.4: Statistical analysis of the light fog

4.2.5 General fog

For the statistical evaluation of the attenuation data for general continental fog, and to observe its characteristics the whole range of attenuation data measured on a second scale on the 80 m FSO link was considered. The descriptive statistics of the selected attenuation data set are presented in Table 4.1, curve fitting were applied on the sampled attenuation data by comparing different probability distribution functions. It was found out that Kumaraswamy's distribution best fits the measured attenuation data for the complete fog condition. For general fog case, the PDF over histogram, CDF, Q-Q plot and P-P plot are given in Figs. 4.5(a), 4.5(b), 4.5(c), 4.5(d). From figure 4.5(a) probability density

plot shows that Kumaraswamy's density function approximate well to general fog. Figure 4.5(b) shows the cumulative distribution function of Kumaraswamy and Gamma distribution. It is visible in figure 4.5(b) that CDF of Kumaraswamy distribution is best fit as compared to Gamma distribution. From figure 4.5(c) the P-P plot for Kumaraswamy distribution is more closer to reference line as compared to Gamma distribution. The Q-Q plot in figure 4.5(d) confirms that Kumaraswamy's distribution have better fit to Complete fog data. If we see the Q-Q plot it is obvious that for higher attenuation Q-Q plot for Kumaraswamy's distribution is converging whereas for Gamma distribution it is diverging but for lower attenuation the situation is reversed. The reason could be in the histogram

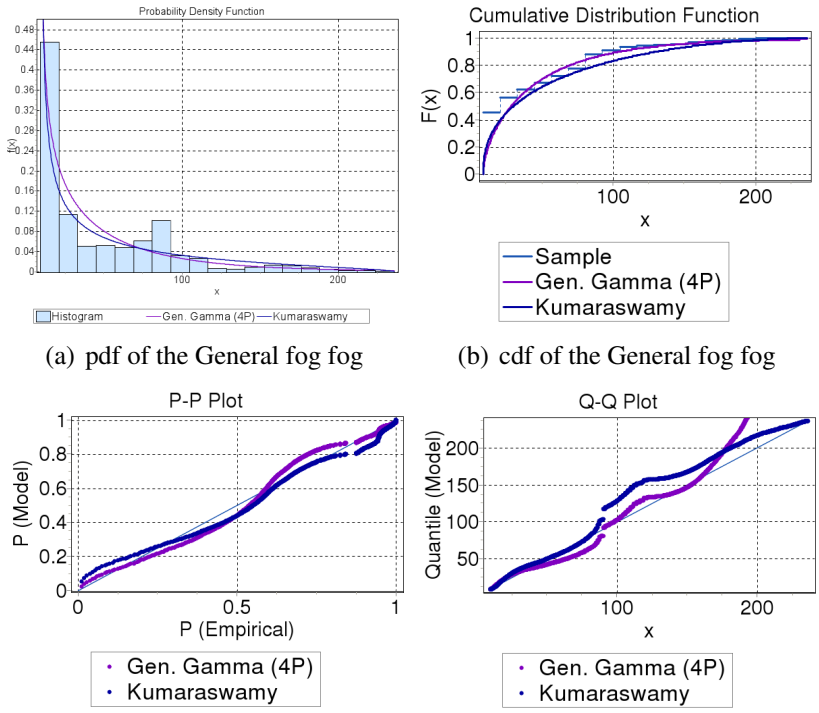

(a) pdf of the General fog fog

(b) cdf of the General fog fog

(c) P-P plot of the General fog fog

(d) Q-Q plot of the General fog fog

Figure 4.5: Statistical analysis of the general fog

(figure 4.5(a)). Figure 4.5(a) shows that it is very difficult to fit a single distribution. The results of goodness of fit in fig 4.5(d) suggest that Kumaraswamy's distribution has reasonable fit of optical attenuations for continental fog case. The calculated parameters for Kumaraswamy and Gamma distribution are given in Table 4.2.

4.3 PDF estimation of Prague Data

Recent research in probability distribution function (PDF), estimation of received signal strength under a foggy channel [75, 116] has diverged in an attempt to provide the appropriate density function under different fog conditions. However, in the current study we have focused on converging multiple density functions into one *PDF* model which should be generic enough to provide the best estimate of received signal strength under continental fog conditions.

We applied distribution fitting techniques on measured data to get the most appropriate probabilistic model for terrestrial free-space optical communication links under continental fog conditions. We fitted all the probability density functions on the actual measured data by visualizing their *PDF* and *CDF*, independently. The goodness of fit has been observed by using graphical methods; probability-probability (PP) plot and quantile-quantile (QQ) plot. To strengthen the graphical findings, Kolmogorov$-$Smirnov test (K-S test) has

also been used to observe the goodness of fit for specified distributions. The summary statistics of fog attenuation for Prague data set are presented in Table 4.3. It is important

Table 4.3: Summary of the data

Statistical parameters	**Value**
Sample Size	2233
Mean	72.54
Variance	843.02
Std. Error	0.61443
Skewness	-0.17
Min	8.3
Max	132.5
25% (Q1)	51.5
50% (Median)	75.2
75% (Q3)	95.1

to mention that the skewness (mentioned in line 6 of Table 4.3) of measured data is negative. Skewness characterizes the degree of asymmetry of a distribution around its mean and the negative skewness observed implies that the left tail of the distribution would be longer. Table 4.3 can be more precisely analyzed by using the box plot. In statistical analysis box plot is a combination of five statistics and provides reasonable information about the shape of distributions and outliers. It can visualize median, upper quartiles, lower quartiles, $1.5th$ of interquartile range and outliers simultaneously. The box plot for Prague data is shown in Fig. 4.6. The upper and lower edges represent the value of $(\pm 1.5th)$ of interquartile range.

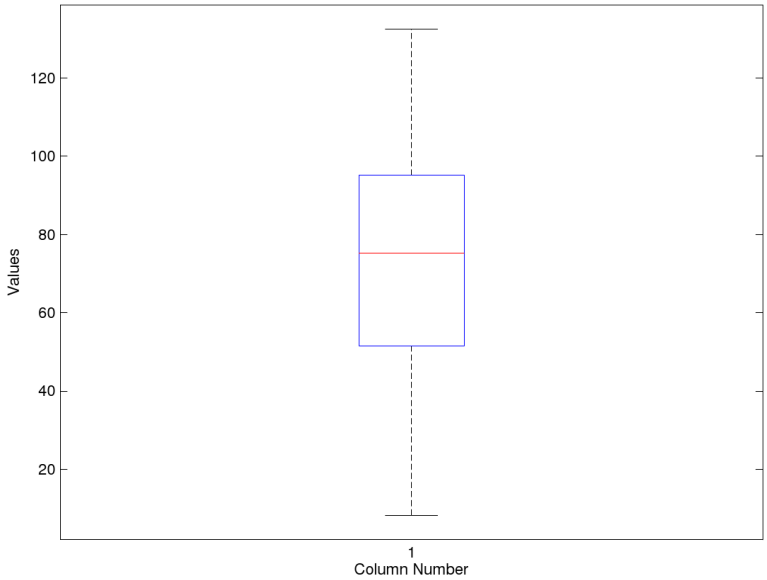

Figure 4.6: Box plot of the optical attenuation

The solid upper and lower lines in the box indicate the *75th* and *25th* percentile point. The

solid line in the box indicates the value of median, if it is not equidistant from the upper and lower quartiles, then the data is skewed. It can be observed from box plot that the median line in the box plot is more closer to upper side of the box, which suggests that data is negatively skewed and strengthens the evaluation of Table 4.3. The points falling outside the edges are outliers, in our case no outliers exist.

Having completed the exploratory data analysis we proceed to find the best fit *PDF* model for measured data. Comparisons have been performed for all the continuous distribution for the measured optical attenuation and an attempt is made to locate the best fit distribution by the K-S test and the observation of the *PP* plot and *QQ* plot. The *PDF*, *CDF*, *PP* plot and *QQ* plot for the measured data is illustrated in Fig. 4.7, 4.8, 4.9 and 4.10 respectively.

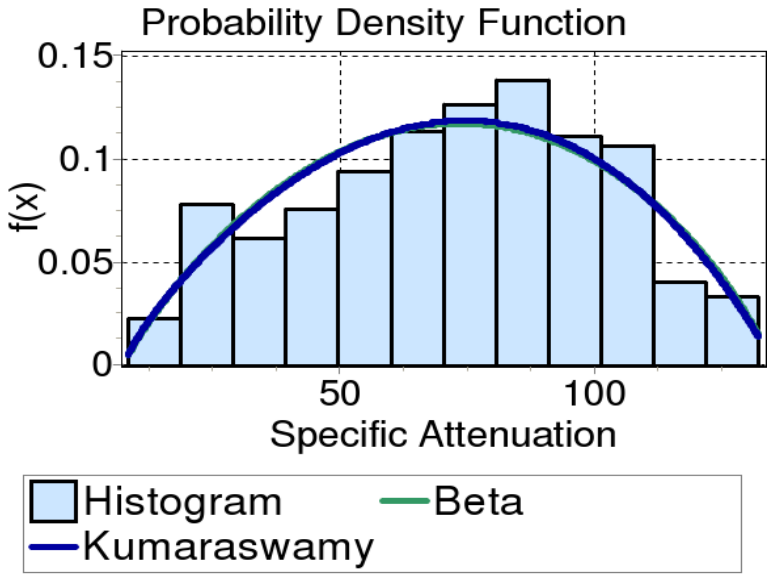

Figure 4.7: PDF over the histogram of the optical attenuation

As, it has been mentioned above that we performed the comparisons for all continuous distributions but selected two best fit distributions on the basis of *QQ* plot, *PP* plot and the results of K-S test. It is obvious from Fig. 4.9 and Fig. 4.10 that *PP* and *QQ* plot are overlapping each other, therefore, we further performed statistical test to select the best fit distribution. A very famous Kolmogorov−Smirnov (K-S) non-parametric test is used for goodness of fit which could test goodness of fit for any specified density function. The results of K-S test suggests that the *Kumaraswamy* is the best fitted *PDF* for optical attenuations.

By using the results of K-S test it is observed from the Table 4.5 that *Kumaraswamy's* distribution is the most appropriate which could describe the characteristics of optical attenuations. The value of test statistics in table 4.5 for *Kumaraswamy's* distribution is less

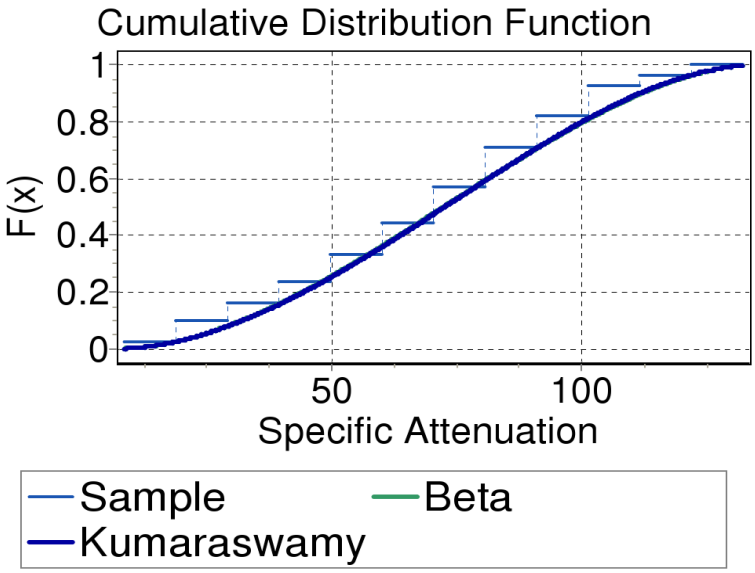

Figure 4.8: CDF of the optical attenuation

Table 4.4: Kolmogorov-Smirnov test

Kumaraswamy					
Kolmogorov-Smirnov					
Sample Size	2233				
Statistic	0.03505				
P-Value	0.00808				
Rank	1				
α	0.2	0.1	0.05	0.02	0.01
Critical Value	0.02271	0.02588	0.02874	0.03212	0.03447
Reject?	Yes	Yes	Yes	Yes	Yes
Beta					
Kolmogorov-Smirnov					
Sample Size	2233				
Statistic	0.03773				
P-Value	0.00338				
Rank	2				
α	0.2	0.1	0.05	0.02	0.01
Critical Value	0.02271	0.02588	0.02874	0.03212	0.03447
Reject?	Yes	Yes	Yes	Yes	Yes

than *Beta* distribution which provide strong evidence that *Kumaraswamy's* distribution is suitable. Test statistics is based on the difference between the theoretical and the empirical CDF.

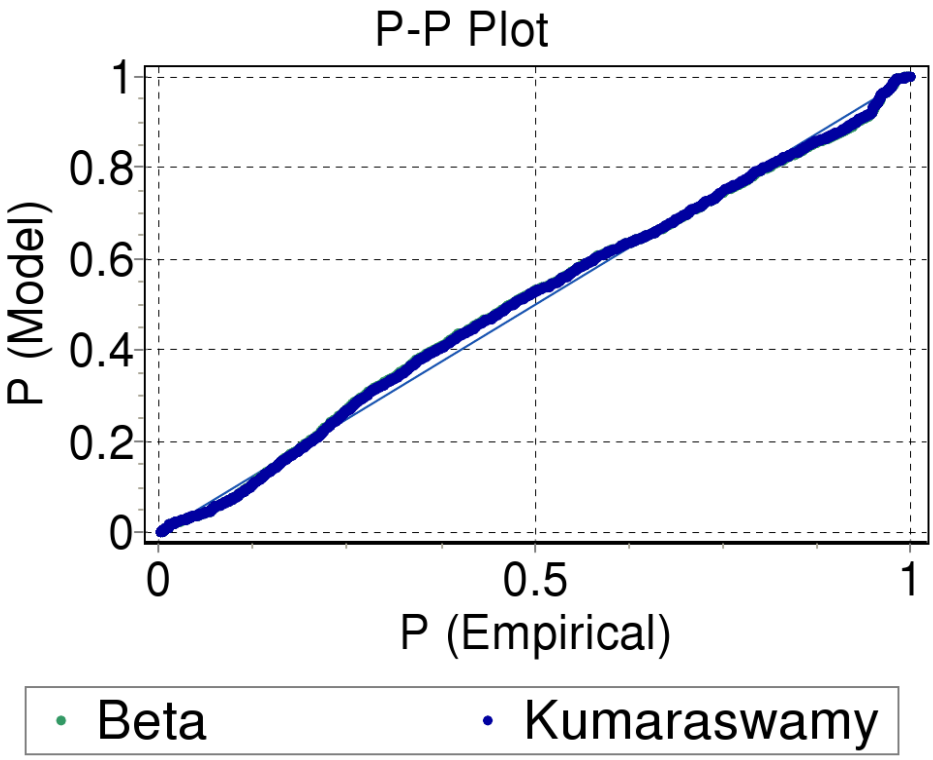

Figure 4.9: P-P plot of the optical attenuation

The optimal parameters of two best fit *PDF* models has been estimated and are provided in Table 4.5.

Table 4.5: Optimum parameters

Serial No	**Distribution Model**	**Parameters**
1	Kumaraswamy	α_1=1.7851 α_2=1.949
		a=7.6101 b=135.48
2	Beta	α_1=1.8957 α_2=1.8265
		a=7.3481 b=134.82

It has been concluded from the results of K-S test that *Kumaraswamy* is the best fit distribution for settled continental fog conditions and thus reinforces the results presented for Graz data. The basic idea in finding the best suited distribution model is to provide the system designer, one appropriate *PDF* model which is a good approximation for RSS, once the fog has settled in, and is not strong enough to have disrupted the link altogether. The con-

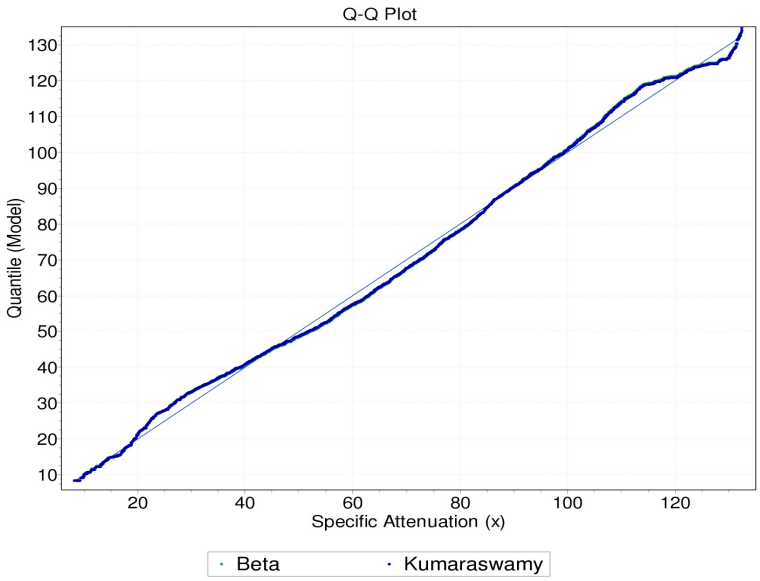

Figure 4.10: Q-Q plot of the optical attenuation

clusion from the analysis provided in this section is that the *Kumaraswamy's* distribution fulfills the stated objective.

5 LWC modeling for FSO links

Liquid water content (LWC) is a microphysical parameter which is used to characterize fog/cloud. Higher density of LWC depicts dense fog, significantly reducing visibility and causing performance degradation of free space optical links for a non-negligible amount of time. Fog formation is directly influenced by microphysical processes within the radiative aerosols and their surface conditions [131]. Visibility is related to droplet number and water mass in a given volume of air [132]. The liquid water content (LWC) is the measure of water density per volume of dry air in a cloud/fog. It is measured per volume of air (g/m^3) or mass of air (g/kg) units. Extinction of light at visible frequencies within different fog conditions result in low visibilities and degradation of the terrestrial FSO link performance. Quantification of LWC in a given volume of air helps characterize different fog and cloud conditions spatially and temporally. Fog, having very low densities, contains very small amount of water thus resulting in lower values of LWC around 0.05 (g/m^3) for a moderate fog (visibility range around 300 m). Much higher values of LWC (around o.4 (g/m^3) usually mean formation of thick or dense fog (visibility range of about 50 m) [133].

5.1 Microphysical Properties of Fog

Microphysical properties of fog as the drop size distribution (DSD), the drop shape and the composition of particles are strongly influenced (both temporally and spatially) by the microclimate and by several other environmental factors. To assess the performance of FSO links in terms of availability and reliability, the sensitivity of signal attenuation to microphysical quantities like the LWC, DSD, average particle size and the number concentration must be investigated well [15]. In order to estimate the optical attenuations particularly in a fog environment, besides from the particle size distribution, LWC (mass of water droplets present per unit volume of air) is another important microphysical property. Within the fog particles LWC is highly influenced by fog particle's DSD and the number concentration.

Attenuation caused by fog particles is highly dependent upon the fog particle radii. For an optical beam propagating through fog, Mie resonance occurs at wavelengths comparable to the fog particle radii. The fog particle radii differs in different climatic regions hence, optical waves propagating through fog conditions even at the same wavelength, face slightly varying attenuation. Assuming spherical shape, fog particles can be categorized into following three classes based on their radii:

- Aitken particles and ultra-fine particles (nucleation mode): These are fine particles with the average size ranging between 0.001 μm and 0.1 μm. These particles contribute to the condensation and formation processes of fogs.
- Fine particles (accumulation mode): The range of these particles lies between 0.1 μm and 1 μm in size. Their number concentration is much higher than the one of ultra-fine and and larger particles.
- The larger particles (coarse mode): The size of these particles goes from 1 μm to 100 μm. These particles mostly contribute to LWC.

The size distribution of fog particles is usually modeled by a modified gamma distribution which is given in Equation (5.2) [98].

$$c(r) = N_0 r^m exp(\Lambda r^\sigma) \tag{5.1}$$

Here, c(r) denotes the number of particles per unit volume per unit increment of the particle having radius r. N_0, m, Λ and σ are the four adjustable parameters that characterize this particle size distribution. Assuming m is specified, and σ = 1 (for fog case) then N_0 and Λ are given by Equation (5.2, 5.3).

$$\Lambda = \frac{(m+3)}{r_e} \tag{5.2}$$

$$N_0 = \frac{(3.10^6.LWC.\Lambda^{m+4})}{(4\pi\Gamma(m+4))} \tag{5.3}$$

where, r_e is the effective particle radius and $\Gamma()$ is the gamma function. One must consider the typical fog droplet radius into account, as several types of fog with different typical droplet radius have been observed in different regions and climates.

If N_d is the number concentration of the fog particles per cubic centimeter of air then the real profile of the fog particles can be obtained through product of $c(r)$ and N_d [134]. Considering the modified gamma distribution in case of fog, the liquid water content in g/m^3 can be calculated as:

$$LWC = \rho_w N_d \frac{4}{3} \int_0^\infty \pi r^3 c(r) dr \tag{5.4}$$

where, r is the fog particle radius and $\rho_w(g/m^3)$ is the density of water. Considering the third power radius in Equation (5.4) suggests that fog droplets smaller than 3 μm have

a very little contribution towards LWC and therefore, could be neglected. The values of LWC resulting from Equation (5.4) and the corresponding set of modified gamma drop size distribution (MGDSD) parameters giving the best fit curves relative to eight size spectra of small water droplets for a visibility range of 1 km are given in [134]. Figure 5.1 demonstrates the effect of modified gamma distribution parameters on the DSD for a LWC value of 0.5 g/m^3.

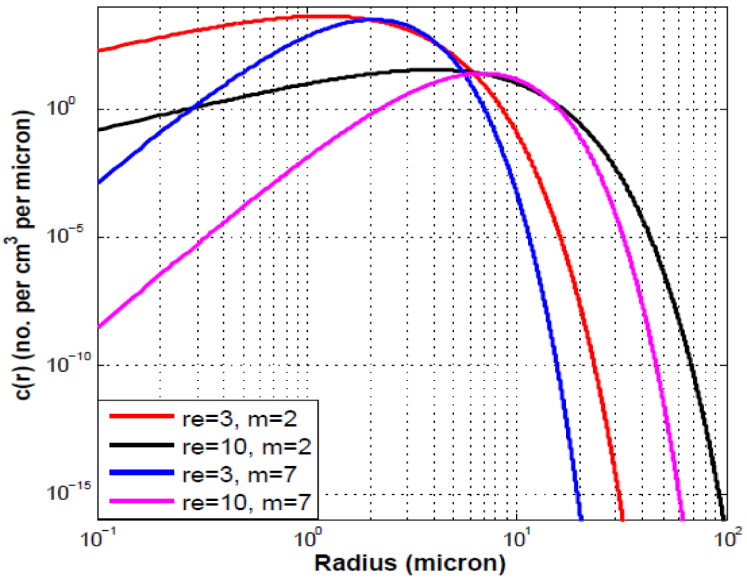

Figure 5.1: Number concentration of fog particles for modified gamma distribution [75]

The effective extinction efficiency $\xi(r)$ and effective droplet radius $r_e(\mu m)$ in terms of DSD can be calculated by Equation (5.5, 5.6).

$$\xi_e = \int_0^\infty \xi(r) r^2 c(r) dr / \int_0^\infty r^2 c(r) dr \tag{5.5}$$

$$r_e = \int_0^\infty r^3 c(r) dr / \int_0^\infty r^2 c(r) dr = 30000 \frac{LWC}{PSA} \tag{5.6}$$

It is important to mention that r_e is the radius of a mono-dispersed particle distribution having the same LWC and particle surface area (hereafter PSA). PSA is the fog particle surface area measured in cm^2/m^3. Assuming spherical shape of fog particles, the relationship between DSD and the PSA is given by Equation (5.7) below,

$$PSA = 10^{-2}.N_d 4\pi \int_0^\infty r^2 c(r) dr \tag{5.7}$$

5.2 Models relating LWC and visibility

Liquid water content (LWC) is a measure of mass of water in fog/cloud in a specified amount of dry air. LWC can be expressed as g/m^3 or mass of air g/kg and varies greatly for different cloud and fog types . The classification of clouds and fog is highly related to the amount of LWC and its origin. The combination of LWC and its origin allows to readily predict the types of conditions that will be, most likely, in the vicinity of the FSO links [75]. Fog having very low densities contains very small amount of water and so eventually results in lower values of LWC i.e., about 0.05 g/m^3 for a moderate fog (visibility range around 300 m). Much higher values of LWC (around 0.5 g/m^3) result in the formation of thick or dense fog (visibility range of about 50 m)[15]. Similarly, clouds may have LWC value of 0.06405 g/m^3, while, 1-3 g/m^3 for Cirrus and Cumulonimbus clouds, measured respectively in the same amount of space [98]. Fog or cloud droplets of the maritime origin tend to have relatively larger size and thus make up fewer water droplets in comparison to the continental fog droplets [98, 135]. The concentration of maritime origin droplets lies between 100 $drops/cm^3$ to 200 $drops/cm^3$, whereas, the concentration of continental origin droplets is about 900 $drops/cm^3$ [136].

Fog characterized by several physical parameters like particle size distribution, temperature, humidity and LWC has been extensively modeled by drop size distribution and visibility range [15]. The variation of visibility and LWC from measured data at Prague is shown in Fig. 5.2.

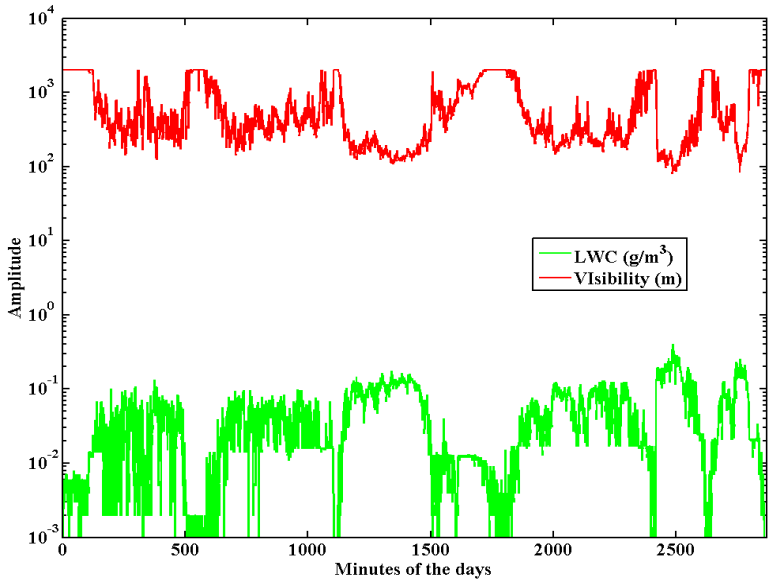

Figure 5.2: Time series analysis of LWC and visibility

This section focuses on the verification of existing LWC based fog modeling. There are two commonly used empirical models that relate visibility to LWC [137]. One such model is given in Equation (5.8).

$$V = b(LWC)^{-\frac{2}{3}} \tag{5.8}$$

where, V is visibility in km and "b" is a constant. The parameter "b" attains a different value for each different type of fog as tabulated in Table 5.1. The simulation results of

Table 5.1: Fog types and different values of coefficient "b"

Fog type	Value of b	Ref.
Dense haze	0.013	[134]
Continental fog	0.034	[134]
Maritime fog (wet and warm)	0.060	[134]
Dense haze and selective fog	0.017	[138]
Stable and evolving fog	0.024	[138]
Advection fog	0.02381	–

equation 5.8 for different values of "b" over the measured data are shown in Fig. 5.3.

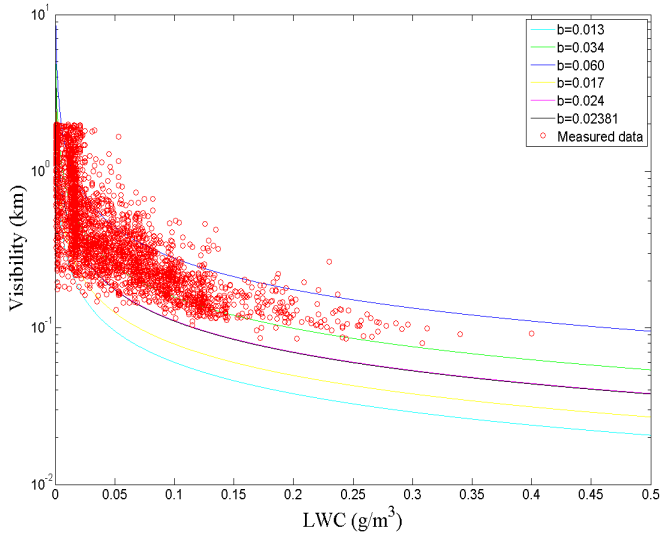

Figure 5.3: Predicted Visibility and LWC alongwith real data for different values of "b"

Fig. 5.3 clearly indicates that for lower values of LWC the spread of measured attenuation values is across different curves depicting haze, maritime fog and continental fog. However, for LWC values between $0.1g/m^3$ to $0.35g/m^3$ the attenuation values are concentrated more closer to the curve of "b" depicting continental fog. Whereas, the reason for spread of data point across different curves for lower value of LWC (below $0.1g/m^3$) is probably due to the fact that our selected data set contains optical attenuation values relating to fog formation, settling and the dissipation phases. Considering different visibility regimes the selected values may be related to haze, mist and continental fog conditions as well hence, some values may be considered as outliers when we speak about continental fog conditions only. However, the evaluations of "b" turn out to be consistent with the values proposed in the literature and thus give evidence for its close dependence on the

shape-parameters of the droplet size distribution, especially with regard to mode radius and the width of the larger-droplet number [134]. Platt [139] suggests that lower values of "b" should be related to "dry" or industrial-type haze and fogs having many more small droplets which grow in probable cold air masses, whereas, gradually higher values of "b" correspond to "wet" natural fogs characterized by increasing and predominant contents of larger but fewer droplets. Eldridge [140] provides an evidence of the influence of width and of the radius range of the droplet size distribution over the coefficient "b". Hence, analysis of measured five months attenuation data provides the possibility of estimating the most proper value of "b". As the next logical step, we tried to estimate the optimum value of "b" depicting continental fog from our measured data. Fig. 5.4 provides the evaluation of the data sets with an aim to minimize the RMSE.

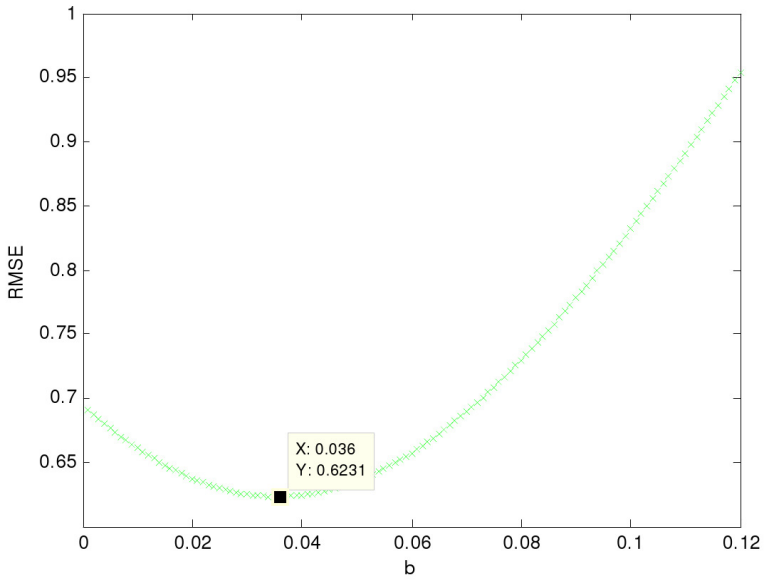

Figure 5.4: Optimum value of "b" for measured optical attenuations

It is obvious from equation 5.8 that one can expect one value of LWC for one value of visibility. For this reason values can be predicted by the bijection. But measured data shows that one can expect different values of visibilities for a single value of LWC $(Fig.5.3)$. Therefore, we use all these possible values in RMSE formula.

Based on our representative data set analysis, the estimated optimum value of "b" for continental fog conditions is "0.036". The simulation of equation 5.8 with newly estimated value of "b" alongwith the measured attenuation data is shown in Fig. 5.5.

As evident from Fig. 5.5 that the newly estimated value of "b" seems a better approximation, we computed mean percentage error to compare the new value of "b" with the already existing value$(b = 0.034)$. We found that mean percentage error for $b = 0.034$ is 67.95, whereas, the mean percentage error for $b = 0.036$ is 66.85. More recently Gultepe

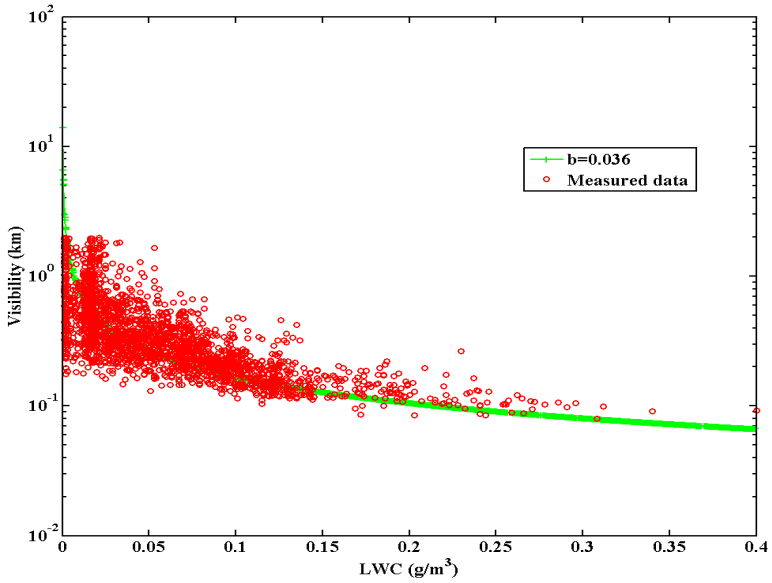

Figure 5.5: Estimated visibility and LWC alongwith real data against new value of b

et al [137] proposed a relationship between visibility range V, and the product of droplet number concentration N_d and LWC as given by equation 5.9.

$$V = 1.002(LWC.N_d)^{-0.6473} \tag{5.9}$$

Here, N_d shows the actual total concentration of fog droplets per cubic centimeter of air. In real atmospheric conditions, however, visibility (extinction of visible light) is related to droplet number and water mass in a given volume of air. Increasing droplet number concentration N_d in warm-fog conditions ($T > 0°C$) for a fixed LWC results in decreasing visibility. The maximum value for N_d and LWC used in the simulation of equation 5.9 are about 400 cm^{-3} and 0.5 g/m^3, respectively, whereas, the minimum values are 1.0 cm^{-3} and 0.005 g/m^3, respectively. This model recognizes the presence of variability in droplet sizes and their contribution towards reduction of visibility range in fog. The simulation results of equation 5.9 are shown in Fig. 5.6 alongwith its comparison with the measured data.

It is obvious from Fig. 5.6 that measured data is close to the value of 400 cm^{-3}. It was attempted to find the optimum value of N_d by calculating RMSE for the measured data and the result is shown in Fig. 5.7. Fig. 5.7 provides valuable insight towards the real values of N_d in continental fog conditions. Fog formation and consequent visibility reduction is observed for values of N_d greater than 100 cm^{-3}.

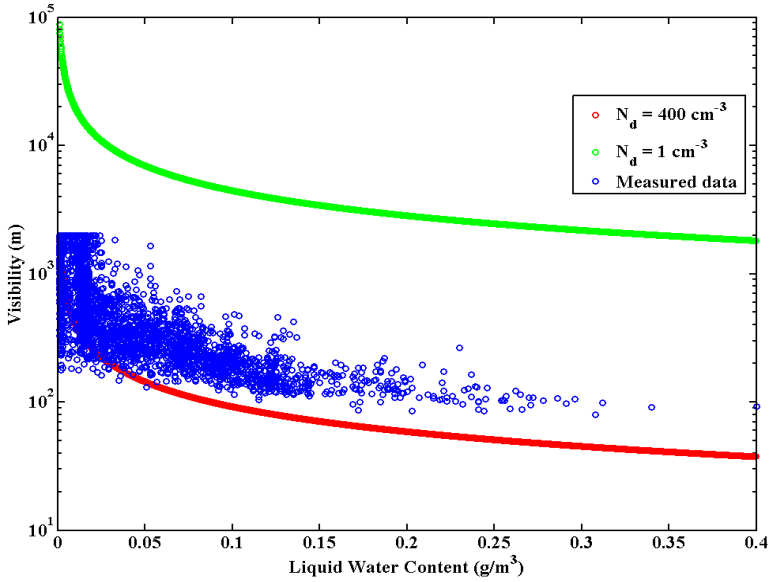

Figure 5.6: Predicted visibility and LWC for different values of N_d

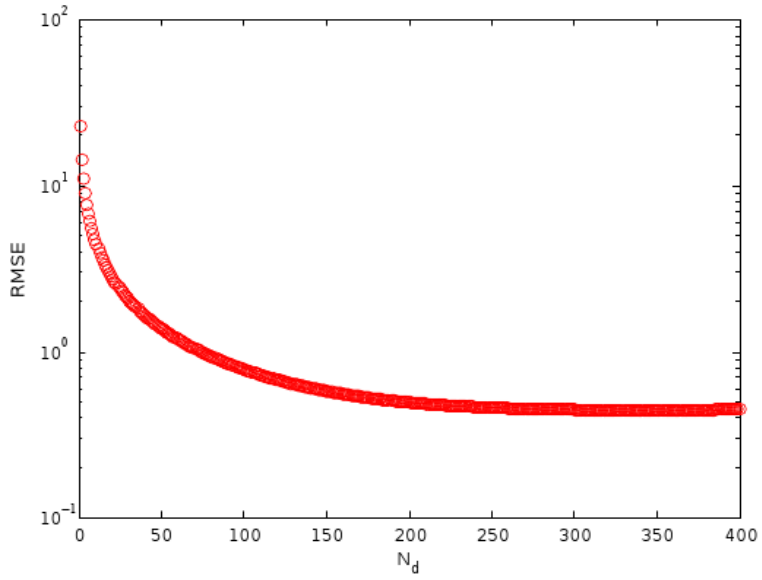

Figure 5.7: Optimum value of N_d for measured data

Estimating fog attenuations through LWC is a useful technique and the existing literature [75, 15] and empirical relation have been found to match closely with real measured data. Generalizing the existing models further does not appear to be an easy task as the value of the coefficient "b" in equation 5.8 and N_d in equation 5.9 would always remain strictly

dependent on the climatic regions of installation and the dynamics (in terms of formation, settling and dissipation phases) of the particular fog event under investigation.

5.3 LWC and optical attenuations

The accurate prediction of optical attenuations in limited atmospheric visibility due to presence of haze, fog and/or clouds remains a challenging task. Very few measurement campaigns have recorded LWC alongside optical attenuation data which reveals interesting insight of the relation between the two. Higher amount of LWC increases the optical attenuation on the link as would appeal to have common scientific understanding of the phenomenon. The graphical illustration of the measured LWC and optical attenuations are provided in Fig. 5.8.

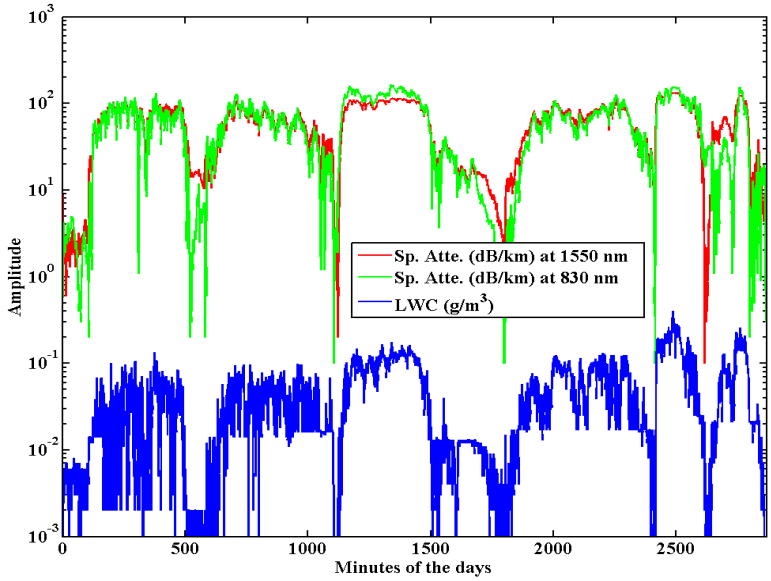

Figure 5.8: Measured data of optical attenuation along with LWC

The Fig. 5.8 plots the LWC (g/m^3) and specific attenuations (dB/km) against the minutes of the day. It is obvious from Fig. 5.8 that higher amount of LWC causes higher optical attenuation. The minimum recorded amount of LWC was 0.001 g/m^3 which caused low optical attenuation, while, the highest recorded amount of LWC was 0.4 g/m^3 which significantly attenuated the transmitted signal (132 dB/km), as seen in Fig. 5.8. It is evident from this plot that optical attenuations decrease with decreasing LWC.

Simultaneous measurements of the liquid water content (LWC), integrated particle surface area (PSA), visibility and optical attenuation have been analyzed to predict optical attenuation caused by fog particles. Attenuation has been measured at two different wavelengths (830 nm and 1550 nm) across co-located links. Five months measured data have been processed to assess an empirical model, which is able to estimate optical attenuation from the

LWC. The proposed model is compared with other published models and it is proven to perform sufficiently well to predict optical attenuation if the LWC values are available.

The purpose of the current work is to use the real measured data of the optical attenuation, LWC, integrated particle surface area (PSA) and visibility, which were measured simultaneously in Prague to predict optical attenuation from the LWC. Five months real time measured data of optical attenuations along with the LWC at Prague provided us a chance to improve and validate an empirical relationship between the LWC and optical attenuation.

5.4 Analysis of Measurements

LWC is the mass of water in a fog/cloud in a specified volume of dry air and it is usually given in g/m^3. Small amounts of LWC ($< 0.05 g/m^3$) usually result in light fog while, high amount of LWC ($> 0.5 g/m^3$) result in the formation of thick or dense fog (approximate visibility range of 50 m) [75].

In the measurement campaign, we sampled data at a rate of one sample per minute. The other instruments were calibrated in a way to measure the specific quantity at the last second of every minute in parallel with the optical attenuation. We selected the data set for analysis where the visibility was less then 1 km. Fig. 5.8 shows the reduced data set of optical attenuation and the corresponding variation of LWC. The LWC is plotted in blue, whereas, optical attenuation is in red for 1550 nm and in green for 830 nm, respectively. It is also important to remark that the time axis in the Fig. 5.8 is not continuous. From Fig. 5.8, a direct relationship between optical attenuation and the LWC can be observed. We selected a subset of the entire data set of Fig. 5.8, to find out the empirical relationship between the LWC and specific optical attenuation. We selected the attenuation data at wavelength 1550 nm. The reason for selecting attenuation data for analysis against this wavelength is its increasing importance for future FSO systems [141]. The remaining data has been used to verify the relationship (see Section 5). The descriptive statistics of the selected data set is provided in Table 5.2.

It is very important to mention that the selected data set which has been used to formulate a model contains a wide range of the LWC varying from 0.001 g/m^3 to 0.4 g/m^3 (Table 5.2). Most fogs have the LWC ranging from 0.001 g/m^3 to 0.4 g/m^3 [142]. We carried out the regression analysis of selected data to find a relationship between optical attenuation and the LWC. The results are shown in Fig. 5.9.

From Fig. 5.9, following relationship between the said parameters have been attained (shown in Equation (5.10)) with R^2 value of 67.84%,

$$A_{1.55\mu m} = 243.57(LWC)^{0.4189} \tag{5.10}$$

Table 5.2: Descriptive statistics of the LWC and Optical attenuations

Statistical parameter	LWC(g/m^3)	Attenuation (dB/km)
Range	0.399	120.5
Mean	0.103	90.921
Variance	0.0039	836.88
Std. Deviation	0.0622	28.929
Minimum	0.001	12
25% (Q1)	0.0585	73.27
50% (Median)	0.099	100.2
75% (Q3)	0.1313	110.52
Maximum	0.4	132.5

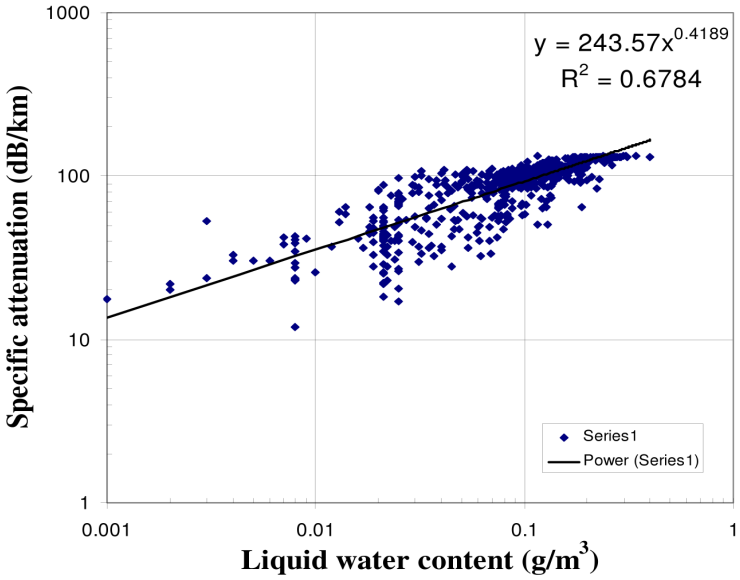

Figure 5.9: Relationship between optical attenuation and the LWC

where, A represents optical attenuation in dB/km and the LWC represents the corresponding liquid water content measured in g/m^3. Hereafter, Equation (5.10) would be referred to as Model A.

5.5 Model Verification

We verified the proposed model by selecting a different set of fog data measured during the campaign. In Fig. 5.10, the model has been plotted and the measured data points have been superimposed. The close match of the proposed model with real measurement from a different fog event validates the model and thus, the simple relationship in Equation (5.10) can be directly used for estimating optical attenuation from the LWC.

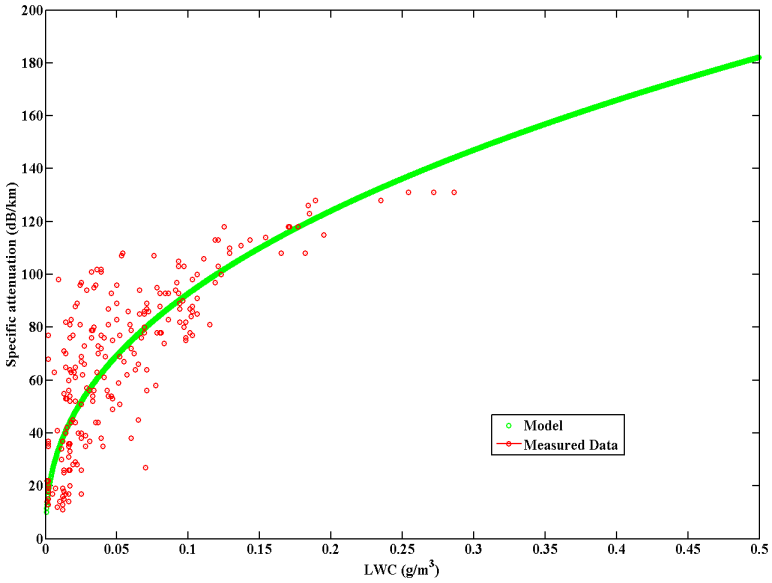

Figure 5.10: Verification of the proposed model

Table 5.3: Verification of random sample point from measured data

Measured Values		Predicted attenuation	RMSE	Percentage error
LWC	A	-	-	-
0.111	93.18	96.98	3.80	4.08
0.131	106.25	103.95	2.30	2.16
0.134	100.29	104.94	4.65	4.64
0.115	97.5	98.43	0.93	0.95
0.112	97.95	97.35	0.60	0.61
0.093	86.44	90.06	4.13	4.18
0.032	59.257	57.60	1.65	2.80
0.03	54.81	56.06	1.25	2.28
0.027	57.84	54.64	3.20	5.53
0.08	84.49	84.55	0.06	0.07

For a more rigorous analysis 10 random samples from the measured data have been selected and the accuracy of prediction has been tabulated in Table 5.3.

Here, in Table 5.3, the LWC is in g/m^3 and attenuation (A) is in dB/km. Table 5.3 shows that the maximum percentage error incurred by the model remains within 5% of the real measured values. In last column of the Table 5.3, it can be observed that the maximum value of RMSE is 4.65 and minimum value is 0.06, which shows that the proposed model is a good approximation of specific attenuation through the LWC. A significant spread

of measured attenuation values for a single value of the LWC can be expected in measurements (as evident from Fig. 5.10), because the LWC is a point-measurement while, attenuation is average along the path. Average values of the LWC could be used to reduce the effect.

Two fog events recorded on 20-21 January 2009 and 07 February 2009 have been selected for further detailed verification of proposed model at wavelength of 1550 nm and 830 nm.

To the best of authors' knowledge there are three other models available in the open literature to calculate optical attenuation from the LWC. These models are provided in Equations (5.11, 5.12, 5.13).

$$A_{0.785\mu m} = 238(LWC)^{0.86} \tag{5.11}$$

Hereafter, Equation (5.11) would be referred to as Model B for further analysis. Model B [83] can perform well under light fog conditions (attenuation level below 40 dB/km) but may not be suitable for moderate, thick or dense fog conditions because the higher attenuation levels (attenuation higher than 40 dB/km) have been extrapolated [83]. Two other models are given in following Equations (Equation 5.12, 5.13) [143].

$$A_{0.63\mu m} = 360(LWC)^{0.64} \tag{5.12}$$

$$A_{0.785\mu m} = 610(LWC) \tag{5.13}$$

Equation (5.11, 5.13) would be referred to as Model C and Model D respectively, for further discussion. The simulation results along with the measured data of fog event recorded on 20-21 January 2009 at operational wavelength of 1550 nm are provided in Fig. 5.11.

The simulation results along with the measured data of fog event recorded on 07 February 2009 at 1550 nm wavelength are provided in Fig. 5.12.

It is obvious from Fig. 5.11 and Fig. 5.12 that there is a close match of measured data with Model A for all ranges of optical attenuations whereas, measured data is highly deviated from Model B and Model D. Model C can be used for higher levels of optical attenuations but it is not suitable for lower levels of optical attenuations. We used mean percentage error criterion to find the best fit model among the above four. The percentage error is given in Equation (5.14)

$$\Delta(\%) = 100.|\frac{M_d - P_d}{M_d}| \tag{5.14}$$

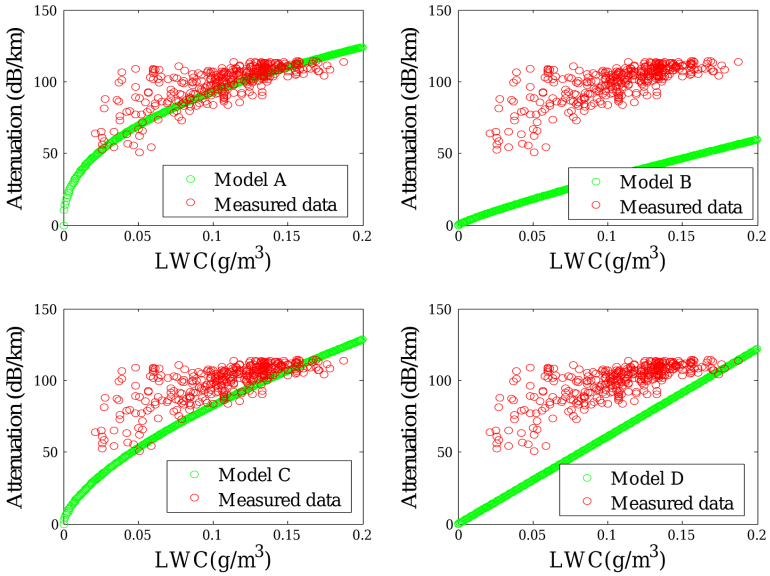

Figure 5.11: Comparison of the models with measured data using 1550 nm wavelength

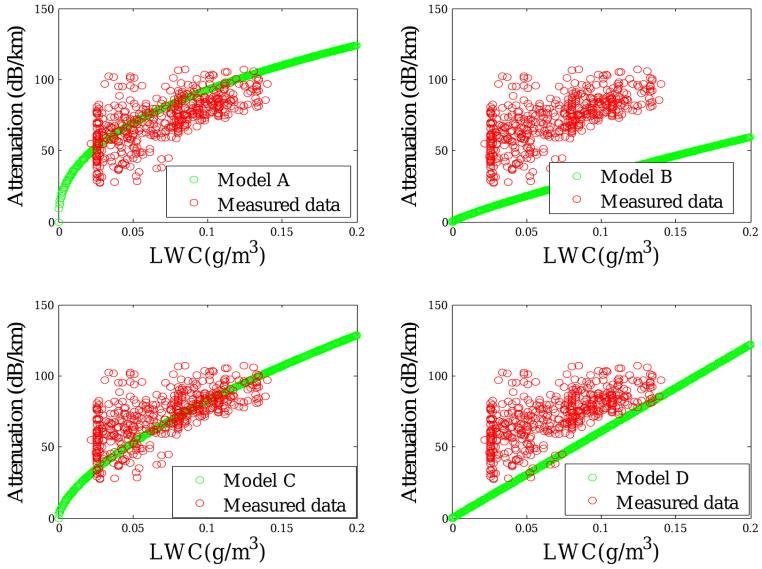

Figure 5.12: Comparison of the models with measured data using 1550 nm wavelength

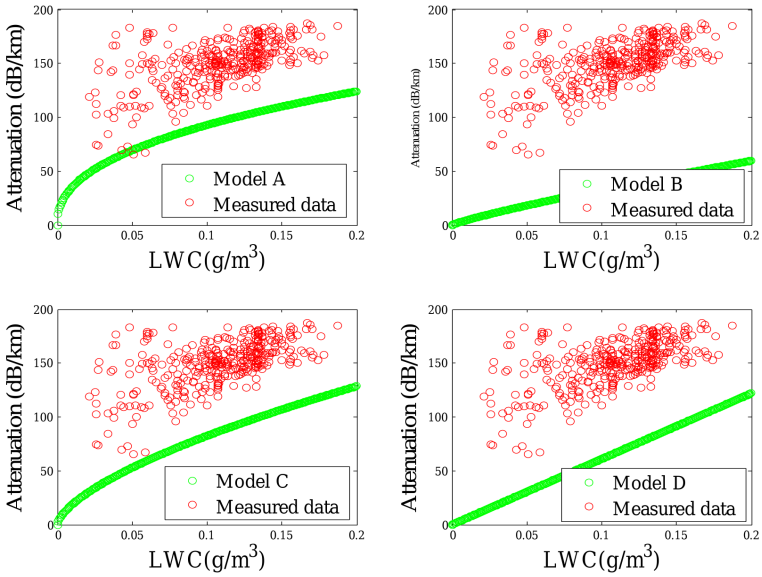

Figure 5.13: Comparison of the models with measured data, wavelength 830 nm

Where, M_d is measured data and P_d is predicted data. And we calculated the mean value of the above given percentage error. The mean percentage error of the fog attenuation is provided in Table 5.4.

Table 5.4: Mean percentage error for considered fog events

Mean percentage error of attenuation				
Fog Event	Model A	Model B	Model C	Model D
20-21 January	26.4	67.4	36.0	49.1
7 February	36.2	58.2	41.7	45.1

It is obvious from Table 5.4 that our proposed model is performing best as compared to other models.

The measured data of optical attenuation at 830 nm, provided us a chance to verify the existing models (including our proposed model) in order to evaluate them at different wavelengths. The simulation results along with the measured data of fog event recorded on 20-21 January 2009 at operational wavelength of 830 nm are provided in Fig.5.13.

The simulation results along with the measured data of selected fog event recorded on 07 February 2009 are provided in Fig. 5.14.

The mean percentage error of the fog attenuation is provided in Table 5.5.

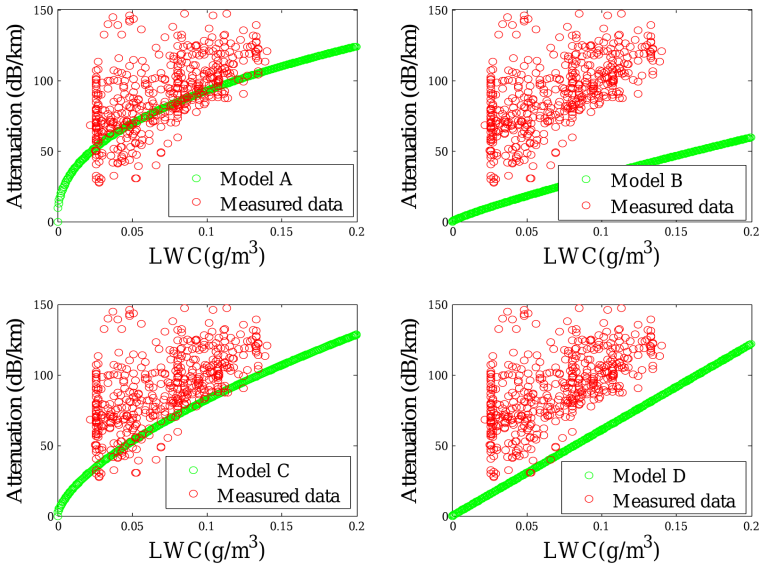

Figure 5.14: Comparison of the models with measured data, wavelength 830 nm

Table 5.5: Mean percentage error for considered fog events

Mean percentage error of attenuation				
Fog Event	Model A	Model B	Model C	Model D
20-21 January	43.5	77.3	49.9	60.1
7 February	24.1	64.8	31.7	44.7

It is also obvious from Table 5.5 that our proposed model with the least value of mean percentage error is performing better as compared to the other models at wavelength of 830 nm. The results in Fig. 5.11, 5.12, 5.13, 5.14 suggest that optical attenuation due to fog does not exhibit significant dependence on wavelengths ranging between 800 and 1600 nm (taking into account uncertainties due to spread of measured data).

6 Conclusions and future work

FSO has great potential to meet the needs of high data rate communication applications. Thorough investigations of weather effects, specially fog, on FSO links is of prime importance to achieve carrier class availability and reliability. This thesis presents the analysis of fog effects using the measured data and provides statistical model under continental fog conditions. This thesis also provided the linearity or homogeneity analysis of optical attenuation using the measured data of across collocated links. The linearity analysis will give a significant insight about the measured campaigns, in future, at longer distance. This thesis also presents the effects of LWC on FSO links and LWC based model to predict optical attenuation.

6.1 Concluding remarks

This thesis presents the detailed analysis of measured optical attenuations caused by reduced visibility due to fog, at three different locations i,e. Graz (Austria); Prague (Czech Republic) and Milan (Italy). The most significant part of the fog attenuation analysis is the linearity or homogeneity analysis of optical attenuation. In Prague (Czech Republic) two collocated links were installed, with different path lengths, during the measurement campaign. The measured data of collocated links, installed at Prague, were used to investigate the linearity of optical attenuation. The linearity of the measured optical attenuations has been investigated by comparing the data of 100 m and 853 m path link. Although the correlation between the optical attenuation measured at 100 m path length and 853 m path length is not strong enough, and that the optical attenuation in 100 m and 853 m is partially linearly correlated which is consistent with the general assumption of the homogeneity of the fog events in a short distance link. The possible reason for such less correlation in the current result is the measurement error in which the fade margin of 853 m path link is about 15 dB. Thus, some optical attenuations of 853 m path link are saturated and can not be precisely compared with that of 100 m path link. The scattering effects due to continental fog have been simulated. The simulation results were compared with the measured data of Prague. The results suggest that there is very less probability of occurrence of multiple scattering for Prague case. This is due to the fact that in Prague there occurred only thick fog. The simulation results show that multiple scattering is not significant for fog particles with diameter 1 μm but multiple scattering becomes critical for the particles having diameter of 50 μm. However, particle concentration is an important factor which affects the multiple scattering, which suggest that multiple scattering occurs at very dense fog conditions.

The measured data of Graz and Prague have been used to analyze statistically and proposed a probabilistic model for FSO links. The high variability of attenuation can cause link outages that could last up to several hours. The empirical models like the famous Kim Kruse and Al-Naboulsi models provide reasonable estimates for optical attenuation under fog. However, they shed no light towards the distribution of the received signal strength. The statistical models presented in this thesis shall yield better understanding of the spatial and temporal variations of the fog attenuation. The Wakeby distribution has been found as appropriate for dense fog, logistic distribution for thick fog, Johnson S_B for moderate and light fog and Kumaraswamy's distribution for general continental fog. These results suggest that these distributions can provide suitable estimates for received signal strength under dense, thick, moderate, light and general continental fog conditions. The measured data at Prague has been used further to investigate and provide the statistics of optical attenuation in another continental environment. The PDF estimation of received signal strength puts forth that Kumaraswamy's distribution as the most appropriate to describe the characteristics of settled continental fog conditions for measured data of optical attenuation at Prague. The Kumaraswamy's distribution has been found best fit probabilistic model for continental fog conditions as it describes well the statistical characteristics of optical attenuations measured at Graz and Prague.

Different atmospheric quantities like LWC, visibility, PSA and optical attenuation have been measured at two different wavelengths and path lengths. The simultaneous measured data of LWC and optical attenuation provides us a chance for thorough investigations of the effects of LWC on optical attenuation. The detailed analysis of effects of LWC on optical attenuations has been presented in this thesis along with a new proposed model. Five months measurement of optical attenuation and the liquid water content (LWC) have been used to draw a new model for direct estimation of optical attenuation from the LWC. A comparison with other existing models shows that the new proposed model performs better and that it provides sufficiently accurate estimates of optical attenuation. The analysis in this thesis has also shown that taking into account the significant spread of measured data, it is generally difficult to establish any clear wavelength dependence of the relation between attenuation and the LWC in the range of 800 - 1600 nm. In this respect however, the model D valid for 10.6 μm has to be treated separately and it was included only for comparison at standard FSO operational wavelengths. It is for this reason, that optical attenuation at wavelengths around 11 μm is known to be linear with LWC, according to the principles of scattering theory. Though there may be some variations for the optical attenuation in the classical optical windows, the model proposed can be used conveniently in the range of wavelengths from 800-1600 nm for estimation of optical attenuation based on LWC with reasonable accuracy.

6.2 Future works

Some studies need to be conducted in future to strengthen our current findings of linearity or homogeneity of fog along the path length. This study can be done by using some

fog sensors in between the transceivers. It is proposed that fade margin of FSO system installed at longer path length should be the multiple of the fade margin and path length of FSO system installed at smaller path length to investigate the affect precisely.

The simulation of scattering under continental fog conditions has been presented. In the future there should also be some detailed investigations on the phenomenon of multiple scattering. The simulation provided in this thesis will provide fundamental concepts and basic knowledge of multiple scattering phenomenon for future investigations. The effects of multiple scattering on data rates and system specification requirements would be a great field to investigate.

Due to high variability of attenuations and atmospheric conditions of Graz and Prague (Specially Graz) a distribution model has been proposed which can be used by any continental environment. Channel estimation and equalization should be of great interest to investigate it in the future, based on Kumaraswamy's distribution.

The effects of LWC on FSO links has been investigated in this thesis. In future the effects of LWC on FSO links during the different stages of fog like fog formation and fog dissipation stages should be investigated.

Much achievements have been gained during the course of this work. Many new questions are foreseen to arise as these newly proposed ideas reach for industrial development and system development with the proposed probabilistic model and LWC based optical attenuation model.

References

[1] S. Arnon and D. Kedar. Urban optical wireless communication networks: The main challenges and possible solutions. *IEEE Commun. Mag*, 42:S2–S7, 2004.

[2] S. S. Muhammed, B. Flecker, E. Leitgeb, and M. Gebhart. Characterization of fog attenuation in terrestrial free space optical links. *Journal of Optical Engineering*, 46(6):066001, June 2007.

[3] M. Jeganathan and P. Ionov. Multi-gigabits per second optical wireless communications. www.freespceotic.com, 2000.

[4] E. Leitgeb and et al. Current optical technologies for wireless access. In *ConTel*, 2009.

[5] K. W. Fischer, M. R. Witiw, J. A. Baars, and T. R. Oke. Atmospheric laser communication: New challenges for applied meteorology. *Bulletin of the American Meteorological Society*, 85(5):725Ű732, May 2004.

[6] H. Willebrand and B.S.Ghuman. *Free space optics: enabling optical connectivity in today's networks*. Sams Publishing, 2002.

[7] M. Gebhart. Optical space communication. Master's thesis, Department of Space Science, Graz University, 2007.

[8] S. Das, H. Henniger, B. Epple, C.I. Moore, R. Sova W. Rabinovich, and D. Young. Requirements and challenges for tactical free-space lasercomm. In *MILCOM*, 2008.

[9] M. Aharonovich and S. Arnon. Performance improvement of optical wireless communication through fog with a decision feedback equalizer. *J. Opt. Soc. Am. A*, 22(8):1646–1654, 2005.

[10] M. K. Carson. *Sterling Biographies: Alexander Graham Bell: Giving Voice to the World*. Sterling Publishing, 2007.

[11] E. Leitgeb, M. Gebhart, A. Truppe, U. Birnbacher, P. Schrotter, and A. Merdonig. Hybrid wireless networks for civil-military-cooperation (cimic) and disaster management. In *Proceedings of SPIE*, volume 5614, 2004.

[12] M. S. Awan, R. Nebuloni, C. Capsoni, L. Csurgai-Horváth, S. Sheikh Muhammad, E. Leitgeb, and F. Nadeem andM. S. Khan. Prediction of drop size distribution parameters for optical wireless communications through moderate continental fog. *International Journal on Satellite Communications and Networks*, 28, August 2010.

[13] H. Willebrand and B. Ghuman. Fiber optics without the fiber. *IEEE Spectrum*, 38:40Ű45, 2001.

[14] A. K. Majumdar and J. C. Ricklin, editors. *Free-Space Laser Communications: Principles and Advances*. Springer, 2008.

[15] M. S. Awan. *Statistical-Dynamical Channel Modeling of Outdoor OpticalWireless Links*. PhD thesis, TU Graz, 2010.

[16] L. Andrews, R. Phillips, and C. Hopen. *Laser Beam Scintillation With Applications*. SPIE Press, New York, 2001.

[17] D. Giggenbach, J. Horwath, and M. Knapek. Optical data downlinks from earth observation platforms. In *Free-Space Laser Communication Technologies*, 2009.

[18] T. Tolker-Nielson and G. Oppenhauser. In-orbit test result of an operational optical intersatellite link between artemis and spot4, silex. In *Proc. SPIE*, 2002.

[19] A. Pavelchek, R. Trissel, J. Plante, and S. Umbrasas. Long wave infrared (10 micron) free space optical communication system. In *In Proceedings of SPIE*, 2004.

[20] A. Soibel, M. Wright, W. Farr, S. Keo, C. Hill, R. Q. Yang, and H. C. Liu. Mid-infrared interband cascade lasers for free-space laser communication. In *In Proceeding of SPIE*, 2009.

[21] Y. Arimoto. Compact free-space optical terminal for multi-gigabit signal transmissions with a single mode fiber. In *In Proceedings SPIE*, 2009.

[22] A. K. Majumdar and J. C. Ricklin. *Free-Space Laser Communications, Principles and Advantages*. Springer Science, 2008.

[23] J. Schuster. Free space optics (fso) technology overview. Presentation given by J. Schuster (Chief Technology Officer Terabeam Corporation) in 2002.

[24] B. R. Strickland, M. J. Lavan, E. Woodbridge, and V. Chan. Effects of fog on the bit-error rate of a free-space laser communication system. *Appl. Opt.*, 38:424–431, 1999.

[25] M. Gebhart, E. Leitgeb, S. S. Muhammad, B. Flecker, C. Chlestil, M. Al Naboulsi, F. de Fornel, and H. Sizun. Measurement of light attenuation in dense fog conditions for fso applications. In *SPIE Proceedings*, 2005.

[26] B. Flecker, M. Gebhart, E. Leitgeb, S. Sheikh Muhammad, and C. Chlestil. Results of attenuation-measurements for optical wireless channels under dense fog conditions regarding different wavelengths. In *SPIE Proceedings*, 2006.

[27] R. Nebuloni and C. Capsoni. Effect of hydrometeor scattering on optical wave propagation through the atmosphere. In *EuCAP 2011*, 2011.

[28] I. Kim, B. McArthur, and E.Korevar. Comparison of laser beam propogation at 785 nm and 1550 nm in fog and haze for optical wireless communications. In *In Proceedings of SPIE*, 2000.

[29] N. Perlot, D. Giggenbach, H. Henniger, J. Horwath, M. Knapek, and K. Zettl. Measurements of the beam-wave fluctuations over a 142 km atmospheric path. In *Proc. SPIE*, 2006.

[30] F. David, D. Giggenbach, R. Landrock, K. Pribil, E. Fischer, R. Buschner, and D. Blaschke. Preliminary results of a 61km ground-to-ground optical im/dd data transmission experiment. In *Free-Space Laser Communication Technologies XIV*, 2002.

[31] N. Perlot. *Characterization of Signal Fluctuations in Optical Communications with Intensity Modulation and Direct Detection through the Turbulent Atmospheric Channel*. PhD thesis, School of Electronique, Université de Valenciennes, 2005.

[32] O. Bouchet, H. Sizun, C. Boisrobert, F. D. Fornel, and P. Favennec. *Free-Space Optics: Propagation and Communication*. ISTE, 2006.

[33] S. Glisic. *Advanced Wireless Communications 4G Technologies*. John Wiley and Sons Ltd, 2004.

[34] H. Hemmati. *Near-Earth Laser communications*. CRC Press, Taylor and Francis Group, 2009.

[35] E. Kube. Information transmission by light beams through the atmosphere. *Nachrichtentechnik*, 6:201–207, 1968.

[36] M. S. Khan, S. S. Muhammad, M. S. Awan, V. Kvicera, M. Grabner, and E. Leitgeb. Further results on fog modeling for terrestrial fso links. *Accepted for Publication in Journal of Optical Engineering*, Vol. 51, 2012.

[37] S. Bloom, E. Korevaar, J. Schuster, and H. Willebrand. Understanding the performance of free space optics. *Journal of Optical Networking*, 2003.

[38] D.J.T. Heathley, D.R. Wisely, I. Neild, and P. Cochrane. Optical wireless: The story so far. *IEEE Communications Magazine*, pages 72–82, 1998.

[39] S. Arnon. *Optical Wireless Communications*, chapter In Encyclopedia of Optical Engineering, pages 1866–1886. Marcel Dekker, New York, USA, 2000.

[40] S. Bloom. The physics of free space optics. White paper (Air Fiber, Inc), 2002.

[41] E. Korevaar, I. Kim, and B. McArthur. Atmospheric propagation characteristics of highest importance to commericial free space optics. In *MRV Communications*, 1998.

[42] M. Gebhart, E. Leitgeb, U. Birnbacher, and P. Schrotter. Ethernet access network based on free-space optic deployment technology. In *Proc. of SPIE*, pages 131–142, 2004.

[43] E. Leitgeb, M. Gebhart, P. Fasser, J. Bergenzer, and J. Tanczos. Impact of atmospheric effects in free space optics transmission systems. In *Proc. of SPIE*, pages 86–97, 2003.

[44] F. de Fornel, M. Gebhart, E. Leitgeb, M. Al Naboulsi, and H. Sizun. Availability prediction for free space optic communication systems from local climate visibility data. In *In Short Term Scientific Report 4. COST270*. 2003.

[45] P. M. Pierce, E. Eisenberg, and J. Ramaprasad. Optical attenuation in fog and clouds. In *Proceedings of SPIE*, volume 4530, 2001.

[46] D. Kedar and S. Arnon. Optical wireless communication though fog in the presence of pointing errors. *Applied Optics*, 42(24):4946–4954, 2003.

[47] S. Arnon. The effects of atmospheric turbulence and building sway on optical wireless communication systems. *Optics Letters*, 28(2):129–131, 2003.

[48] S. A. Zabidi, W. A. Khateeb, Md. R. Islam, and A.W. Naji. The effect of weather on free space optics communication (fso) under tropical weather conditions and a proposed setup for measurement. In *ICCCE 2010*, 2010.

[49] M. S. Awan, Marzuki, E. Leitgeb, F. Nadeem, M. S. Khan, and C. Capsoni. Weather effects impact on the optical pulse propagation in free space. In *VTC*, 2009.

[50] A. A. G. Abushagur, F. M. Abbou, M. Abdullah, and N. Misran. Performance analysis of a free-space terrestrial optical system in the presence of absorption, scattering, and pointing error. *Opt. Eng*, 50:075007, 2011.

[51] S. A. Zabidi, W. A. Khateeb, and et al. The effect of weather on free space optics communication (fso) under tropical weather conditions and a proposed setup for measurement. In *ICCCE*, 2008.

[52] D. C. O'Brien. Improving coverage and data rate in optical wireless systems. In *Proc. of SPIE*, 2005.

[53] S. Arnon. Optimization of urban optical wireless communication systems. *IEEE Transcations on Wireless Communications*, 2(4):626–629, 2003.

[54] E. Korevar, B. McArthur, and I. Kim. Debunking the recurring myth of a magic wavelength for free space optics. In *In Proceedings of SPIE*, 2002.

[55] D.A. Rockwell and G.S. Mecherle. Wavelength selection for optical wireless communication systems. In *In Optical Wireless Communications IV, Proc. of SPIE*, 2001.

[56] H. Manor and S. Arnon. Performance of an optical wireless communication system as a function of wavelength. *Applied Optics*, 42(21):4285–4294, 2003.

[57] M. Achour. Free-space optics wavelength selection: 10 micrometer versus shorter wavelengths. *Journal of Optical Networking*, 2(6):127–143, 2003.

[58] E. Leitgeb, M. Gebhart, and P. Fasser. Reliability of free space laser communications: Investigations at technical university graz. In *In Proceedings and Presentations at the 8th Annual WCA Technical Symposium*, 2002.

[59] E. Leitgeb, S.S. Muhammad, C. Chlestil, M.Gebhart, and U. Birnbacher. Reliability of fso links in next generation optical networks. In *In 7th International Conference on Transparent Optical Networks ICTON*, 2005.

[60] V. V. Ragulsky and V. G. Sidorovich. Availability of a free-space optical communication link operating under various atmospheric conditions. In *In Optical Wireless Communications IV, Proc. of SPIE*, 2001.

[61] A. Al-Habash, K.W. Fischer, C.S. Cornish, and J. Nash. Comparison between experimental and theoretical probability of fade for free-space optical communications. In *In Optical Wireless Communications V, Proc. of SPIE*, 2002.

[62] D.S. Sica and E.H. Castro. Conditions for free-air laser communications in buenos aires. In *In Free Space Laser Communications V, Proc. of SPIE*, 2005.

[63] A. Prokes. Atmospheric effects on availability of free space optics systems. *Opt. Eng*, 48:066001, 2009.

[64] E. Leitgeb, S. S. Muhammad, C. Chlestil, M.Gebhart, G.Kandus, and T. Javornik. Importance of reliable optical wireless links in the evolving broadband network. In *In The 9th World Multi-Conference on Systemics, Cybernetics and Informatics (WMSCI)*, 2005.

[65] E. Leitgeb, M. Gebhart, U. Birnbacher, W. Kogler, and P. Schrotter. High availability of hybrid wireless networks. In *In SPIE International Symposium Photonics Europe, Proc. of SPIE*, 2004.

[66] I.I. Kim and E.J. Korevaar. Availability of free-space optics and hybrid fso/rf systems. In *In Optical Wireless Communications IV, Proc. of SPIE*, 2001.

[67] S. H. Bloom and W. H. Hartley. Hybrid fso radio (hfr): some preliminary results. In *In Optical Wireless Communications V, Proc. of SPIE*, 2002.

[68] J. Llorca, A. Desai, E. Baskaran, S. Milner, and C. Davis. Optimizing performance of hybrid fso/rf networks in realistic dynamic scenarios. In *In Free Space Laser Communications V, Proc. of SPIE*, 2005.

[69] F. Nadeem. *Investigation on Switching Technologies for HybridWireless Networks (RF and FSO)*. PhD thesis, Institute for Broadband Communication, 2010.

[70] L. C. Andrews, R. L. Phillips, and C. Y. Hopen. *Laser Beam Scintillation With Applications*. SPIE Press Monograph Series. Bellingham, WA: SPIE Optical Engineering Press, 2001.

[71] F. S. Vetelino, C. Young, and L. C. Andrews. Fade statistics and aperture averaging for gaussian beam waves in moderate-to-strong turbulence. *Appl. Opt*, 46:3780, 2007.

[72] G. Parry. Measurement of atmospheric turbulence induced intensity fluctuations in a laser beam. *J. Mod. Opt*, 28:715Ű728, 1981.

[73] L. C. Andrews and R. L. Phillips. Measured statistics of laserlight scattering in atmospheric turbulence. *J. Opt. Soc. Am*, 71(12):1440Ű1445, 1981.

[74] M. A. Al-Habash, L. C. Andrews, and R. L. Phillips. Mathematical model for the irradiance probability density function of a laser beam propagating through turbulent media. *Opt. Eng*, 40(8):1554Ű1562, 2001.

[75] S. S. Muhammad, M. S. Awan, and A. Rehman. Pdf estimation and liquid water content based attenuation modeling for fog in terrestrial fso links. *Radioengineering*, 19, 2010.

[76] B. Epple. Simplified channel model for simulation of free-space optical communications. *J. Opt. Commun. Netw.*, 2(3):293–304, 2010.

[77] C. Kontogeorgakis. Millimeter through visible frequency waves through aerosols particle modeling, reflectivity and attenuation. Master's thesis, Virginia Polytechnic Institute and State University, 1997.

[78] P.W. Kruse and al. *Elements of infrared technology: Generation, Ttransmission and Detection*. J. Wiley and Sons, New York, 1962.

[79] M. Al Naboulsi, H. Sizun, and F. de Fornel. Fog attenuation prediction for optical and infrared waves. *Optical Engineering*, 43(2):319–329, 2004.

[80] R. E. Roberts and L. N. Seekamp. Infrared attenuation by aerosols in limited atmospheric visibility: relationship to liquid water content. In *IDA PAPERMarch*, 1979.

[81] G. Tonna and C. Valenti. optical attenuation coefficients and liquid water content relationship in fog, at seventy four wavelengths from 0.35 to 90 micrometer. *Atmospheric Environment*, 17(10):2075–2080, 1983.

[82] G. Tonna. Backscattering, extinction, and liquid water content in fog: a detailed study of their relations for use in lidar systems. *Applied Optics*, 30(9):1132–1140, 1991.

[83] L. Csurgai-Horvath and I. Frigyes. Characterization of fog by liquid water content for use in free space optics. In *In Proceedings of ConTEL*, 2011.

[84] H. Vasseur, C. Oestges, and A. V. Vorst. Influence de la troposph?cre sur les liaisons sans fil aux ondes millimt'etriques et optiques. In *in Propagation t'electromagnt'etique du dt'ecamt'etrique t'r lŠangstrĺom, Rennes*, 1997.

[85] E. Leitgeb, J. Bregenzer, M. Gebhart, P. Fasser, and A. Merdonig. Free space optics - broadband wireless supplement to fiber-networks. In *In the proceeding of SPIE*, volume 4975, 2003.

[86] M. S. Khan et al. Probabilistic model for free-space optical links under continental fog conditions. *Radioengineering*, 19, 2010.

[87] M. S. Khan, M. S. Awan, E. Leitgeb, F. Nadeem, and I. Hussain. Selecting a distribution function for optical attenuation in dense continental fog conditions. In *In the Proceeding of ICET*, 2009.

[88] V. Kvicera M. Grabner. The wavelength dependent model of extinction in fog and haze for free space optical communication. *Optics Express*, 19(4):3376–3386, 2011.

[89] Z. Z. Wei and W. Zhen-Sen. Millimeter-wave attenuation due to fog and clouds. *International Journal of Infrared and Millimeter Waves*, 21(10):1607–1615, 2000.

[90] Federal Meteorological Handbook No. 1. Surface weather observations and reports. In *U.S. DOC/NOAA, Washington, DC*. 1995.

[91] H. R. Pruppacher and J. D. Klett. *Microphysics of Clouds and Precipitation*. Kluwer Pub, 2nd edition edition, 1997.

[92] I. Gultepe et al. Fog research: a review of past achievements and future perspectives. *J. of Pure and Applied Geophy*, 164:1121–1159, 2007.

[93] M. Gazzi, V. Vincentini, and C. Pesci. Dependence of a black targetŠs apparent luminance on fog droplet size distribution. *Atmos. Environ*, 31:3441Ű3447, 1997.

[94] L. R. Bissonnette. Imaging through fog and rain. *Opt. Eng*, 31:1045Ű1052, 1992.

[95] M. Gazzi, T. Georgiadis, and V. Vincentini. Distant contrast measurements through fog and thick haze. *Atmos. Environ*, 35:207Ű222, 2001.

[96] H. C. van de Hulst. *Light Scattering by Small Particles*. Dover Publications, Leiden Observatory, 1981.

[97] C. F. Bohren and D. R. Huffman. *Absorption and Scattering of Light by Small Particles*. Wiley-Interscience , first edition, 1998.

[98] E. P. Shettle. Models of aerosols, clouds, and precipitation for atmospheric propagation studies. *presented at Atmospheric Propagation in the UV, Visible, IR, and MM Wave Region and Related System Aspects, AGCARD Conf. 454(15)*, page 1Ű13, 1989.

[99] D. Harris. The attenuation of electromagnetic waves due to atmospheric fog. *International Journal of Infrared and Millimeter Waves*, 16(6):1091Ű1108, 1995.

[100] O. Gaceu. Climate characteristics of the fog phenomenon and its influence on the tourists and the tourist activities in the apuseni mountains. *GeoJournal of Tourism and Geosites*, 3:29–34, 2009.

[101] M. S. Awan et al. Prediction of drop size distribution parameters for optical wireless communications through moderate continental fog. *International journal of satellite communications and networking*, 29:97Ű116, 2009.

[102] P. W. Kruse, L. D. McGlauchlin, and R. B. McQuistan. *Elements of Infrared Technology: Generation, Transmission, and Detection*. J. Wiley & Sons, 1962.

[103] R. M. Pierce, J. Ramaprasad, and E. C. Eisenberg. Optical attenuation in fog and clouds. In *Proc. SPIE*, 2001.

[104] T. H. Carbonneau and D. R. Wisely. Opportunities and challenges for optical wireless: the competitive advantage of free space telecommunications links in todayŠs crowded marketplace. In *SPIE Proceedings*, page 119Ű128, 1998.

[105] G. S. Mecherle. Mitigation of atmospheric effects on terrestrial free space optical communication systems. In *SPIE Proceedings*, 2004.

[106] F. Nadeem and E. Leitgeb. Dense maritime fog attenuation prediction from measured visibility data. *Radioengineering*, 19, 2010.

[107] J. Pesek, O. Fiser, J. Svoboda, and V. Schejbal. Modeling of 830 nm fso link attenuation in fog or wind turbulence. *Radioengineering*, 19, 2010.

[108] M. Achour. Simulating atmospheric free-space optical propagation: Part i, rainfall attenuation. In *SPIE Proceedings*, volume 4635, page 192Ű201, 2002.

[109] W. G. Tam and A. Zardecki. Multiple scattering corrections to the beer-lambert law w. g. tam and a. zardecki,1: Open detector. *Applied Optics*, 21(13):2405–2412, 1982.

[110] A. Zardecki and W. G. Tam. Multiple scattering corrections to the beer-lambert law. 2: Detector with a variable

eld of view. *Applied Optics*, 21(13):2413–2420, 1982.

[111] S. Arnon, D. Sadot, and N.S. Kopeika. Simple mathematical models for temporal, spatial, angular, and attenuation characteristics of light propagating through the atmosphere for space optical communication. *Journal of Modern Optics*, 41(10), 1994.

[112] V. Brazda, O. Fiser, and J. Svoboda. Fso and radio link attenuation: meteorological models verified by experiment. In *Proc. SPIE*, volume 8162, 2011.

[113] L. Csurgai-Horvath and I. Frigyes. Characterization of fog by liquid water content for use in free space optics. In *Contel*, 2011.

[114] M. Al Naboulsi, F. de Fornel, H. Sizun, M. Gebhart, E. Leitgeb, S. S. Muhammad, B. Flecker, and C. Chlestil. Measured and predicted light attenuation in dense coastal upslope fog at 650, 850, and 950 nm for free-space optics applications. *Optical Engineering*, 47(3):036001, 2008.

[115] V. Kvicera and and O. Fiser M. Grabner. Visibility and attenuation due to hydrometeors at 850 nm measured on an 850 m path. In *CSNDSP*, 2008.

[116] M. S. Khan, M. S. Awan, S. S. Muhammad, M. Faisal, Marzuki, F. Nadeem, and E. Leitgeb. Probabilistic model for free-space optical links under continental fog conditions. *Radioengineering*, 19(3):460–465, 2010.

[117] Czech Hydrometeorological Institute. http://www.chmi.cz/meteo/ok/klemintroe.html. visited on 10 October 2010.

[118] E. Leitgeb and et al. Current optical technologies for wireless access. In *ConTel 2009*, Zagreb, Croatia, 2009.

[119] Dirk Giggenbach, Hennes Henniger, Nicolas Perlot, and Florian David. Multiple-wavelength free-space laser communications. In *Proc. SPIE*, volume Vol. 4975, pages 12–19, July 2003.

[120] A. Biswas and S. Lee. Ground-to-ground optical communications demonstration. *Jet Propulsion Laboratory, Pasadena, CA, Telecommunications and Mission Operations Progress*, Rep. 42-141, May 2000.

[121] X. Zhu and J. M. Kahn. Free-space optical communication through atmospheric turbulence channels. *IEEE Trans. Commun*, 50(8):1293Ű1300, Aug 2002.

[122] B. Epple. Simplified channel model for simulation of free-space optical communications. *J. OPT. COMMUN. NETW*, VOL. 2, NO. 5:293–304, MAY 2010.

[123] B. R. Strickland, M. J. Lavan, E. Woodbridge, and V. Chan. Effects of fog on the bit-error rate of a free-space laser communication system. *Applied Optics*, 38:424–431, 1999.

[124] M. S. Khan, M. S. Awan, E. Leitgeb, F. Nadeem, and I. Hussain. Selecting a distribution function for optical attenuation in dense continental fog conditions. In *ICET*, 17-18 October 2009.

[125] J. C. Houghton. Birth of a parent: the wakeby distribution for modeling flood flows. *Water resources research*, 14(6):1105–1110, 1978.

[126] S. R. Bowling, M. T. Khasawneh, S. Kaewkuekool, and B. R. Cho. A logistic approximation to the cumulative normal distribution. *Journal of Industrial Engineering and Management*, Vol 2, No 1:114–127, 2009.

[127] Michael R. Flynn. Fitting human exposure data with the johnson sb distribution. *Journal of Exposure Science and Environmental Epidemiology*, 16:56Ű62, 2006.

[128] M.C. Jones. KumaraswamyŠs distribution: A beta-type distribution with some tractability advantages. *Statistical Methodology*, 6:70Ű81, 2009.

[129] Warren G. Gilchrist. *Statistical Modelling with Quantile Functions*. CHAPMAN & HALL/CRC, 2000.

[130] Eric B. Holmgren. The p-p plot as a method for comparing treatment effects. *Journal of the American Statistical Association*, 90(429):360–365, Mar 1995.

[131] I. Gultepe and G. A. Isaac. Scale effects on averaging of cloud droplet and aerosol number concentrations observations and models. *Journal of Climate*, 12, 1999.

[132] I. Gultepe, G. A. Isaac, and K. B. Strawbridge. Variability of cloud microphysical and optical parameters obtained from aircraft and satellite remote sensing measurements during race. *International Journal of Climatology*, page 507Ű525, 2001.

[133] M. S. Awan, R. Nebuloni, C. Capsoni, and et al. Prediction of drop size distribution parameters for optical wireless communications through moderate continental fog. *International Journal of satellite communications and networking*, 29(1):97Ű116, 2009.

[134] C. Tomasi and F. Tampieri. Features of the proportionality coefficient in the relationship between visibility and liquid water content in haze and fog. *Atmosphere*, 14(2), 1976.

[135] ITU-R P.840-3. Attenuation due to clouds and fog. 1999.

[136] J. M. Wallace and P. V. Hobbs. *Atmospheric Science: An Introductory Survey*. Elsevier Publisher London (UK), 2006.

[137] I. Gultepe, M. D. Mller, and Z. Boybeyi. A new visibility parameterization for warm-fog applications in numerical weather prediction models. *Journal of applied meteorology and climatology*, 45, 2006.

[138] R. G. Eldridge. Haze and fog aerosol distributions. *J. Atmos. Sci.*, 23, 1966.

[139] C. M. R. Plat. Transmission of submillimeter waves through water clouds and fogs. *J. Atmosph. Sci*, 27, 1970.

[140] R. G. Eldridge. The relationship between visibility and liquid water content in fog. *J. Atmos. Sci*, 28(7), 1971.

[141] M. S. Khan, S. S. Muhammad, M. S. Awan, V. Kvicera, M. Grabner, and E. Leitgeb. Further results on fog modeling for terrestrial fso links. *Accepted for publication in Journal of Optical Engineering, March 2012*, 51(3), 2012.

[142] I. Gultepe and et al. Fog research: A review of past achievements and future perspectives. *J. of Pure and Applied Geophysics*, 164:1121Ű1159, 2007.

[143] O. Bouchet and et al. *Free-Space Optics: Propagation and Communication*. Wiley-ISTE, 2006.

[144] E. A. Bucher and R. M. Lerner. Experiments on light pulse communication and propagation through atmospheric clouds. *Applied Optics*, 12(10):2401–2414, 1973.

Appendix A: Own Publications

The work provided in this thesis has been published in the following journals and refereed conference proceedings.

As First Author

1. ***M. S. Khan***, M. S. Awan, E. Leitgeb, F. Nadeem, I. Hussain, *"Selecting a Distribution Function for Optical Attenuation in Dense Continental Fog Conditions"*, ICET 2009, October 19-20, 2009, Islamabad, Pakistan.

2. ***M. S. Khan***, M. S. Awan, et al., *"Probabilistic Model for Free-Space Optical Links Under Continental Fog Conditions"*, Journal Radioengineering, vol. 19, NO. 3, September 2010.

3. ***M. S. Khan***, M. S. Awan, et al., *"Linearity in Optical Attenuations for Free-Space Optical Links in Continental Fog"*, EuCAP 2011, 1-15 April 2011, Rome, Italy.

4. ***M. S. Khan***, S. S. Muhammad, et al., *"Validating Relationship between Aerosol's Liquid Water Content and Optical Attenuation for Terrestrial FSO Links"*, ConTEL 2011, 15-17 June , 2011, Graz, Austria.

5. ***M. S. Khan***, S. S. Muhammad, et al., *" Further Results on Fog Modeling for Terrestrial FSO Links"*, Accepted for publication in Journal of Optical Engineering, vol. 51, No. 03, March 2012.

6. ***M. S. Khan***, E. Leitgeb, et al., *"Effects of PSA on Free-space Optical Links"*, Accepted for EuCAP 2012, 26-30 March 2012, Prague, Czech Republic.

7. ***M. S. Khan***, S. S. Muhammad, et al., *" Modeling of Liquid Water Content for Optical Attenuation Prediction"* Submitted to Journal Radioengineering.

As Co-Author

1. F. Nadeem , ***M. S. Khan***, E. Leitgeb, *"Optical Wireless Link Availability Estimation through Monte Carlo Simulation"*, ConTEL 2011, 15-17 June, 2011Graz, Austria.

2. M. S. Awan, Marzuki, E. Leitgeb, B. Hillbrand, F. Nadeem, ***M. S. Khan***, *"Cloud Attenuations for Free-Space Optical Links"*, International Workshop on Satellite and Space Communications (IWSSC) 2009, Siena-Tuscany, Italy.

3. M. S. Awan, L.C. Horwath, S. S. Muhammad, E. Leitgeb, F. Nadeem, ***M. S. Khan***, *"Characterization of Fog and Snow Attenuations for Free-Space Optical Propagation"*, J. Communications, vol. 4, no. 8, September 2009.

4. M. S. Awan, R. Nebuloni, C. Capsoni, L. Csurgai-Horváth, S. S. Muhammad, E. Leitgeb, F. Nadeem, ***M. S. Khan***, *"Prediction of Drop Size Distribution Parameters for Optical Wireless Communications through Moderate Continental Fog"*, International Journal of Satellite Communications and Networking (IJSCN) Volume 29, Issue 1, 2009.

5. F. Nadeem, M. S. Awan, E. Leitgeb, ***M. S. Khan***, S. S. Muhammad, G. Kandus, *"Comparing the Cloud Attenuation for Different Optical Wavelengths"*, IEEE International Conference on Emerging Technologies, 2009, Islamabad, Pakistan.

6. E. Leitgeb, M. S. Awan, T. Plank, N. Perlot, C. Capsoni, R. Nebuloni, T. Javornik, G. Kandus, F. Nadeem, P. Brandl, S. S. Muhammad, M. Loeschnigg, ***M. S. Khan***, E. Duca, S. Betti, *"Investigations on Free-Space Optical Links within SatNEx II"*, European Conference on Antennas and Propagation, 2009, Berlin, Germany.

7. M. S. Awan, Marzuki, E. Leitgeb, F. Nadeem, ***M. S. Khan***, C. Capsoni, *"Weather Effects Impact on the Optical Pulse Propagation in Free Space"*, IEEE Vehicular Technology Conference, 2009, Barcelona, Spain.

8. M. S. Awan, E. Leitgeb, C. Capsoni, R. Nebuloni, Marzuki, F. Nadeem, ***M. S. Khan***, *"Attenuation Analysis For Optical Wireless Link Measurements Under Moderate Continental Fog Conditions at Milan and Graz"*, IEEE Vehicular Technology Conference (VTC) 2008 - Fall, Calgary, Canada.

9. F. Nadeem, E. Leitgeb, M. S. Awan, ***M. S. Khan***, G. Kandus, *"Bandwidth efficient solution for hybrid wireless network"*, International Workshop on Satellite and Space Communications (IWSSC), 2008, Toulouse, France.

10. F. Nadeem, B. Flecker , E. Leitgeb , ***M. S. Khan*** , M. S. Awan , T. Javornik, *"Comparing the fog effects on hybrid network using optical wireless and GHz links"*, CSNDSP 2008 , Graz Austria.

11. M. S. Awan, E. Leitgeb, S. S. Muhammad, Marzuki, F. Nadeem, ***M. S. Khan***, C. Capsoni, *"Distribution Function for Continental and Maritime Fog Environments for Op-*

tical Wireless Communication", CSNDSP 2008 , Graz Austria.

12. M. S. Awan, C. Capsoni, O. Koudelka, E. Leitgeb, F. Nadeem, ***M. S. Khan***, *"Diurnal variations based fog attenuations analysis of an optical wireless link"*, IEEE Photonics Global, 2008, Singapore.

13. M. S. Awan, E. Leitgeb, Marzuki, F. Nadeem, ***M. S. Khan***, *"Evaluation of Fog Attenuation Results for Optical Wireless Links in Free Space"*, International Workshop on Satellite and Space Communications (IWSSC), 2008, Toulouse, France.

14. M. S. Awan, C. Capsoni, R. Nebuloni, E. Leitgeb, Marzuki, F. Nadeem, ***M. S. Khan***, *"FSO-Relevant New Measurement Results Under Moderate Continental Fog Conditions at Graz and Milan and Modified Gamma Drop Size Distribution"*, Advanced Satellite Mobile Systems Conference (ASMS) 2008, Bologna, Italy.

15. F. Nadeem, E. Leitgeb, M. S. Awan, ***M. S. Khan***, G. Kandus, *"Simulations and Analysis of Bandwidth Efficient Switch-over between FSO and mmW Links"*, International Conference on Software, Telecommunications and Computer Networks (SoftCom), 2008, Split, Croatia.

16. F. Nadeem , E. Leitgeb, ***M. S. Khan***, M. S. Awan, *"Availability simulation of Switch over for FSO and mmW"*, IEEE International Conference on Information and Emerging Technologies (ICIET), 2007, Karachi, Pakistan.

Appendix B: Proposed setup to measure Dispersion for FSO links

Performance of terrestrial FSO links mainly depends on local weather conditions. At times, moderate clouds and fog may emerge between the transceiver of FSO links. The fog may impose a temporal broadening of the pulse, causing an intersymbol interference (ISI). In adverse weather conditions ISI may significantly reduce the system throughput. ISI may reduce the signal-to-noise ratio (SNR) and degrade the system's bit error rate (BER). We found that the presence of ISI was due to the reason of multiple scattering of laser beam with fog [9, 144].

Some experiments have bee performed to investigate the light pulse propagating through the atmospheric clouds [144]. The schematic diagram of the used setup is shown in Fig .1 (for transmitter) and in Fig .2 (for receiver) section respectively.

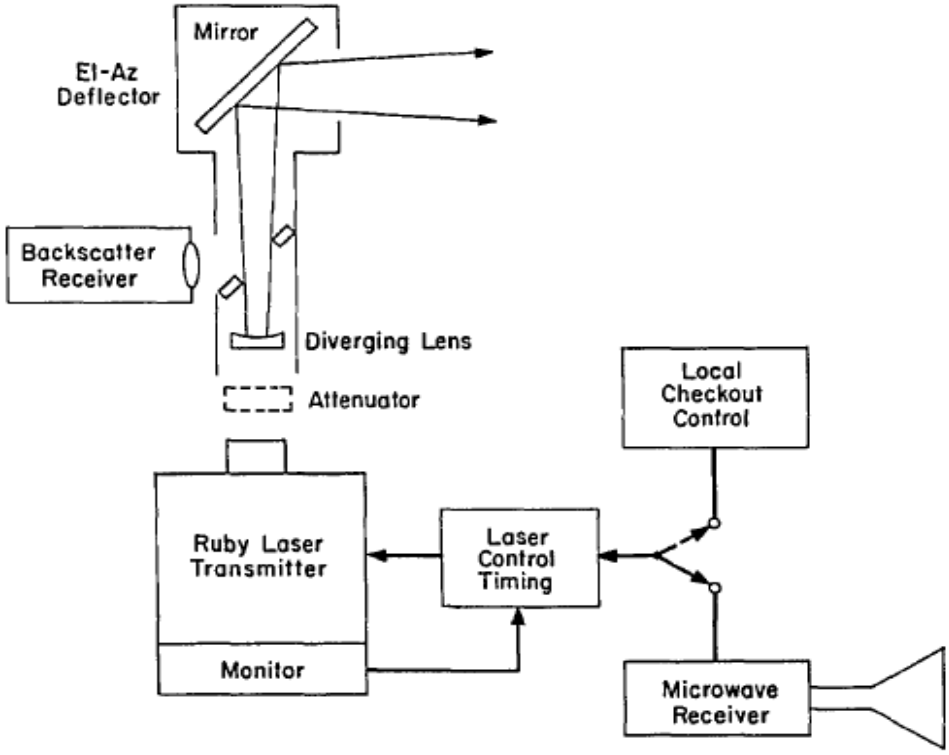

Figure .1: Schematic diagram of Transmitter

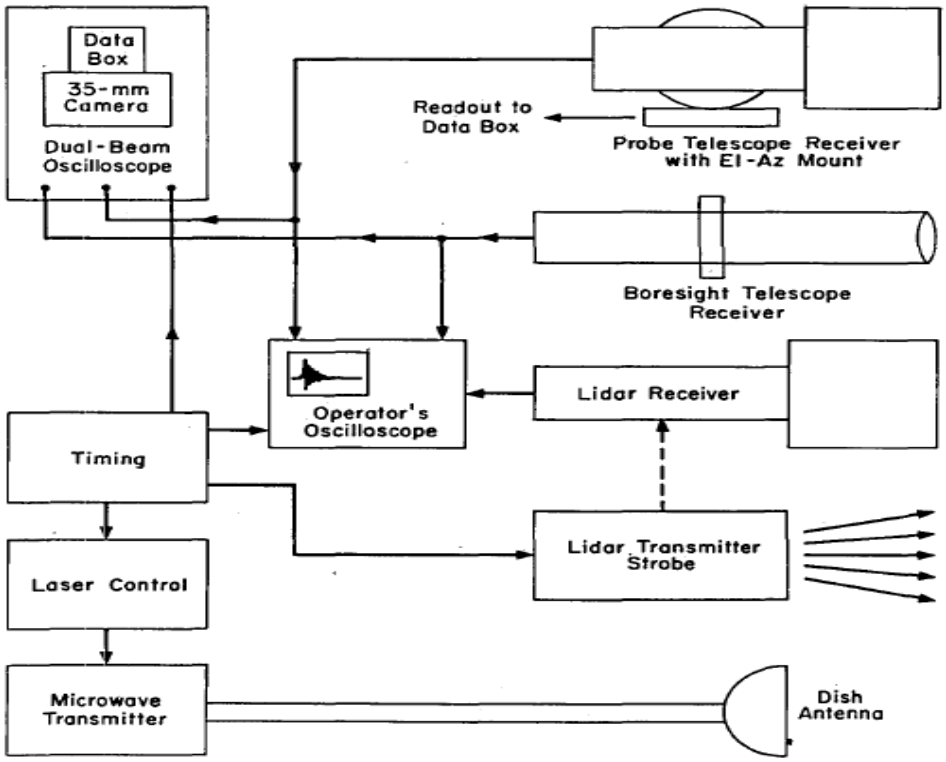

Figure .2: Schematic diagram of Receiver

In this experiment (demonstrated in [144]) a light pulse was transmitted using a Q-switched ruby laser producing 0.5-J pulses at 694 nm wavelength for less than 30 nsec. The period of laser pulse was limited to approximately 1 pulse in 5 sec. In this experiment only one wavelength was used and there was lack to understand and analyze the frequency dependent attenuations.

B.1 Background

Optical wireless communication system uses atmosphere as propagation medium. Earth's atmosphere occasionally contains fog, which is the main limiting factor for optical wireless communication. In the recent years, the main focus of the research community has been to counteract the problem of fog. Different modulation and coding schemes were proposed to improve the performance of optical wireless communication.

Fog causes very high attenuation over significant amounts of time. In the case of fog light energy is scattered, so the light rays loose direction of propagation. Dispersion means, the total amount of power (or energy) at the point of transmission is split up into several parts, which arrive at the receiver at slightly different times. The underlying process will be multi path propagation or dispersion. For the air conditions, the two interesting effects

will be scintillation and fog, causing multiple scattering. There are different causes for the effect, e.g different group velocities for different optical wave lengths in a glass fiber, or different distances due to multiple particles scattering for light propagation in free air with fog particles. If the power at the transmitter is modulated by a continuous frequency, at the receiver the different parts of the power containing the modulation signal with different phase shifts are summed up at one time. This causes a frequency dependent attenuation. Typically, the transmission power will not be split up into a few discrete parts, but it will rather have a continuous distribution function (e.g. over wavelength). For a simple example, let us assume only two parts for the power: The first part needs 0.334 μs to propagate 100 meters from Transmitter to Receiver, the second part needs 0.335 μs from Transmitter to Receiver. The difference is one Nanosecond. Let us assume a comparatively low frequency square wave modulation signal of 10 kHz. This means a time period of 100 μs, for a duty cycle of 50% to 50% this means 50 μs of light state, and 50 μs of dark state. For the simplified example of dispersion with 1 ns difference in two equal parts of the transmission power, the effect will be negligible.

Let us assume a comparatively high frequency square wave modulation signal of 500 MHz. This means a time period of 2 ns, for a duty cycle of 50% to 50% at the transmitter, with 1 ns light state and 1 ns dark state. At the receiver, this means, that the modulation signal cancels out, because half of the energy arrives at time t and contains light state with half of the power, and half of the energy arrives at time t + 1 ns and contains light state with half of the power. So there is no difference between light state and dark state. For the receiver (which uses a high pass), this means a complete attenuation of the modulation signal. So, the important point is, that dispersion will introduce wavelength dependent attenuation, if it exists at all. And it will be interesting for modulation frequencies in the range of 500 MHz, as data rates in the order of 1 Gbit/s are interesting for FSO. So this method would investigate the existence or non-existence of the effect at the same frequencies as used for the intended application. To be able to measure this accurately, it would help to change the modulation frequency continuously, starting from a low frequency, where dispersion will not have an effect. But it is expected that dispersion itself (if existent at all) may change characteristics over time.

B.2 Prosposed Setup

The affects of dispersion is related to the system used, the local weather and air conditions. For the system especially the receiver acceptance angle, also known as Field of View (FOV) will be interesting.

For terrestrial FSO links, under good weather conditions and possibly in presence of scintillation there should be no dispersion effect up to 10 GHz and over several km distances. The only possible mechanism in this context would be, change in the fractional index n which according to Fermatt's principle could cause different propagation ways for the

light, but for fog case it is very unlikely that the ray would find its way back to the receiver, when it was deviated somewhere in the link distance.

For the case of fog, the light energy is scattered, so the light rays loose directivity. If the transmitted power and the received power is considered, this means that rays directly pointing from TX to RX will be attenuated most because free-space optic receivers usually have a very narrow acceptance angle and so can nearly only detect the direct light rays.

If multiple scattering is considered, which happens in reality, it is possible that light will be scattered a second time, and comes back to the receiver, although from a different angle. This part of the light energy then also has had a longer distance to propagate. So, basically, this scenario using wide TX and RX angles could allow less fog attenuation on the expense of higher dispersion. And possibly this effect could also cause ISI in typical FSO systems.

A signal of a high pulse frequency (switch between light and dark states) like 200 MHz or 1 GHz should be produced. Then a counter should be used to produce a low pulse frequency out of the first signal, like 10 kHz. Then combine both signals with an AND gate. Use this signal to modulate a FSO transmit unit. FSO receiver (possibly with a wide acceptance angle) should be used which should be able to detect the first signal, after it has crossed the link through free air (fog, scintillation...). The receiver then should have two band-pass filters to select the high frequency and the low frequency. Both shall be amplified and the (averaged) signal amplitude shall be measured. Now the idea is, that for the case of fog, the light will be attenuated. But if the affect is present, the high frequency amplitude would be much more attenuated than the low frequency amplitude (due to phase-shifted parts of the pulse engergy, which are summed up).